CHEMICAL ABUNDANCES AND PHOTOMETRIC PARAMETERS IN THE BULGES OF SPIRAL GALAXIES

by

Todd Allan Boroson

A Dissertation Submitted to the Faculty of the

DEPARTMENT OF ASTRONOMY

In Partial Fulfillment of the Requirements
For the Degree of

DOCTOR OF PHILOSOPHY

In the Graduate College

THE UNIVERSITY OF ARIZONA

1 9 8 0

THE UNIVERSITY OF ARIZONA
GRADUATE COLLEGE

As members of the Final Examination Committee, we certify that we have read the dissertation prepared by Todd Allan Boroson

entitled CHEMICAL ABUNDANCES AND PHOTOMETRIC PARAMETERS IN THE BULGES OF SPIRAL GALAXIES

and recommend that it be accepted as fulfilling the dissertation requirement for the Degree of Doctor of Philosophy.

	June 2, 1980 Date
Ray J. Weymann	June 2, 1980 Date
	2 Jun 1980 Date
	2 June, 1980 Date
	Date

Final approval and acceptance of this dissertation is contingent upon the candidate's submission of the final copy of the dissertation to the Graduate College.

I hereby certify that I have read this dissertation prepared under my direction and recommend that it be accepted as fulfilling the dissertation requirement.

Ray J. Weymann Dissertation Director	June 2, 1980 Date

STATEMENT BY AUTHOR

This dissertation has been submitted in partial fulfillment of requirements for an advanced degree at The University of Arizona and is deposited in the University Library to be made available to borrowers under rules of the Library.

Brief quotations from this dissertation are allowable without special permission, provided that accurate acknowledgment of source is made. Requests for permission for extended quotation from or reproduction of this manuscript in whole or in part may be granted by the head of the major department or the Dean of the Graduate College when in his judgment the proposed use of the material is in the interests of scholarship. In all other instances, however, permission must be obtained from the author.

SIGNED: Todd A. Brown

ACKNOWLEDGMENTS

This dissertation represents an attempt to plan, carry out, and understand the results of an extensive observational project. When I decided, about three years ago, to work on stellar populations in galaxies, it was with the knowledge that there was no one at Steward actively working in this field. I believed that this fact would slow down my progress over what it would have been if there had been someone with whom to discuss each step of my work. However, I also believed that ultimately I would learn more by proceeding on my own. I think that this latter expectation has been fulfilled. A combination of two factors have lessened the extent of the former expectation. One was the excellent luck I had with the weather during my observing runs. I ran well above 90% for more than thirty nights in Kitt Peak. The other factor was the great support and assistance I received from many people while I have been working on this project. I thank everyone with whom I have discussed all the different aspects of this study, and I want to single out several in particular.

First, I wish to thank Drs. Steve Strom, Ray Weymann, Sandy Faber, Paul Schechter, Jim Liebert, John Kormendy, Hy Spinrad, and Dave Burstein. Each of these astronomers has had a major impact on my dissertation and on what I believe about galaxies. I also want to acknowledge helpful conversations with Drs. Leonard Searle, Marc Aaronson, Pete Stockman, Dave Monet, Doug Rabin, Eric Jensen, Jeremy

Mould, Tom Sargent, and Doug Richstone. A special thanks goes to Her Majesty's Pundit, Dr. W. L. W. Sargent, who got me started in astronomy as well as single malt scotch whisky. I also want to extend thanks to Dr. Keith Hege, who designed, built, and maintained the Reticon scanner I used, and to the mountain staffs at Steward Observatory and Kitt Peak National Observatory.

Finally, I want to thank my parents and family, whose support and understanding have been an inspiration to me.

TABLE OF CONTENTS

	Page
LIST OF ILLUSTRATIONS	vii
LIST OF TABLES	ix
ABSTRACT	x
CHAPTER	
I. INTRODUCTION	1
II. METALLICITIES IN THE BULGES OF SPIRAL GALAXIES	12
Observations	17
The Mgb-CN39 Diagram	21
Discussion	36
III. THE DISTRIBUTION OF LUMINOSITY IN SPIRAL GALAXIES	41
Observations and Preliminary Reductions	44
Decomposition of the Profiles	68
NGC 488	118
NGC 628	119
NGC 1058	119
NGC 2268	120
NGC 2336	120
NGC 2344	120
NGC 2655	120
NGC 2681	121
NGC 2775	121
NGC 2841	121
NGC 2855	122
NGC 2967	122
NGC 3147	122
NGC 3277	122
NGC 3368	122
NGC 3642	123
NGC 3898	123
NGC 4378	123
NGC 4594	124
NGC 4725	124
NGC 4736	124
NGC 4941	125
NGC 5194	125

TABLE OF CONTENTS--Continued

	Page
NGC 6340	125
NGC 7217	126
NGC 7331	126
Discussion	126
Conclusions	140
IV. THE METALLICITY-LUMINOSITY RELATION FOR SPIRAL GALAXIES	142
Discussion	154
REFERENCES	163

LIST OF ILLUSTRATIONS

Figure		Page
1.	Reduced spectrum of the elliptical galaxy NGC 4889	22
2.	Reduced spectrum of the Sc galaxy NGC 5194 (M51)	23
3.	A comparison of the Mgb index values measured in this study with Mg_2 index values measured by Faber (1979) for 21 objects in common	26
4.	The Mgb-CN39 diagram for elliptical galaxies (crosses) . .	27
5.	The Mgb-CN39 diagram for spiral galaxies (triangles) and M32 (cross)	29
6.	The relationship between the %Y parameter and (left) revised morphological type and (right) Yerkes concentration class	37
7.	The distribution of the $(Mgb)_c$ parameter with Yerkes concentration class	39
8.	Prints from the long plates of the program spiral galaxies	45
9.	A typical characteristic curve for the plates obtained in this study	58
10.	A comparison of surface brightness measurements of NGC 3379 made in this study with those of other authors	66
11.	A comparison of surface brightness measurements of NGC 4486 made in this study with those of other authors	67
12.	Elliptically averaged major axis profiles	69
13.	The relations between bulge-to-disk ratios and qualitative classifications	131
14.	The residuals of the relation between T type and log (B/D) plotted against an indicator of the fraction of the disk in neutral atomic hydrogen	135

LIST OF ILLUSTRATIONS--Continued

Figure Page

15. The distribution of disk central surface brightnesses in this study (lower panel) and in the study of Freeman (1970) (upper panel) 137

16. The distribution of true bulge flattenings in this study 139

17. One sigma error ellipses showing possible values of slope and intercept for the first four pairs of variables listed in Table 14 153

18. The metallicity (Mgb) vs. luminosity (M) diagram for elliptical galaxies (crosses) and spiral bulges (triangles) 155

19. Histograms of the observed distributions of bulge-to-disk mass ratios for spirals (from this study) and for SO's (from Burstein 1979b) 159

LIST OF TABLES

Table		Page
1.	Parameters of Program Spiral Galaxies	9
2.	Parameters of Program Elliptical Galaxies	10
3.	Measured Line Indices and Dispersions	24
4.	Metallicities and Young Star Fractions as Deduced from Mgb-CN39 Analysis	34
5.	Plate Material	52
6.	Photoelectric Aperture Photometry	55
7.	Precision of Zero-Point Determinations	61
8.	Aperture Radii and Positions	63
9.	Elliptically Averaged Major Axis Profiles	95
10.	Parameters of Decomposed Spiral Galaxies	114
11.	Derived Overall Parameters of Program Spirals	115
12.	H I Properties of Program Spirals	133
13.	Metallicity-Luminosity Data for Program Spirals	144
14.	Statistical Tests	150

ABSTRACT

The relation between central or mean metallicity and luminosity in elliptical galaxies is a well observed phenomenon. Theoretical explanations proposed for this relation include scenarios in which peak metallicities are determined either by the epoch at which the remaining gas is expelled from the galaxy by supernova-driven winds, or by the efficiency of star formation following a series of mergers by small stellar/gaseous subsystems. These explanations suggest that an investigation of the metallicity-luminosity relation for spiral galaxies might have implications for galaxy formation models and for the origin of SO galaxies. The existing evidence concerning SO's points to a relation between mean metallicity and total luminosity.

The problem of measuring metal abundances in the nuclei of spiral galaxies is that the line strength variations due to metallicity changes must be distinguished from those due to a filling in of the lines by the continuum from a young population. This was accomplished by measuring absorption line indices for Mg b and for a CN band at λ3880. Nuclear spectra of twenty ellipticals, obtained with a reticon detector, show these two indices to be well correlated for pure old populations; models including the effects of young stars show a very different trajectory for age effects. A procedure is thus defined for determining the metallicity of the population and the fraction of light coming from the young component, and this procedure is applied to observations of 25 spiral galaxies. A comparison of the results of

this analysis with detailed population syntheses for six galaxies confirms the correctness of the procedure.

In order to obtain bulge luminosities and bulge-to-disk ratios, photographic plates of twenty-two of the spirals were obtained. This material was digitized and reduced to a series of radial luminosity profiles for each galaxy. A procedure was established for decomposing the profiles into disk and bulge contributions. In addition to the desired gross parameters of the bulge and disk, the inclinations and true bulge flattenings for some of the galaxies are accurately determined. A discussion of the results of this analysis deals with the nature of departures from the exponential fitting function for some disks, a decomposition of the Hubble sequence into quantitative parameters, and the implication of the distribution of true bulge flattenings.

The metallicities and luminosities are then combined, and two tests indicate that in spiral galaxies, central metallicity and bulge luminosity follow the same relation seen in ellipticals. The implications of this result are twofold. First, galaxy formation models in which the disk material can affect the processes which determine the central metallicity in the bulge are ruled out. Specifically, it is likely that the disks of spiral galaxies are not undergoing vigorous star formation at the time the bulge ceases forming stars. A picture in which the disk material has not yet accreted on to the galaxy at this time is also quite consistent. A somewhat more straightforward implication comes from a comparison of the results of this study with similar studies of S0 galaxies. It is concluded that, aside from the uncertain

effects of radial gradients, the evidence is inconsistent with the theory that most SO's were at one time spiral galaxies.

CHAPTER I

INTRODUCTION

It has often been assumed that the bulges of spirals and S0 galaxies are stellar systems with properties very similar to elliptical galaxies. Support for this assumption comes from the similarity of the luminosity distributions and stellar populations in bulges and elliptical galaxies. The fact that galaxies with disks must represent some change in the initial conditions of galaxy formation or early evolution from galaxies without disks, however, implies that at some level the two types of systems must differ. Recent studies of rotation of galaxies have revealed one such difference. Apparently, ellipticals are not supported by rotation (Illingworth 1977), whereas bulges do contain most of their kinetic energy in rotation (Kormendy and Illingworth 1980). Further properties which distinguish bulges from elliptical galaxies are sure to be found, and such distinctions provide an important input to models of galaxy formation. One such property which holds promise for supplying information about conditions at the time of galaxy formation is the metallicity-luminosity relation.

The existence of variations in colors of elliptical galaxies has been known for more than 20 years (Baum 1959, deVaucouleurs 1961, Lasker 1970, Faber 1973). These variations are correlated with the strengths of metal lines in the integrated spectra and with luminosity, in the sense that brighter galaxies tend to have stronger metal lines

and redder colors (Faber 1973, 1977). The interpretation which has evolved for these variations is that they are due to a range of mean metal abundances in the stellar populations of different galaxies. In terms of the colors, increasing metallicity implies increasing line-blanketing in the UV and a cooler giant branch, so the observed correlation between color and line strength is qualitatively as expected. Furthermore, synthetic galaxy population models which vary the star formation rate or the mass function are unable to reproduce the observed features, although it is likely that very blue dwarf ellipticals do have current or recent star formation which serves to bluen their colors even more. A good review of metallicity variations within and between galaxies is given by Faber (1977).

Two different explanations for the trend of metallicity with luminosity in elliptical galaxies have been proposed. In what we shall refer to as the supernova-driven wind model (Larson 1974b), the star formation, and hence the nucleosynthesis, is terminated at a time when enough energy has been imparted to the remaining interstellar gas by supernova explosions to blow the gas out of the galaxy. This has the effect of making both the mean and central metal abundance higher in galaxies which can hold on to their gas longer. How tightly a galaxy can hold its gas is a measure of its escape velocity which depends on the mass of the galaxy.

The other explanation, the star formation efficiency argument, depends upon the merger picture of galaxy formation. According to this theory (White and Rees, 1978, Tinsley and Larson 1979) galaxies are constructed by the successive mergers of small subsystems containing stars

and gas. Chemical enrichment in this model accompanies bursts of star formation induced by the compression of gas in each merger. Tinsley and Larson (1979) show that a simple consequence of this model is an efficiency of star formation which is proportional to the total mass of the subsystems involved in the merger.

Thus, each of these processes accounts for the metallicity-luminosity relation in elliptical galaxies. Their application to spiral and SO galaxies, however, is less straightforward. In particular, the effect of the disk is uncertain. Does the very existence of a disk affect the properties which cause the metallicity-luminosity relation? Or is the disk added on at a later time, after the bulge star formation has ceased? We present the four following possible metallicity-luminosity relations for galaxies with disks:

1. A correlation between metallicity and bulge luminosity identical to the metallicity-luminosity relation for ellipticals.
2. A correlation between metallicity and total luminosity identical to the metallicity-luminosity relation for ellipticals.
3. A correlation between metallicity and bulge luminosity offset to lower metallicity than the elliptical relation and a correlation between this offset and bulge-to-disk ratio (lower metallicity for smaller bulge-to-disk).
4. A correlation between metallicity and total luminosity offset to lower metallicity than the elliptical relation and a correlation between this offset and bulge-to-disk ratio (lower metallicity for smaller bulge-to-disk).

These four possible cases can be thought of as expressing the formula:

$$M = \alpha L_{bulge} + \beta L_{disk}$$

where M is some measure of the metallicity, L_{bulge} and L_{disk} are the bulge and disk luminosities, and α and β are relative measures of the degree of correlation. For instance, relation 1 described above would have α positive and β zero; relation 2 would have α and β positive and equal; relations 3 and 4 would have α positive and β smaller or negative.

Each of these four possible relations can be justified in terms of a theoretical scenario of galaxy formation. Relation 1, in which bulges are most like elliptical galaxies, might occur if disks have no effect on the processes which cause the metallicity-luminosity relation. A specific picture with this effect is one in which, at the time that star formation in the bulge ceases, the disk material is not mixed with the bulge material. This might occur if the structural formation of the galaxy, disk and bulge, is complete. Then, for instance, supernova explosions among the newly formed bulge stars could expel the remaining gas from the bulge region with minimal effect from the disk material. Another, completely different scenario in which relation 1 is the expected outcome is one in which the bulges are produced by mergers of stellar/gaseous subsystems, but disks are created by the slow infall of low density clouds over a long period of time.

Relation 2 might be most easily explained in terms of the previously described multiple merger model in which both disk and bulge

material are contained in the smaller subsystems. In this case, star forming efficiency, and therefore chemical enrichment, is related to the total mass of the system, and the gas which does not immediately form stars settles into the disk.

Relation 3 might arise from a picture like the hydrodynamic models constructed by Larson (1974a, 1974b, 1975, 1976). One important consequence of these models is that the bulge-to-disk ratio of the galaxy is primarily controlled by the density of the gas in the protogalactic cloud. Similar results are obtained by Gott and Thuan (1976) who suggest that the fraction of the protogalaxy which will become the bulge is that fraction of the gas which has formed stars within one collapse timescale after the galaxy begins to collapse. The idea is that the stars which form as the protogalaxy collapses initially will form a dissipationless system, while the gas remaining will quickly settle into a disk. Since the collapse timescale is proportional to the inverse of the gas density, $t_c \propto \rho_g^{-1}$, and the star formation timescale may be proportional to ρ_g^{-2}, as in the calculations of Schmidt (1959), a lower density cloud will become a galaxy with a smaller bulge-to-disk ratio. If this picture is combined with the supernova-driven idea, in which the relevant parameter is the escape velocity, also dependent on the density, a simple consequence is that at a given bulge luminosity, a small bulge-to-disk ratio galaxy will have a lower central metallicity than a large bulge-to-disk ratio galaxy. These effects would produce a metallicity-luminosity relation similar to relation 3.

Relation 4 might be expected in a scenario which strings together the multiple merger models with the bulge-to-disk ratio

explanation given for relation 3. It is reasonable to expect that the star forming efficiency depends on the gas density as well as the mass of the merging subsystems. In this case, as for the previous relation, gas with a lower density will produce a galaxy with less chemical enrichment and a smaller bulge-to-disk ratio, if it is assumed that the disk is formed from the residual gas.

It is apparent from the previous discussion that the whole situation is quite complex. We will not attempt to construct quantitative models for all possible cases, both because many of the input parameters are unknown and because such models would not be unique. It is likely, however, that an investigation of the metallicity-luminosity relation in galaxies with disks would supply an important piece of information to the process of sorting out the galaxy formation pictures.

The existing observational data on this subject are not very extensive. Visvanathan and Sandage (1977) have obtained broad-band colors and magnitudes for 105 elliptical and S0 galaxies. They find that the metallicity-<u>total</u> luminosity relations for the two types of systems are indistinguishable in slope or intercept. However, their (u-V) colors may be affected by the age of the population in addition to metallicity, although it is quite unlikely that the two effects conspire to produce the result seen. Visvanathan and Griersmith (1977) have obtained similar colors and magnitudes for 41 early type spirals. They also conclude that the colors correlate with total magnitude in the same relation seen in ellipticals and S0's, but in this case, contamination by younger stars in the disk as well as effects of dust are not negligible. Burstein (1979a) obtained line strength measurements

indicative of the Mg b absorption for 5 SO galaxies. Using a red continuum color, he showed that in these objects there is little or no contamination from young stars, but, because this color is not reddening free, his method is subject to the problem that dust can mast the effect of young stars. His results confirm those of Visvanathan and Sandage. The metallicity-total luminosity relation for SO galaxies is the same as that for elliptical galaxies.

A comment on radial gradients and their effects on these measurements is in order. Both the color measurements of Visvanathan and Sandage and Visvanathan and Griersmith and the line strength measurements of Burstein were obtained with large apertures. Since it is known that both elliptical galaxies and SO galaxies show radial gradients in these colors and line strengths (Faber 1977, Burstein 1979a), we must distinguish between mean and nuclear metallicity measurements. While qualitatively, the same results are expected to obtain for both mean and nuclear metallicities, a systematic difference in the shape or steepness of the gradients in different types of galaxies could alter the quantitative comparison. An obvious example of this is that if one galaxy has a radial gradient much steeper than another galaxy, it is possible for their nuclear metallicities to be the same, while the one with the shallower gradient has a much larger mean metallicity. This problem will be discussed further in a later chapter.

The fact that some data exist for SO galaxies and the possibility of distinguishing between the various galaxy formation pictures are the motivations for the study that follows, a determination of the metallicity-luminosity relation for spiral galaxies, and a comparison of

this relation with the elliptical and SO galaxy relations. It was decided to choose a sample of approximately 25 spiral galaxies to be studied spectroscopically and photometrically. The requirements applied to the objects in this sample were that they be classified SO/a or later, that they have a significant bulge component visible on the Sky Survey or other published photographs, and that they have a radial velocity of less than about 3000 km sec^{-1}. The reason for this last qualification was to attempt to minimize the effects of radial gradients in the populations by sampling close to the same region in all galaxies. Most of the galaxies chosen are close to face-on as dust absorption and inclination effects are then least important. The spiral galaxies in the sample, and relevant information about them are listed in Table 1. The adopted distances come from Aaronson, Huchra, and Mould (1979) and Aaronson (1980).

Nineteen elliptical galaxies were also observed spectroscopically to establish their metallicity-luminosity relation on the same scales which were to be used for the spirals. Information on these galaxies is presented in Table 2. It should be noted that these samples are not expected to be free from selection effects. For example, late type spirals are certainly underrepresented in terms of the relative numbers of objects along the Hubble sequence. It is expected, however, that the method by which the sample was chosen will have little or no effect on the primary test to be performed, the comparison of the metallicity-luminosity relation for spirals with that for elliptical galaxies.

Table 1. Parameters of Program Spiral Galaxies

NGC	Hubble type	Revised type	Yerkes type	Distance (Mpc.)	B_0^T
224	Sb	3	gkS	0.65	3.59
488	Sb	3	gkS	35.3	10.83
628	Sc	5	fgS	12.2	9.48
2268	Sbc	4	fS	37.9	11.55
2336	Sbc	4	fgS	36.8	10.49
2344	Sc	5	-	15.4	12.42
2655	SO/a	0	kEp	25.0	10.49
2681	Sa	0	kS	15.7	10.79
2775	Sab	2	gkDS	14.8	10.85
2841	Sb	3	kS	15.7	9.58
2855	SO/a	0	kD	25.5	12.06
3031	Sb	2	gkS	3.6	7.24
3147	Sb	4	gkS	41.2	11.07
3277	Sab	2	kS	21.6	12.31
3368	Sab	2	gS	10.0	9.79
3642	Sbc	4	gkS	26.6	11.29
3898	Sab	2	kS	15.8	11.28
4378	Sa	1	kS	49.0	12.35
4594	Sa	1	kS	18.4	8.97
4725	Sb	2	gkSB	17.4	9.64
4736	Sab	2	gDS	5.2	8.58
5194	Sc	4	fgS	8.7	8.62
6340	Sa	0	gDS	33.0	11.45
7217	Sb	2	gkSD	18.9	10.49

Table 2. Parameters of Program Elliptical Galaxies

NGC	Distance (Mpc.)	B_0^T	M_B
596	32.4	11.53	-21.02
1209	38.6	12.03	-20.90
1407	17.0	10.51	-20.64
2300	33.3	11.47	-21.14
2314	42.5	12.39	-20.75
2768	23.1	10.60	-21.22
3193	19.7	11.63	-19.84
3377	10.0	10.85	-19.15
3379	10.0	10.00	-20.00
4374	15.7	10.11	-20.87
4387	15.7	12.75	-18.23
4406	15.7	9.93	-21.05
4464	15.7	13.31	-17.67
4478	15.7	11.92	-19.06
4621	15.7	10.55	-20.43
4649	15.7	9.62	-21.36
4889	78.0	12.16	-22.30
6482	43.4	11.59	-21.60
7619	41.6	11.78	-21.32

The following part of this dissertation divides quite naturally into three sections. Chapter II reports on the spectroscopic observations of the galaxies and the discovery of a technique for separating the effects of metallicity variations from those of age, an important distinction when comparing spiral nuclei to elliptical nuclei. The metallicities of the program galaxies are listed and several correlations between the quantitative parameters derived and qualitative classification schemes are examined.

Chapter III discusses the surface photometry measurements for the sample galaxies, including a description of observation and reduction techniques. The decomposition of radial luminosity profiles into bulge and disk components is discussed and a procedure is devised and applied to the data obtained here. The relevant photometric parameters are derived and an investigation of the nature of the Hubble sequence in terms of these parameters is made. Chapter IV combines the results of Chapters II and III to construct the spiral metallicity-luminosity relation and compare it with the elliptical relation. Implications for the processes of galaxy formation and the nature of SO galaxies are discussed.

CHAPTER II

METALLICITIES IN THE BULGES OF SPIRAL GALAXIES

Variations among the spectra of the central regions of galaxies were first explored by Morgan and collaborators (Morgan and Mayall 1957; Morgan 1958, 1959; Morgan and Osterbrock 1969). Using photographic spectrograms of the nuclei of bright galaxies, these workers were able to establish a classification scheme using some of the same criteria as were used for individual stars. It was recognized that a correlation exists between the spectroscopic appearance of the nuclear stellar population of a galaxy and that galaxy's morphological appearance. This correlation is in the sense that spectra dominated by the earliest type stars (A in Morgan's system) correspond to those galaxies with the latest morphological appearance (Sc or Ir in Hubble's [1936] classification sequence). This is not a surprising result as there are several indications that the population of the disk component of a galaxy contains a significant fraction of young stars while that of the bulge does not. The evidence for this includes broad-band colors, the presence of H II regions and OB associations in nearby galaxies, and the distribution of neutral hydrogen. Thus, the range of spectral variation in galactic nuclei can be thought of as the effect of varying amounts of the young disk population showing through the old bulge population.

The quantitative study of stellar populations in galaxies has progressed slowly from this qualitative beginning. The main technique used has been population synthesis, in which a collection of

measurements (photometric colors or strengths of spectroscopic features) of different stellar types are combined to yield composite measurements which are then compared with observations of galaxies. In terms of physically meaningful quantities, each star in the population can be described by an age, a mass, and a metallicity. Of course, the abundance of each element is different, but [Fe/H] is often used to represent the entire array. The stellar population, then, can be thought of as the distribution of stars over these three parameters.

Three different methods have been used to produce the combination of stellar measurements which are to be compared to the galaxy measurements. The first and simplest is to determine, with linear or quadratic programming techniques, or by trial and error, the relative numbers of each star in the library of stellar observations needed to match the actual galaxy (Spinrad 1966, Wood 1966, Spinrad and Taylor 1971, Faber 1972, Turnrose 1976, Pritchet 1977). There are two rather serious drawbacks to this method. First, it is impossible to construct a catalog of stellar observations representing all possible values of mass, age, and abundances, within reasonable limits. Abundances are a particular problem in this regard as in the solar neighborhood we see a rather restricted range of metallicities, subsolar metallicities being observable only in the limited populations of old globular clusters and supersolar metallicities being essentially absent. The second problem inherent to the empirical population synthesis is that of uniqueness. Since the observations of different stellar types do not represent orthogonal vectors but only slightly oblique ones, the best fit solution is not well determined and is very sensitive to observational noise.

This limitation was recognized by the early workers in this field (Spinrad 1966), but its effect was demonstrated quite dramatically by Williams (1976). The procedure which has generally been used to avoid the problem of nonuniqueness is to constrain the allowed solution with various reasonable assumptions. These include the prevention of negative numbers of stars and various continuity criteria. However, one has to be careful in this case not to overinterpret the model; while the gross features of the synthesized population reflect the information in the spectrum, the details are often due solely to the constraints (Wilkinson and Searle 1977).

The other two methods of population synthesis are attempts to build the constraints into the technique by which the best fit model is found. Williams (1976) parameterized the HR diagram with such quantities as the turnoff spectral type and the slope of the mass function above and below the turnoff. He then solved for the values of the parameters for which the composite light most resembled the observed galaxies. This led to solutions which were stable to perturbation although the values derived may still be poorly determined.

The third type of population synthesis contains the constraints in the form of an evolutionary model. The model is defined in terms of a mass function, an age, a star formation rate, and a metallicity. The model is constructed by translating the mass and age of each star into a temperature and luminosity using stellar evolution tracks. The metallicity of the population enters into the solution in terms of both the evolutionary tracks and the measurements of the individual stars. This

type of analysis has been performed by Searle, Sargent, and Bagnuolo (1973); Moore (1968); Tinsley and Gunn (1976); and O'Connell (1976).

What have we learned about stellar populations from population syntheses? The general picture that has evolved is that all galaxies are about 10 billion years old (Searle et al. 1973). In ellipticals and presumably in the bulges of spirals all the star formation took place in a comparatively brief burst. In spiral disks, however, star formation has persisted to the present day, at a declining or steady rate, or in separate bursts (Searle et al. 1973). Visible light measurements have proven to be quite insensitive to the mass function (Tinsley and Gunn 1976) indicating only that if expressed as a power law, its slope must be flatter than -3, i.e., $\frac{dN}{dm} = Am^{\alpha}$, where $\alpha > -3$. Further information on this slope comes from observations of infrared features extremely sensitive to luminosity. Measurements of the Wing-Ford band (Whitford 1977, Tinsley and Gunn 1976) and similar studies of the 2.3μ CO absorption feature (Frogel et al. 1978) supply evidence that $\alpha > -2$.

Metallicity and age variations tend to be confused, as a decrease in [Fe/H] produces an effect very much like a decrease in the mean age of a population. One unambiguous limit on metallicities, however, is that the nuclei of luminous elliptical galaxies are dominated by stars with metal abundances greater than solar. Metallicity variations lead quite naturally into the work of Faber (1973) who used an approach very much different from population synthesis to study stellar populations in galaxies. In the event that one is more interested in how the populations of galaxies differ than the properties they have in common, one can examine the variations in a straighforward

way. Clearly, observed variations could indicate differences in metallicity, star formation rate, or mass function, so it is interesting to ask in how many ways galaxy spectra differ. That is, how many dimensions of variation are there, and can they be interpreted in terms of physically meaningful quantities? Faber found that in elliptical galaxies almost all the variation was correlated, that only one dimension was required to explain the differences seen. She interpreted this variation as being due to changes in metallicity and found that it was correlated with the luminosity of the galaxy. The fact that more luminous ellipticals have redder colors was known previously (Baum 1959, de Vaucouleurs 1961, Tifft 1969), but she added evidence that the color variations were metallicity induced.

More recently, an outgrowth of Faber's approach to the problem has proven effective in studying metallicities quantitatively. Mould (1978) has related the strength of the Mg b index measured by Faber and others to [Fe/H] values for stellar populations. He also showed that this particular line index is much more sensitive to metallicity than to the details of the stellar population. Similarly, Cohen (1978) and Aaronson et al. (1978) have examined the behavior of individual spectral features in terms of variations in the different parameters.

Since this technique has yielded some interesting results for the predominantly old populations of elliptical galaxies, it might be expected that something could be learned about the populations in the nuclei of spirals in a similar way. It is expected that when the old bulge population is contaminated by the younger disk population, changes will occur in the spectrum which can be distinguished from metallicity

variations. It should be recalled, however, that to first order, the changes will mimic a metallicity decrease. A decrease in metallicity and the presence of young stars will both tend to weaken the metal lines, strengthen the hydrogen lines, and make the continuum bluer. However, using the accepted interpretation that the spectra of elliptical galaxies form a one parameter (metallicity) family, it will be demonstrated that a second parameter is present in the spectra of galaxies having a disk population. Several lines of evidence show that this second parameter is the presence of a younger population. Finally, a quantitative procedure will be devised to determine the fraction of light arising in the young component and the metallicity inherent to the bulge population on a system which can be used to compare the bulges of spirals with elliptical galaxies.

Observations

Spectra of twenty elliptical galaxies and twenty-five spiral galaxies were obtained with the Steward Observatory 2.3 meter telescope. The detector used was a two-line by 938 diode reticon chip operated in an analog mode (Hege, Cromwell, and Woolf 1979) behind a two-stage RCA C33063 image tube and a three-stage Varo image tube booster. This whole system was mounted on Steward Observatory's Boller and Chivens cassegrain spectrograph. The observations were made in five separate runs between 6 October 1978 and 19 November 1979. In all cases a 3.5 arcsecond diameter aperture was used, centered on the nucleus of the galaxy. The second aperture looked at the sky 20 arcseconds to the east or west. A 400 line per millimeter grating was used in second order,

giving a reciprocal dispersion of about 100 Å/mm which corresponds to about 2 Å per diode on the detector. The grating tilt used produced spectral coverage from about λ3600 to λ5400, and a $CuSO_4$ filter eliminated the possibility of contamination from the first order spectrum.

Each observation consisted of a series of short integrations, usually 5 seconds long. After four such integrations, the telescope was wobbled 20 arcseconds east or west so that the nucleus fell into the other aperture. After each wobble cycle, i.e., when the object was moved back to the original aperture, the spectrum was moved one-half diode along the reticon array. A complete cycle consisted of 8 such substeps, 4 in one direction and then 4 in the other direction. These substeps allow the spectrum to be oversampled but introduce a 4 channel (1 channel = 1/2 diode) periodic noise which must be removed in the reduction procedure. A complete observation generally consisted of three or four cycles, as described above, followed by a helium-argon comparison lamp observation and a continuum lamp flat-field observation, followed by three or four more cycles on the object. Thus, the total integration time on each galaxy was about 30 to 40 minutes.

In most cases the instrument was used in a mode in which the sky spectrum was automatically subtracted from the galaxy plus sky spectrum at the end of the observation, the two arrays being kept separate. Because of the angular size of the galaxies in the sample, the sky beam was usually looking at some off-nuclear region in the galaxy. In general, the galaxy was fainter than the sky in this beam and the sum was only a few per cent of the galaxy plus sky flux. Therefore, effects of this contamination were ignored. In three cases, NGC 224, NGC 3031,

and NGC 5194, this mode was not used, but a sky spectrum was obtained several degrees away from the galaxy and later subtracted from the galaxy plus sky spectrum.

Two problems associated with this instrument should be mentioned. The first is that a large amount of light is scattered at small angles in the system. By replacing the grating in the spectrograph with a mirror, it was possible to examine this effect by projecting an unresolved spot through the system. It was found that the diodes outside the points at which the intensity fell to one-tenth its central value contained more than 15% of the total intensity in the spot. For comparison a gaussian distribution contains about 3% of its total intensity in a corresponding region. The effect of this scattering is to make observed equivalent widths of both emission and absorption lines smaller than their true values. This happens because more light is scattered from regions of high intensity than into them. The scattering problem was traced to the Varo image tubes, but no attempt was made to correct the measurements for it.

The second problem is much more serious as it introduces random errors. The spectra are centered on the reticon arrays in the direction perpendicular to the dispersion by adjusting the tilt of a quartz block behind the focal plane. This alignment is judged by comparing the continuum lamp spectrum falling in the two arrays. Because of geometrical distortions in the image tubes, the positional accuracy required to ensure that each spectrum falls completely on each array is quite high. It proved to be very difficult to maintain this alignment over the course of several hours. Possible reasons for this include

the four to five foot unsupported length of the image tube-reticon package and the magnetic focusing of the RCA image tube. As a result, variations in the precision of this alignment produce anomalous continuum shapes in the 200Å regions at each end of the spectrum. Unfortunately, these variations affect the strengths of some of the spectral features measured, but repeated observations of several of the objects as described below should give a realistic estimate of the true uncertainties.

The spectra were reduced in the following manner. First, about ten comparison lines from a helium-argon arc observed before or after each galaxy were identified, and a third order polynomial was fit to the wavelengths. Residuals in this fit were almost always less than one-half angstrom. Small scale variations in sensitivity were removed using the continuum lamp spectrum. Large scale variations were removed from the spectra using observations of spectrophotometric standard stars, one or two of which were observed each night. This procedure also corrected the spectra to units of energy per anstrom. The spectra were then convolved with a four channel rectangle to remove the noise generated by the substepping described previously. The two arrays were added, with adjustment being made for differents in the wavelength fit. Then the spectra were all converted to rest wavelengths, after using a cross-correlation technique to determine the redshift of each galaxy. Finally, the spectra were all rebinned using linear interpolation on a uniform wavelength scale, i.e., such that the wavelength of the center of any channel, λ_n is given by $\lambda_n = \lambda_o + n\Delta\lambda$, where λ_o was λ3201.0 and

$\Delta\lambda$ was 2.0Å. Reduced spectra for two of the 45 galaxies observed are shown in Figures 1 and 2.

The Mgb-CN39 Diagram

Two line indices, Mgb and CN39, were measured for each of the galaxies. Mgb is almost identical to the Mg_2 index described by Faber (1977). It measures the strength of both the atomic Mg triplet and the MgH bandhead. It has been shown (Mould 1978) that an index measuring these features is sensitive to metallicity variations. The index is defined as:

$$\text{Mgb} = -2.5 \log \left(\frac{F_\lambda\,(5156\text{-}5198)}{F_\lambda(4898\text{-}4960) + 0.609\,(F_\lambda(5304\text{-}5368) - F_\lambda(4898\text{-}4960)} \right)$$

where $F_\lambda(\lambda_1 - \lambda_2)$ is the average flux per angstrom between λ_1 and λ_2.

The CN39 index measures the depth of the broad trough, due mostly to CN at λ3860. The red continuum band for this index is longward of the λ4000 break and the blue continuum band is shortward of the Balmer limit. The index is defined as:

$$\text{CN39} = -2.5 \log \left(\frac{F_\lambda(3850\text{-}3870)}{F_\lambda(3610\text{-}3630) + 0.6\,(F_\lambda(4010\text{-}4030) - F_\lambda(3610\text{-}3630)} \right)$$

The coefficients 0.609 and 0.6 in the definitions of the indices are used to linearly interpolate the continuum flux to the position of the center of the line band. A list of the galaxies and their measured indices is presented in Table 3.

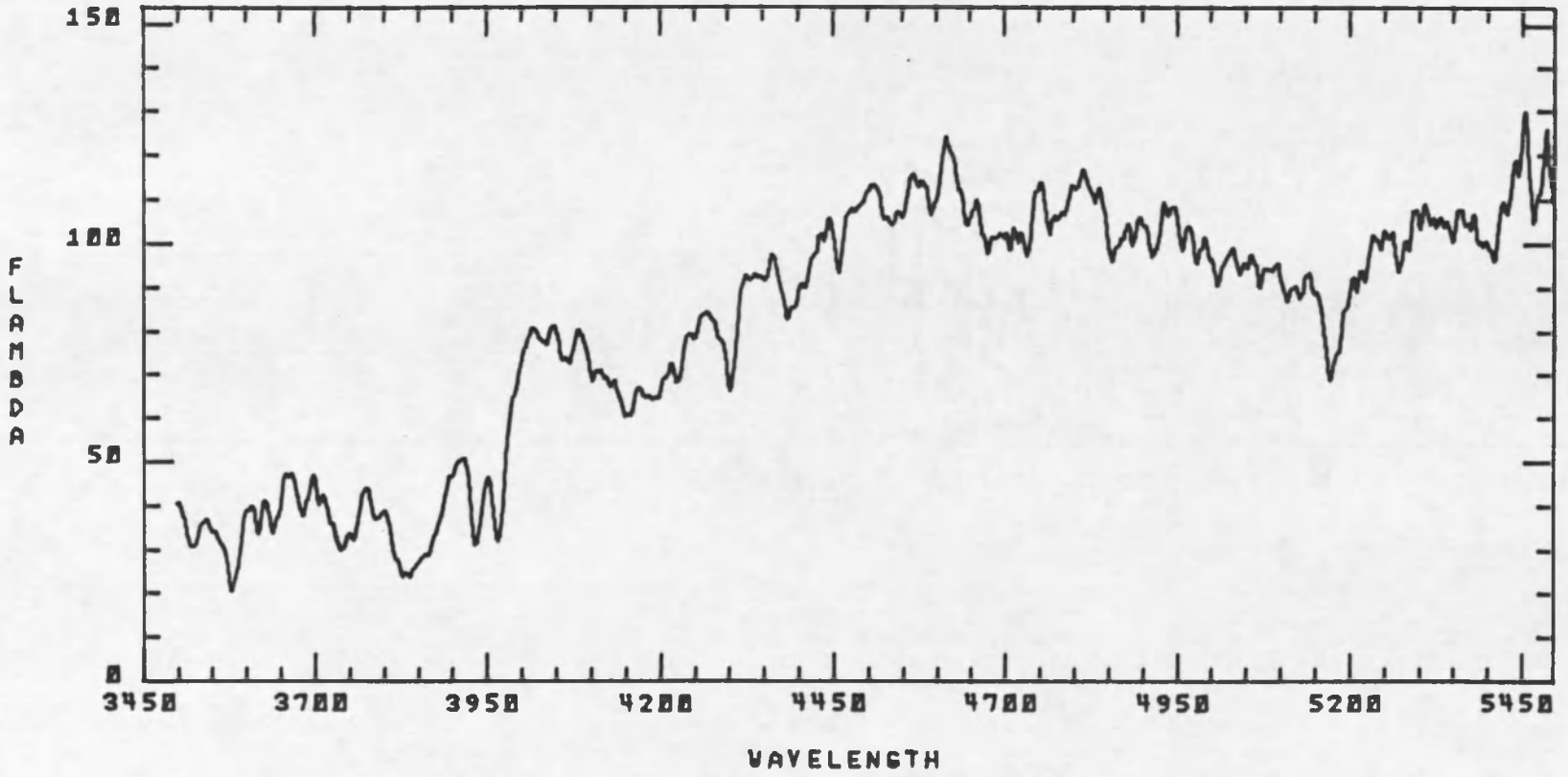

Figure 1. Reduced spectrum of the elliptical galaxy NGC 4889 -- Vertical scale is in arbitrary units.

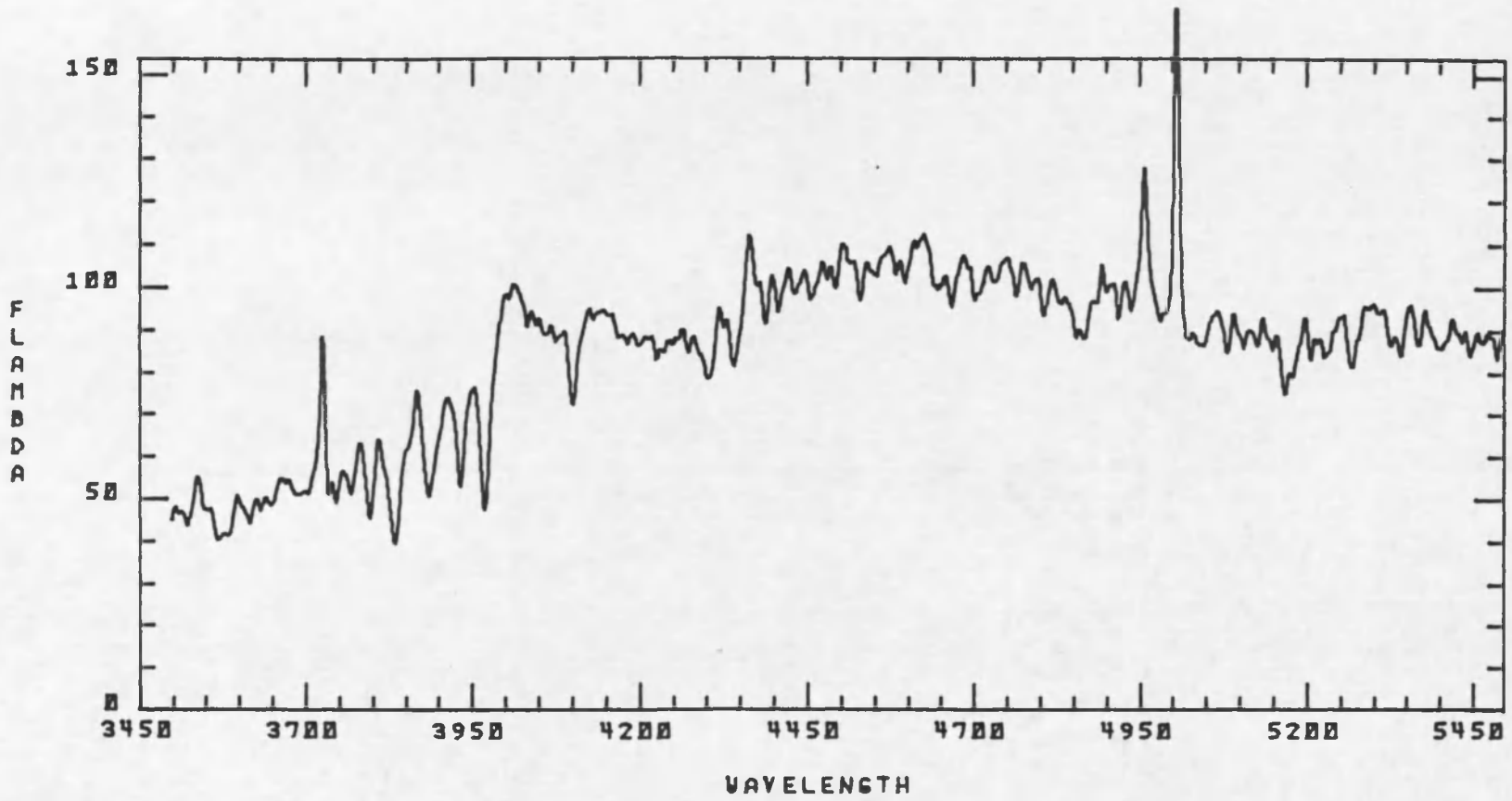

Figure 2. Reduced spectrum of the Sc galaxy NGC 5194 (M51) -- Vertical scale is in arbitrary units.

Table 3. Measured Line Indices and Dispersions

NGC	Hubble type	Mgb	Δ(Mgb)	CN39	Δ(CN39)
221	E2	.158		.443	
224	Sb	.295		.999	
488	Sb	.240		.688	
596	E0	.204		.697	
628	Sc	.145		.390	
1209	E6	.278		.729	
1407	E0	.244		.795	
2268	Sbc	.162		.365	
2300	E2	.266		.824	.064
2314	E3	.267	.033	.780	.177
2336	Sbc	.200		.660	
2344	Sc	.176	.001	.418	
2655	S0/a	.160		.411	
2681	Sa	.132	.012	.163	
2768	E6	.267		.722	.001
2775	Sab	.264	.009	.780	
2841	Sb	.322	.019	.906	
2855	S0/a	.188		.358	.169
2985	Sb	.156		.385	
3031	Sb	.240		.554	.067
3147	Sb	.194		.736	.053
3193	E2	.256		.814	
3277	Sab	.234		.543	
3368	Sab	.125		.387	
3377	E6	.274	.050	.730	.051
3379	E0	.315	.039	.875	.017
3642	Sbc	.124	.030	.222	
3898	Sab	.302	.010	.750	
4374	E1	.292		.801	
4378	Sa	.239		.573	
4387	E5	.222		.728	
4406	E2	.279		.926	
4464	E3	.212	.035	.732	.059
4478	E2	.218		.703	
4486B	E0	.206		.874	
4594	Sa	.339		.881	
4621	E5	.316		.963	
4649	E2	.365	.022	.880	.096
4725	Sb	.222		.516	
4736	Sab	.176	.040	.407	
4889	E4	.319		.844	
5194	Sc	.139	.002	.093	.110
6340	Sa	.269	.000	.728	
6482	E2	.324		.733	
7217	Sb	.308		.697	
7619	E3	.271		.862	

Two tests have been used to estimate the uncertainties in the measurements of these indices. First, 21 of the galaxies observed in this study have also been observed spectroscopically by Faber (1979). A comparison between her index Mg_2 and the Mgb index measured here shows a good correlation (Figure 3). A straight line fit to the points ($Mgb = 0.00 + 0.90\ Mg_2$) is also shown. The fit was determined assuming that all the uncertainty was in Mgb. The fit shows the result expected from the scattering problem described earlier. The line intersects the origin and has a slope less than unity. The average deviation of the Mgb measurements from the values predicted by Faber's Mg_2 indices and the derived relation is 0.02 or about 8% of the mean Mgb value.

A second check on the precision of the measurements is their reproducibility. Ninteeen of the galaxies were observed on two different nights. For these galaxies, the total ranges measured in the Mgb index, Δ(Mgb), and the CN39 index, Δ(CN39), are also listed in Table 3. Some of the galaxies have two reliable measurements for only one of the indices. The average values for half the dispersion between repeated measurements are 0.011 for the Mgb index, and .039 for the CN39 index. We adopt 0.020 and 0.050 as the accuracies of the Mgb and CN39 index measurements, respectively.

Figure 4 shows the location of the elliptical galaxies in the Mgb-CN39 diagram. A correlation is seen (significant at the 99.5% confidence level), and the straight line through the points has been fit by minimizing the sum of the squares of the residuals in <u>both</u> indices. The scatter around the line is roughly consistent with the uncertainties

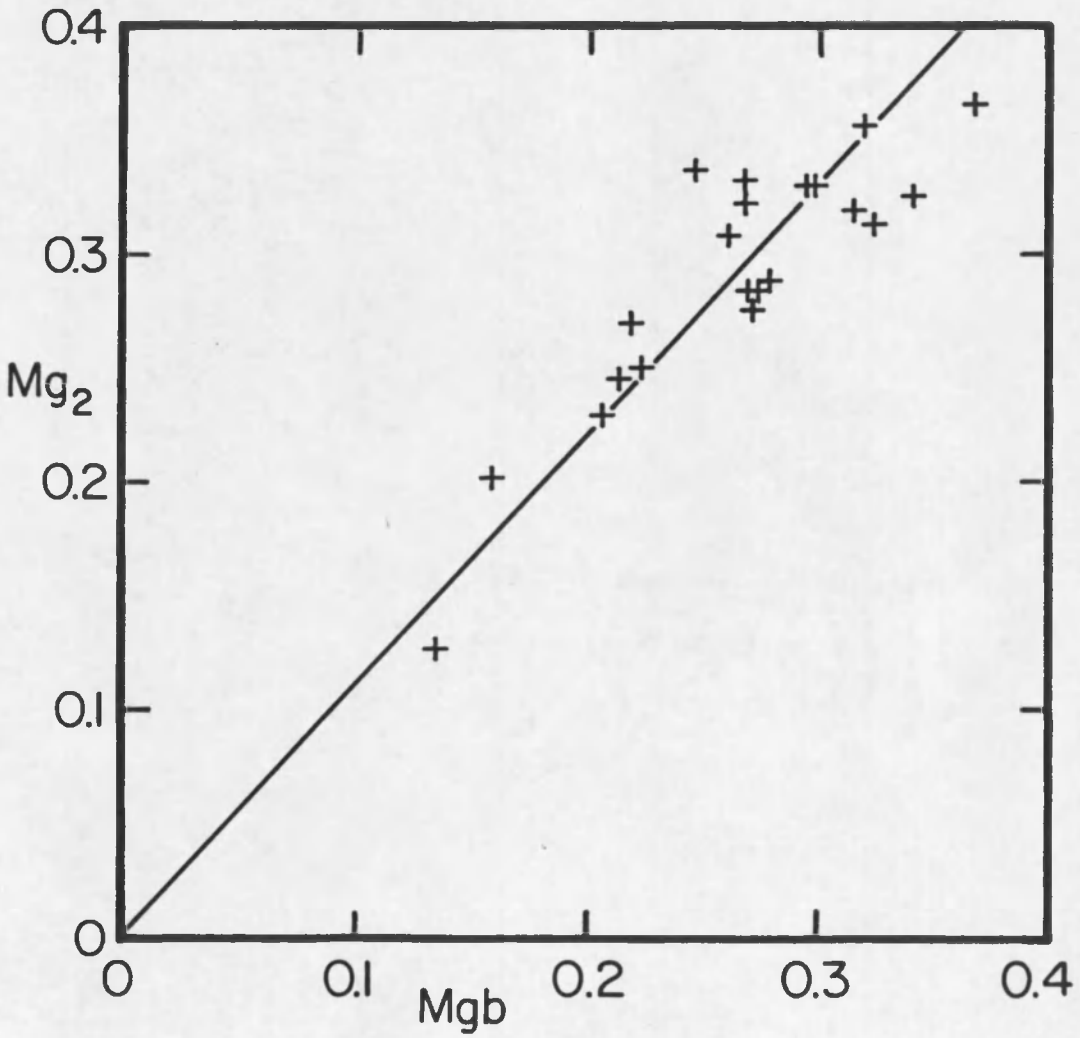

Figure 3. A comparison of the Mgb index values measured in this study with Mg_2 index values measured by Faber (1979) for 21 objects in common.

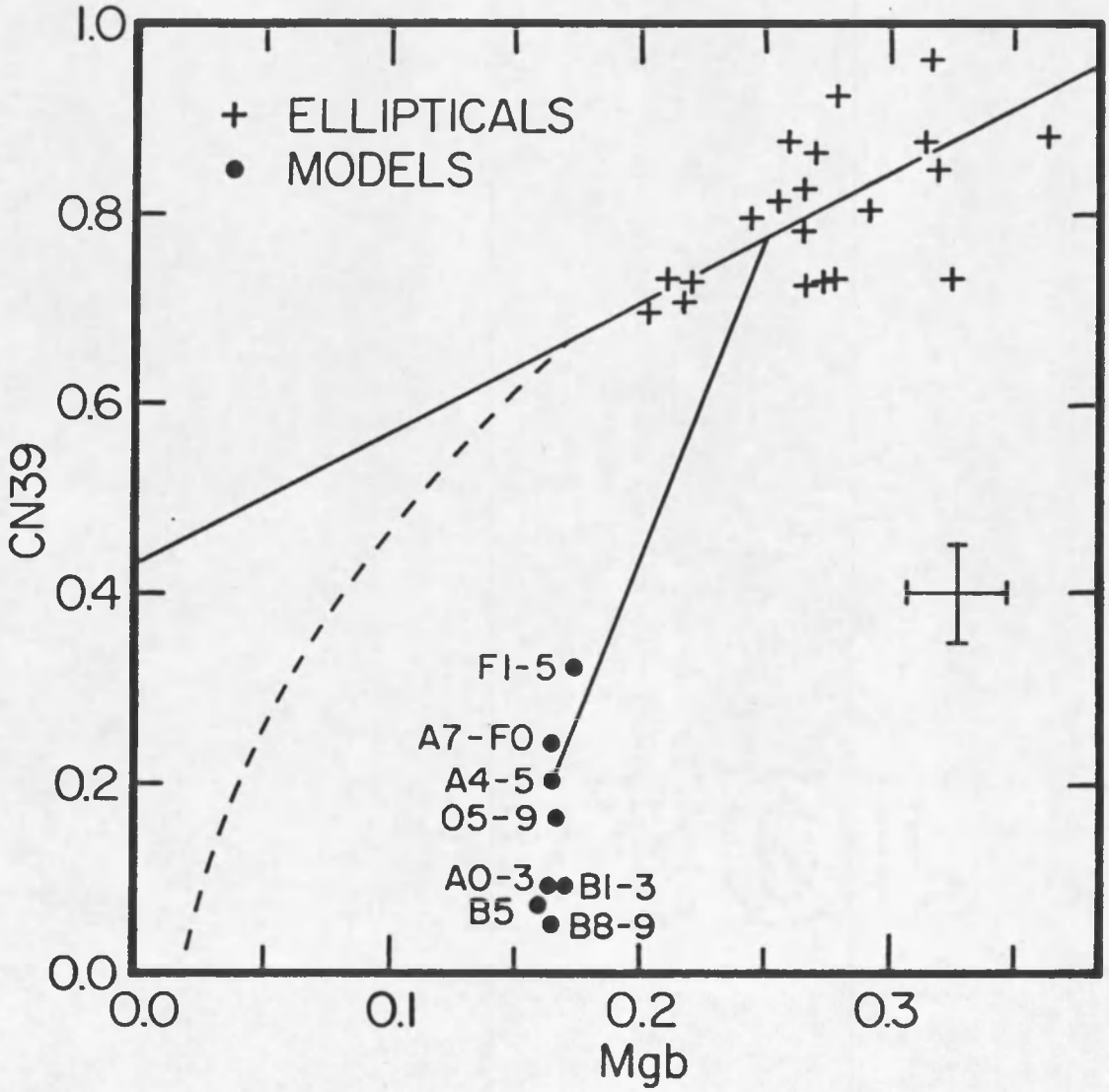

Figure 4. The Mgb-CN39 diagram for elliptical galaxies (crosses) -- The line through the points minimizes the sum of errors in both indices. The dashed line is a guess at the extrapolation to low metallicities. The models, indicated by dots, are explained in the text.

in the measurements. Since it is reasonable that variation in the Mgb strength in elliptical galaxies be interpreted as a metallicity effect, the regression line is taken to be a metallicity sequence, with abundances increasing upward and to the right in the diagram. It is not expected that this line can be extended indefinitely to the left (lower metallicity). Qualitatively, at very low metallicities, the Mgb absorption will go to zero and the CN39 index will become negative because the increased hydrogen absorption will lower the blue continuum band which is shortward of the Balmer limit. This can be deduced from the measurements for an A star which has Mgb = 0.0 and CN39 = -.3. A guess at a more realistic extrapolation of the metallicity line is shown as a dashed line in Figure 4. Observations of low metallicity ellipticals and globular clusters are necessary to confirm this expectation. The insensitivity of the CN39 index to metallicity is a result of the band being saturated at the typical metallicities ([Fe/H] > 0.) found in galactic nuclei. For this reason, decoupling of CNO and Fe variations has little or no effect on the relation between CN39 and Mgb. The possible existence of a band such as CN39 in this region of the spectrum and its use for separating metallicity and age effects was first discussed by Burstein (1979a).

Figure 5 shows the locations of the nuclei of the spirals and the dwarf elliptical M32 in the Mgb-CN39 diagram. The metallicity line from Figure 4 is also plotted. M32 is included in this diagram because it is suspected of having a young component in its population (O'Connell 1980). There is a striking difference between the distributions of spiral and elliptical points. While about one-third of the spiral

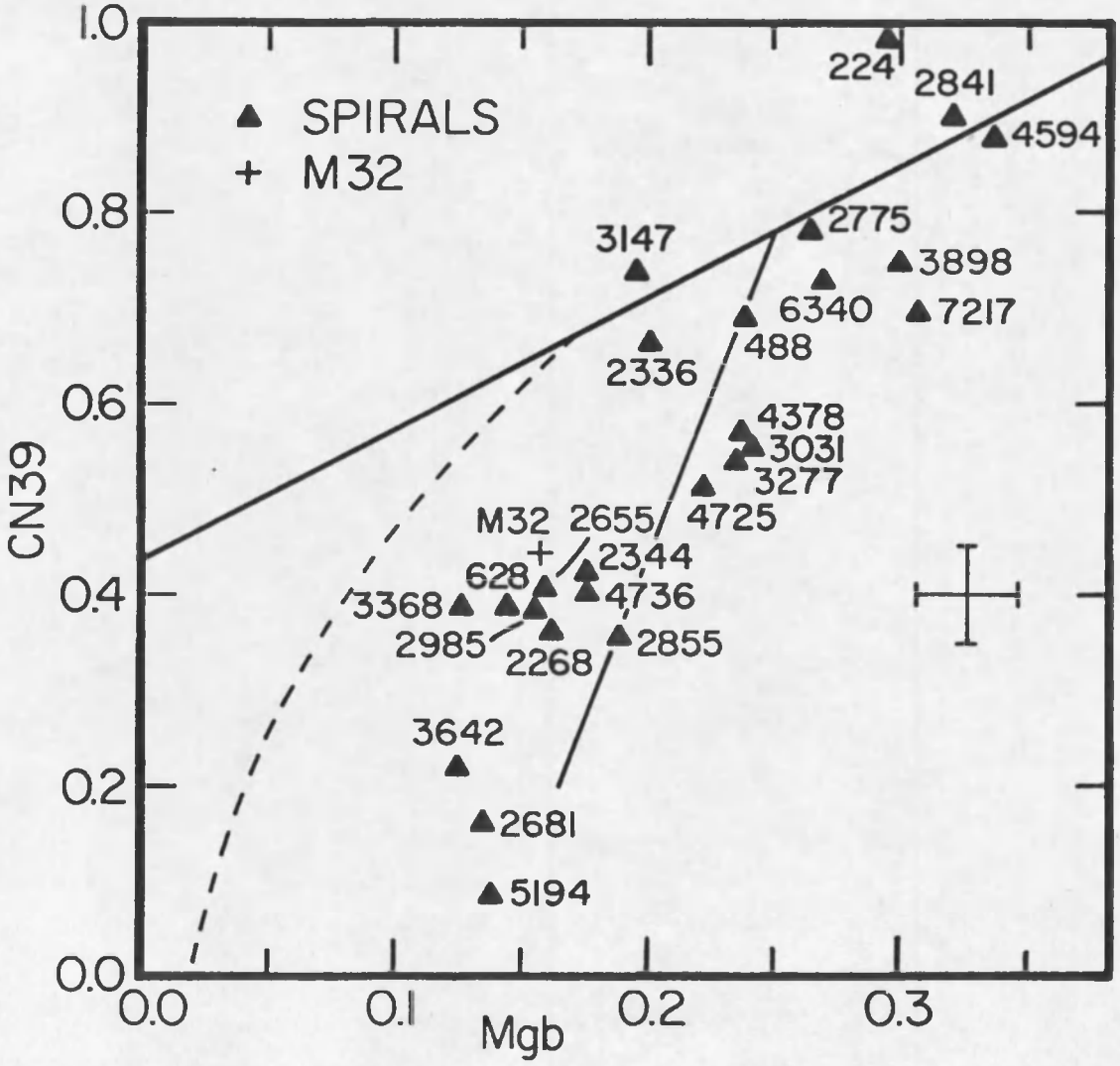

Figure 5. The Mgb-CN39 diagram for spiral galaxies (triangles) and M32 (cross) -- Each spiral is labelled with its NGC number. The lines are as in Figure 4.

nuclei fall around the elliptical metallicity relation, most fall significantly below the line. It is clear from a comparison of the two diagrams that the effect of a second parameter is present in the Mgb-CN39 diagram for spiral galaxies.

The most obvious way to move a point in the Mgb-CN39 diagram from the metallicity line downward is to add a blue continuum. A continuum bluer than a typical red old population will fill in the CN39 band more quickly than the Mgb band. Thus, a composite population consisting of an old elliptical-like component and a hot stellar component will fall in the region populated by the spiral nuclei. In order to investigate the properties of such composite populations, several models were generated. These models consist of two components. One-half of the light at $\lambda 4500$ comes from an elliptical galaxy on the metallicity line (Mgb = 0.25, CN39 = 0.775) and one-half comes from an early type star. Fluxes in bands suitable for the calculation of the indices for the stars were obtained from Turnrose (1976). The models were calculated for stars with spectral types of O5 to F5 and are plotted in Figure 4. Two inferences can be drawn from the location of the models in the diagram. First, the addition of a hot stellar continuum does move a point from the elliptical metallicity line down to the region occupied by spirals. Second, the range of angles defined by the different spectral types is small compared to the angle between the metallicity line and the line to any of the models. Therefore, in the first approximation, the extra parameter chosen to describe the hot population, the spectral type, can be ignored and an average hot star line can be drawn. This is shown in Figure 4. The direction of this

line indicates the effect of adding a hot population to an elliptical; its length represents the case in which equal amounts of light at λ4500 arise in each component. Conversely, an observation of a spiral nucleus can be moved up this hot star line until it reaches the metallicity line defined by the ellipticals. The point at which it crosses the metallicity line gives the Mgb index intrinsic to the old component of the population. The distance it must move to reach the line gives the fraction of light in the composite spectrum coming from the hot component. The adoption of an average hot star line produces an uncertainty of ∿0.01 in the Mgb index and about 10% in the fraction of light coming from hot stars.

There are two possible explanations for the picture presented by the diagram. The light which has been described as the hot star component could arise from a relatively recent burst of star formation or it could come from metal-poor blue horizontal branch stars. An argument against the latter interpretation can be made from the Mgb-CN39 diagram itself. In globular clusters blue horizontal branches occur only when [Fe/H] $\leq$ -1.3 in solar units. This corresponds to a Mgb index of essentially zero, using the conversion given by Terlevich et al. (1980). Since all the spirals observed have Mgb > 0.1 (and in fact have the Mg triplet easily visible in the spectrum), the presence of blue horizontal branch stars would require that in spiral nuclei such branches occur at very much higher metallicities than in globular clusters (or elliptical galaxies). For this reason it seems to us much more likely that the blue continuum represents a contribution from a relatively young group of stars, and the second component present in

the spiral nuclei will hereafter be referred to as the young component of the population. Note, however, that a consistent pattern could be constructed if a very large range of metallicities were present in the spiral nuclei. In that case, a substantial fraction of the light could come from a population with [Fe/H] very low and dominated by blue horizontal branch stars while a large fraction comes from a population with [Fe/H] > 0 and strong Mgb absorption.

The use of a single spectral type to represent a young population is not a great oversimplification. Inspection of color-magnitude diagrams of open clusters shows that the integrated light from a population with a main sequence turnoff up to early F is dominated by the the main sequence rather than the giant branch. Calculation of the relative contributions of different stellar types in main sequences with a Salpeter mass function indicates that the earliest spectral type, the turnoff, dominates the light at $\lambda 4500$. Thus, in a young population, the single spectral type used as a parameterization represents the turnoff of that population. Note that although the models constructed here consist of two discrete components, it is not necessary that the star formation occur in that manner. We are unable to distinguish a recent burst of star formation from star formation up to a recent epoch. Models with bursts of continuous star formation have previously been proposed to explain particularly blue galaxies such as Markarian objects or interacting systems (Huchra 1977, Larson and Tinsley 1978). In those more dramatic cases, the optical integrated light is dominated by the young component, while in the cases under consideration here, it is expected that the old component dominates.

The prescription, then, for using the Mgb-CN39 diagram is as follows. Each galaxy in the diagram will be moved upward and to the right, parallel to the average young star line until it reaches the elliptical metallicity relation. The distance it must be moved, divided by the length of the average young star line, times 50%, gives the fraction of light at λ4500 coming from the young population. This parameter will hereafter be called %Y. For comparison with other analyses, it is expected that this fraction corresponds to the fraction of light at λ4500 coming from stars with spectral types earlier than G0. This spectral type is approximately the turnoff type for a pure old population. Any galaxy for which the %Y measured is less than 10 will not be corrected. This limit is consistent with the measurement uncertainties and the scatter of points around the line in Figure 4. Similarly, all galaxies above the metallicity line will not be corrected but will have %Y = 0. The $(Mgb)_c$ index is the value of Mgb at which the correcting line drawn from each galaxy intersects the metallicity relation. For all galaxies requiring no correction, the observed Mgb index will be used. Although it is recognized that different mixtures of two populations in the Mgb-CN39 diagram would not be represented as a linear relation, detailed calculation shows that the errors due to this simplifying approximation are much smaller than the other inherent uncertainties. Table 4 lists all the spiral galaxies observed plus the dwarf elliptical M32 (NGC 221), their revised morphological types (T), and their %Y and $(Mgb)_c$ values.

It is desirable to demonstrate empirically that the proposed interpretation of the distribution of points in the Mgb-CN39 diagram is

Table 4. Metallicities and Young Star Fractions as Deduced from Mgb-CN39 Analysis

NGC	T	$(Mgb)_c$	%Y	<GO	Reference[a]
221	-6	.200	24	22,25	B,C
224	3	.295	0	0	B
488	3	.240	0		
628	5	.195	28	40	A
2268	4	.218	32		
2336	4	.200	0		
2344	5	.226	29		
2655	0	.209	28		
2681	0	.221	51		
2775	2	.264	0		
2841	3	.322	0		
2855	0	.249	36		
2985	2	.206	30		
3031	2	.277	22	21	B
3147	4	.194	0		
3277	2	.272	26		
3368	2	.170	26		
3642	4	.199	43		
3898	2	.302	0		
4378	1	.271	19		
4594	1	.339	0		
4725	2	.263	24		
4736	2	.228	30	37	B
5194	4	.238	58	48,43	B,A
6340	0	.269	0		
7217	2	.332	15		

[a]References: A = Turnrose (1976); B = Pritchet (1977); C = O'Connell (1980).

a correct or unique one. As a crude attempt to do this, we have calculated, from the detailed population synthesis models of Turnrose (1976), Pritchet (1977), and O'Connell (1980), a parameter analogous to our %Y. These are listed in a column labeled < GO in Table 4 for six galaxies in common. It can be seen that the agreement is quite good, especially considering the ± 10 uncertainty in %Y due to the use of the mean young star line.

Another piece of evidence supportive of our analysis is the general correlation between morphological appearance and fraction of light coming from the young population. Those objects which fall close to the elliptical line are those having obviously bulge dominated nuclei and no indications of nuclear activity. NGC 4594, NGC 2841, NGC 224, NGC 2775, and NGC 3898 are in this category. The two galaxies which fall farthest from the elliptical line, however, have nuclear spectra very different in appearance. NGC 5194 has a very small bulge and a disk of high surface brightness. Strong [O II] and [O III] emission suggest nuclear activity. NGC 2681, although classified an Sa, is not typical of that class. It has an extremely bright nucleus with a spectrum which looks like that of a late A star. In particular, the hydrogen lines are very strong and the metal lines very weak. Evidence that the metallicity is not extremely low can be obtained from the CO absorption at 2.3 μ. Although this band is primarily used as a luminosity indicator, in low metallicity integrated spectra it becomes very weak. Also, its wavelength makes it quite sensitive to the presence of hot blue stars regardless of their nature. From the measurements of Aaronson (1977) and Frogel et al. (1978), it is clear

that the CO band strength in NGC 2681 (CO = 0.164) is much more consistent with the high metallicity ellipticals than the low metallicity globular clusters (see Figure 3 in Frogel et al. 1978).

Discussion

Several interesting aspects of this spectral decomposition are apparent. First, it might be expected that there is a correlation between the morphological type and the fraction of light coming from the young population. This would be a quantification of the relation found by Morgan and Mayall (1957) between central concentration (bulge-to-disk ratio) and spectral type. Figure 6 shows the %Y parameter plotted against the revised morphological type (T) and the Yerkes type. It should be kept in mind that the Yerkes types are not spectroscopically derived but come from subjective estimates of the degree of central concentration. No obvious correlations are visible between the fraction of light arising in the young component of the population and either of the classification systems. This is a rather surprising result; there are large bulge-to-disk galaxies which have a significant young central concentration and small bulge-to-disk galaxies which do not. A closer examination of the relation between classification schemes and quantitative morphological parameters will be made in Chapter III.

Since we will ultimately wish to explore the metallicity-luminosity relation for spiral bulges, it is important to consider possible sources of systematic error which might affect that relation. Because the young star line and metallicity relation are not orthogonal in the Mgb-CN39 diagram, it is possible that an error in the slope of

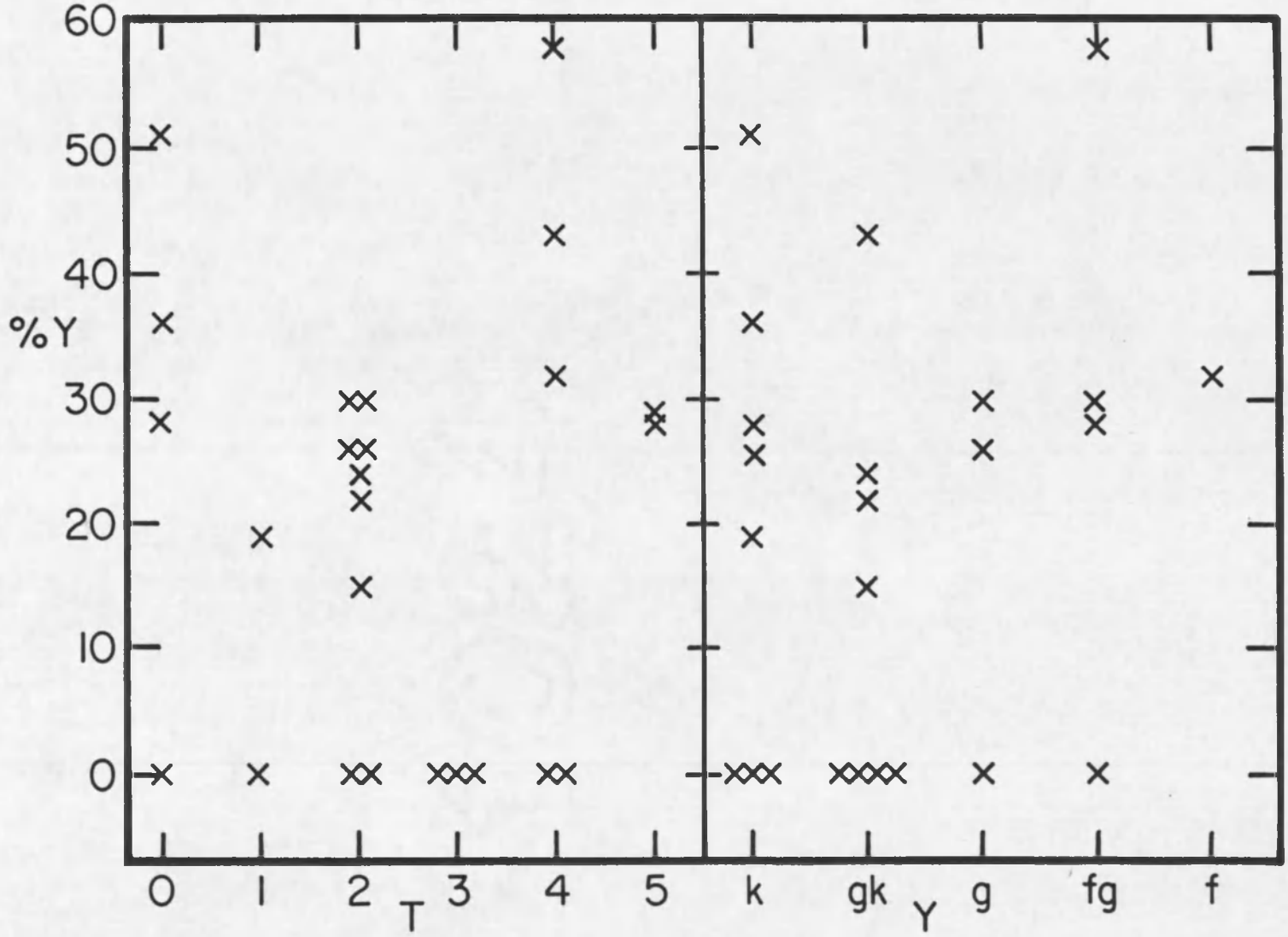

Figure 6. The relation between the %Y parameter and (left) revised morphological type and (right) Yerkes concentration class.

young star line will have such an effect. Suppose, for example, that the proper young star line to use for all galaxies was the one corresponding to the model with the F5 star. Then, we would have erred in using a line with a steeper slope than the correct one. The result of this would be an error in the $(Mgb)_c$ index which was proportional to the young star correction made. Those galaxies with the largest young star correction would have $(Mgb)_c$ indices which were the lowest with respect to their proper values. Such an error might produce an anomalous correlation between metallicity and any of the photometric measurements we intend to investigate.

It is simple to show that such an effect appears in the data. This can be seen by merely examining Figure 5, the Mgb-CN39 diagram for spiral galaxies. With the exceptions of NGC's 2336, 3147, and 2855, all the spiral galaxies below M32 are to the left of the young star line while above M32, they are all to the right. If $(Mgb)_c$ is plotted against Yerkes type (Figure 7), a correlation is seen at the 99% confidence level. This is either an indication that we have used too steep a young star line or evidence of a real relation between metallicity and the degree of central concentration of a galaxy. We can estimate the largest possible systematic error by considering the range of slopes derived from the young population models. This largest error is found to be 0.0004 %Y. If 0.0004 %Y is added to all the $(Mgb)_c$ values and the correlation coefficient is recalculated, it changes only from 0.52 to 0.50, indicating a 1% decrease in the confidence level of significance. Thus it appears that this correlation is real; we are seeing evidence that small bulge-to-disk ratio galaxies tend to have lower central

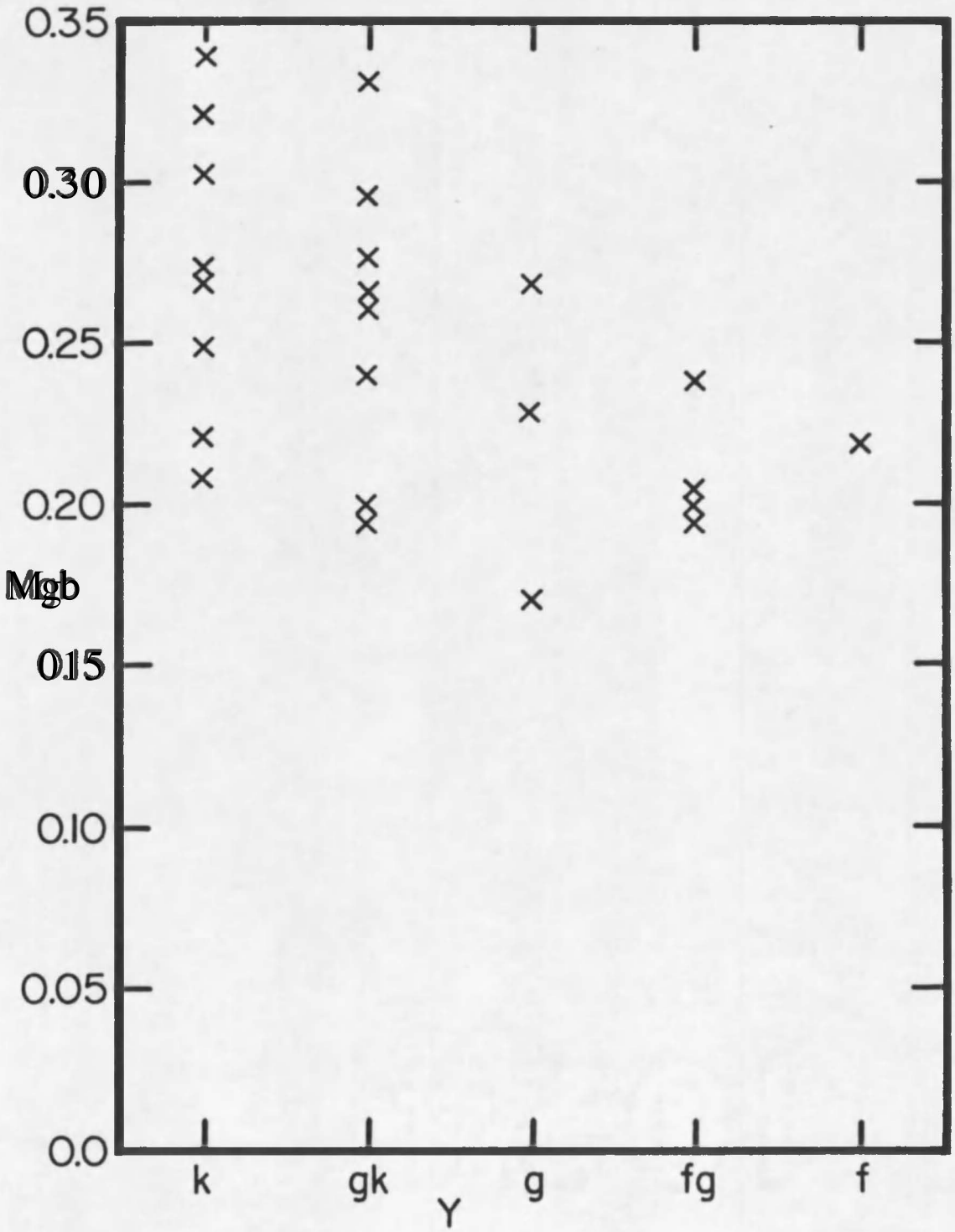

Figure 7. The distribution of the $(Mgb)_c$ parameter with Yerkes concentration class.

metallicities in the old part of their stellar populations. Note that even a modest error in the slope of the metallicity line in the Mgb-CN39 diagram will not produce this same effect. It will merely stretch out or compress the Mgb scale, independent of the %Y parameter. This result will be explored further in Chapter IV.

In summary, we have obtained digital spectra of 20 elliptical galaxies and 25 spiral galaxies, and have defined and constructed the Mgb-CN39 diagram. Using this diagram:

1. We have demonstrated that a variation in some quantity other than metallicity is present in the central regions of spiral galaxies.
2. We have shown that this quantity is most likely the presence of a young component in the stellar population.
3. We have quantified the variations in such a way as to recover the Mgb index of the old part of the population and the fraction of light arising in the young part.
4. We have explored the relation first discussed by Morgan and Mayall (1957), a correlation between spectral type and central concentration. This correlation is surprisingly poor, i.e., there are large bulge-to-disk galaxies with a strong young population and small bulge-to-disk galaxies with no young stars.
5. We have found evidence for a correlation between corrected central metallicity and Yerkes type. A test was performed which demonstrates that this is not due to a systematic error introduced by the analysis procedure.

CHAPTER III

THE DISTRIBUTION OF LUMINOSITY IN SPIRAL GALAXIES

The study of surface brightness distributions in spiral galaxies has been limited by the availability of observational data. While in the past several years observational studies of elliptical galaxies have fueled controversies over oblateness, low surface brightness envelopes, and dynamics, the folklore concerning spirals has remained relatively unchanged for a decade. This folklore is based on a rather heterogeneous collection of studies of individual or few systems, mostly limited to fairly high surface brightnesses compared to what is possible today. Both because ho homogeneous set of observations exists and because current technology permits routine measurements at fainter light levels than were achieved in previous work, it was decided to obtain and investigate surface photometry for a representative sample of spiral galaxies. We begin by reviewing the conventional wisdom,

It is generally believed that there are two major morphological constituents of spiral galaxies. These are a spheroidal component, usually called the bulge, and a disk component in which the spiral structure is embedded. The ratio of luminosity (or mass) between the two components is thought to be one of the primary variations along the Hubble sequence. The bulge is thought to be similar to an elliptical galaxy, and therefore, the same functions which are fit to elliptical galaxy luminosity distributions, the Hubble law (Hubble 1930), the de

Vaucouleurs law (de Vaucouleurs 1953), and the King model (King 1962) are used to describe bulges. The various advantages and disadvantages of each of these fitting functions has been discussed by Kormendy (1977b).

The disk component in spiral galaxies is believe to be well described in the radial coordinate by an exponential (de Vaucouleurs 1959, Freeman 1970). Freeman (1970) made a study of published surface brightness profiles of 36 spiral and SO galaxies and found that almost all showed exponential disks. His analysis of these data produced two interesting conclusions. The scale lengths determined for the exponential section of the profiles were smaller in galaxies with late morphological types. Completely unexpected, moreover, was the discovery that the central surface brightness of the disks, measured by extrapolating the exponential fit to the center of the galaxy, was almost always the same, having a value of 21.65 B-magnitudes per square arcsecond ($B\mu$).

Several other authors have investigated more sophisticated methods for decomposing the profile into bulge and disk contributions. A good review of these techniques and their shortcomings, as applied to SO galaxies, is found in Burstein (1979b). Briefly, the problem is that each of the two components dominates the profile at radii which vary from object to object. Thus, in galaxies in which the transition region is small, Freeman's technique of extending an exponential, fit to the outer part of the disk, to the center is sufficient. In galaxies with bulge-to-disk ratios (B/D) of about unity, however, this method is unsatisfactory, and Kormendy (1977c) devised an iterative procedure which is better. Kormendy (1977c) showed that Freeman's

incorrect fitting procedure may have anomalously produced the observed near constancy of disk central surface brightness. Iterative and other methods of decomposition will be discussed further in a later section.

Kormendy (1977a, 1977b, 1977c) and Burstein (1979b, 1979c, 1979d) have studied the luminosity profiles of SO galaxies, which are thought to have some properties similar to spirals. Kormendy's findings include evidence that exponential disks sometimes have inner or outer cut-offs. Burstein's aim was to measure B/D's for a sample of SO's to compare with those for spirals, this comparison testing the hypothesis that SO's are spirals in which the gas has been stripped out. His result was that almost all B/D's were within a factor 2 of unity, a value much larger than the B/D's for the three spirals which have been studied in detail. However, these 3 spirals hardly constitute a representative sample, and so a further goal of this study will be to derive B/D's for as many spirals as possible for comparison with Burstein's SO numbers.

In the following sections we will discuss the surface photometry observations of a sample of 26 spiral galaxies, most of which are close to face-on. We will describe reduction procedures and will present major and minor axis profiles and "elliptically averaged" major axis profiles. We will discuss the implications of the large scale shapes of these profiles and will attempt to decompose them into bulge and disk contributions.

Observations and Preliminary Reductions

Direct plates of 28 galaxies were obtained during three observing runs between 6 October 1978 and 22 September 1979 with the Harrison #1 camera on the Kitt Peak National Observatory #1-36 inch telescope (f/7.5). IIa-O plates and a GG13 filter were used, giving a bandpass similar to the Johnson B band. The plates were hypersensitized by baking in forming gas (2% H_2, 98% N_2) at 65°C for one to two hours depending on the emulsion batch. For each galaxy at least one long plate (usually 120 minutes) and one short plate (15 to 20 minutes) were obtained. Figure 8 shows a print of each of the 26 spirals from a long plate. Scales and directions are indicated. Details of the observations are listed in Table 5. Simultaneous with each exposure, a plate was exposed on a tube-type spot sensitometer belonging to Steward Observatory. The sensitometer was kept on the observing floor in order to reproduce the conditions (temperature, humidity) in which the plates were exposed. A GG13 filter was used in the sensitometer also. All plates were developed five minutes in D19, generally two plates at a time.

In addition to the sample of spirals observed, several other plates were obtained for various sorts of checks and calibrations. A plate of the open cluster NGC 2632 (Praesepe) was obtained to accurately measure the plate scale (28.77 arcseconds per mm). Plates of the elliptical galaxies NGC 3379 and NGC 4486 were obtained in order to estimate the quality of the surface photometry by comparing measurements of these galaxies with published values. One field with no galaxy in it was observed in order to measure any vignetting or other

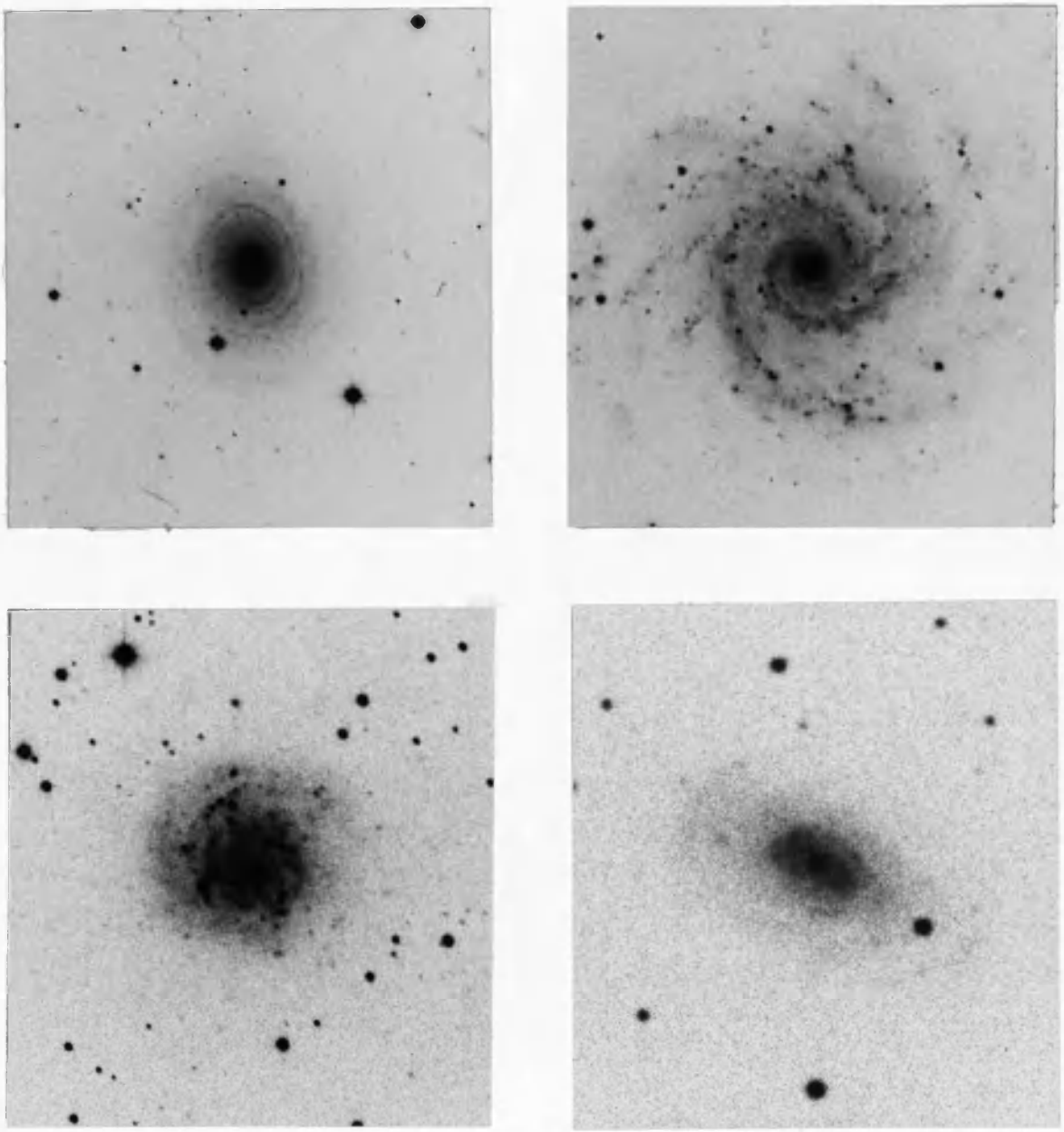

Figure 8. Prints from the long plates of the program spiral galaxies -- North is up and east is to the left. The scale is such that three inches corresponds to 512 pixels for all galaxies. Upper left = NGC 488, upper right = NGC 628, lower left = NGC 1059, lower right = NGC 2268.

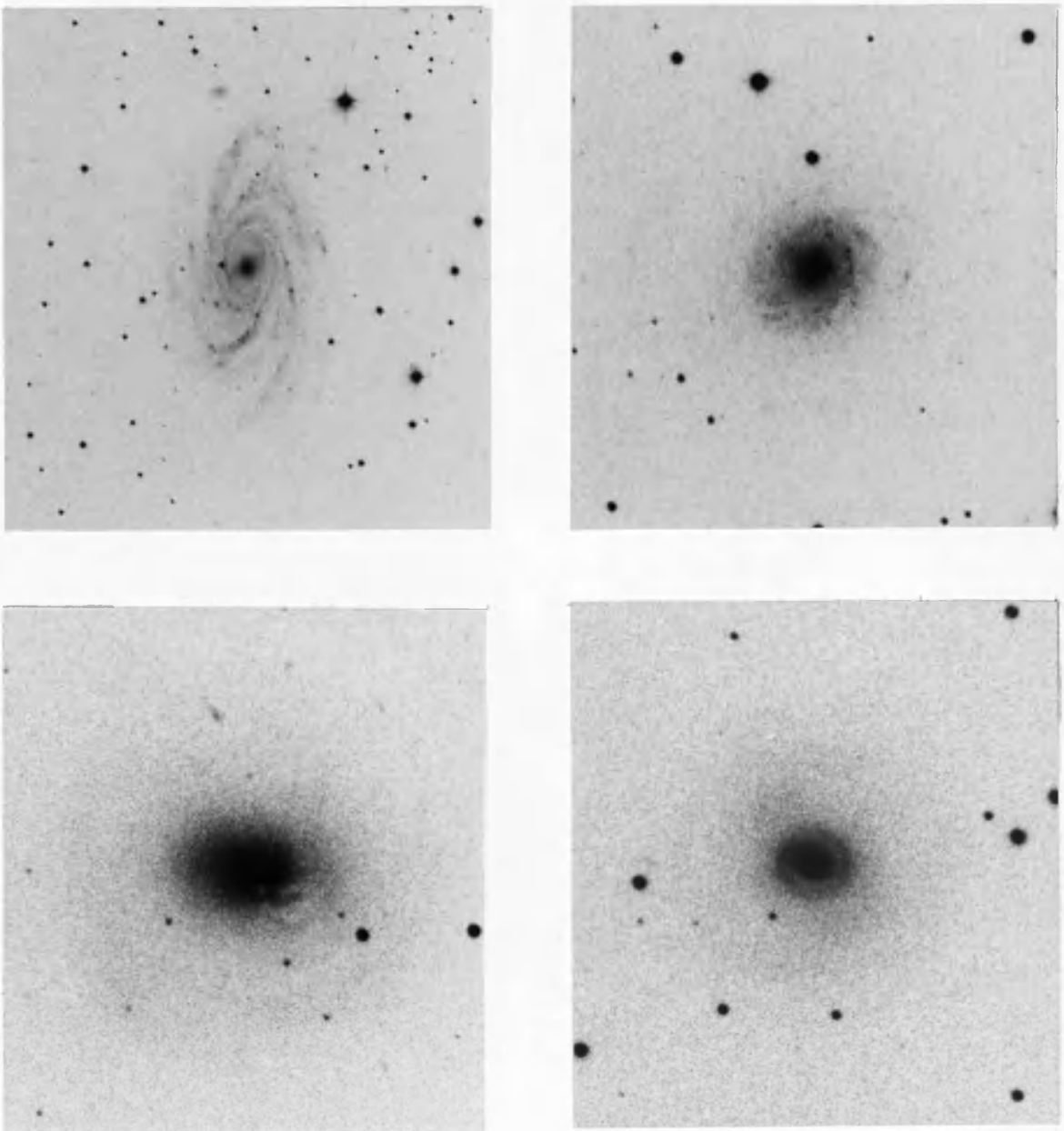

Figure 8.--Continued Prints from the long plates of the program spiral galaxies -- North is up and east is to the left. The scale is such that three inches corresponds to 512 pixels for all galaxies. Upper left = NGC 2336, upper right = NGC 2344, lower left = NGC 2655, lower right = NGC 2681.

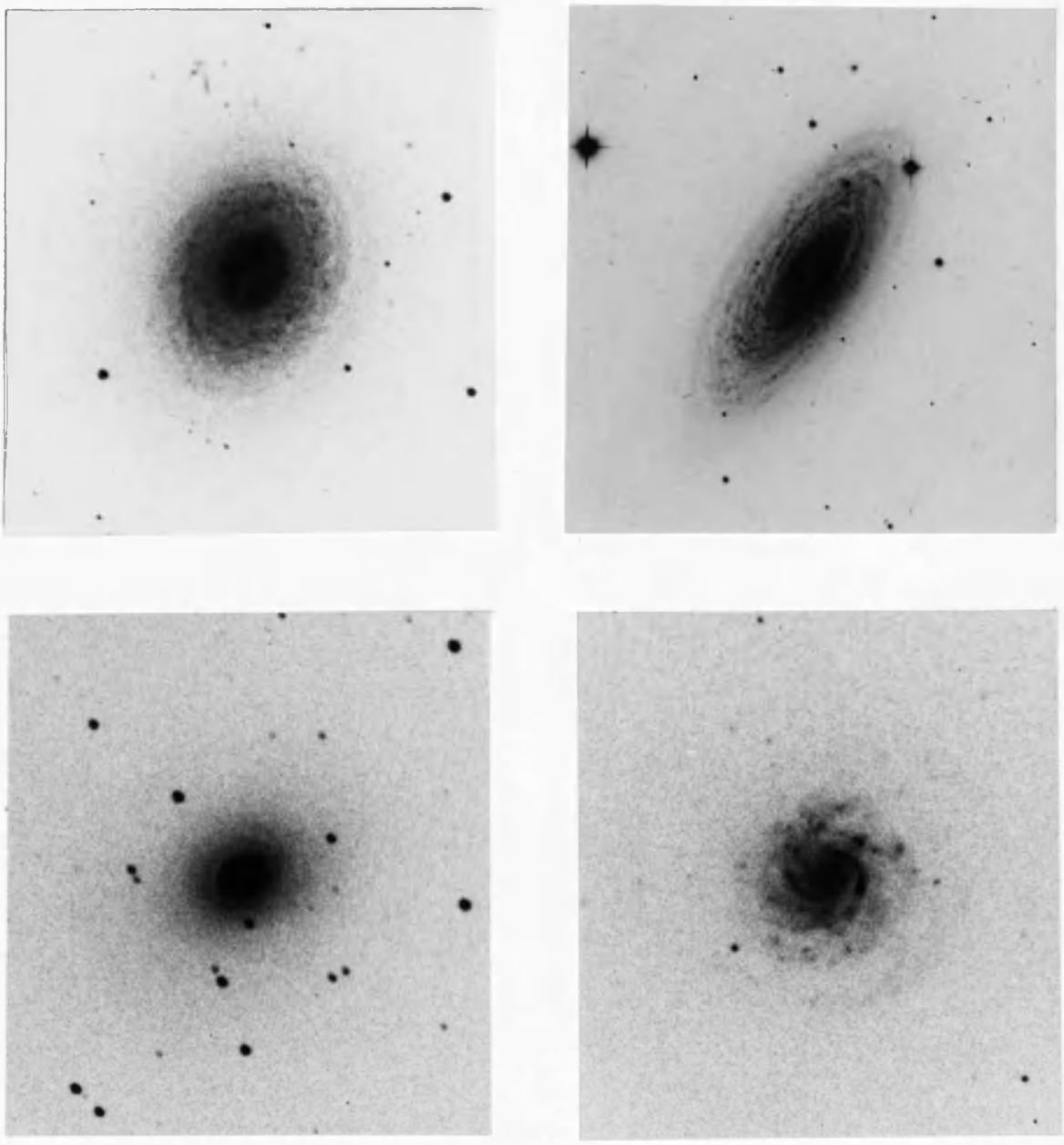

Figure 8.--Continued Prints from the long plates of the program spiral galaxies -- North is up and east is to the left. The scale is such that three inches corresponds to 512 pixels for all galaxies. Upper left = NGC 2775, upper right = NGC 2841, lower left = NGC 2855, lower right = NGC 2967.

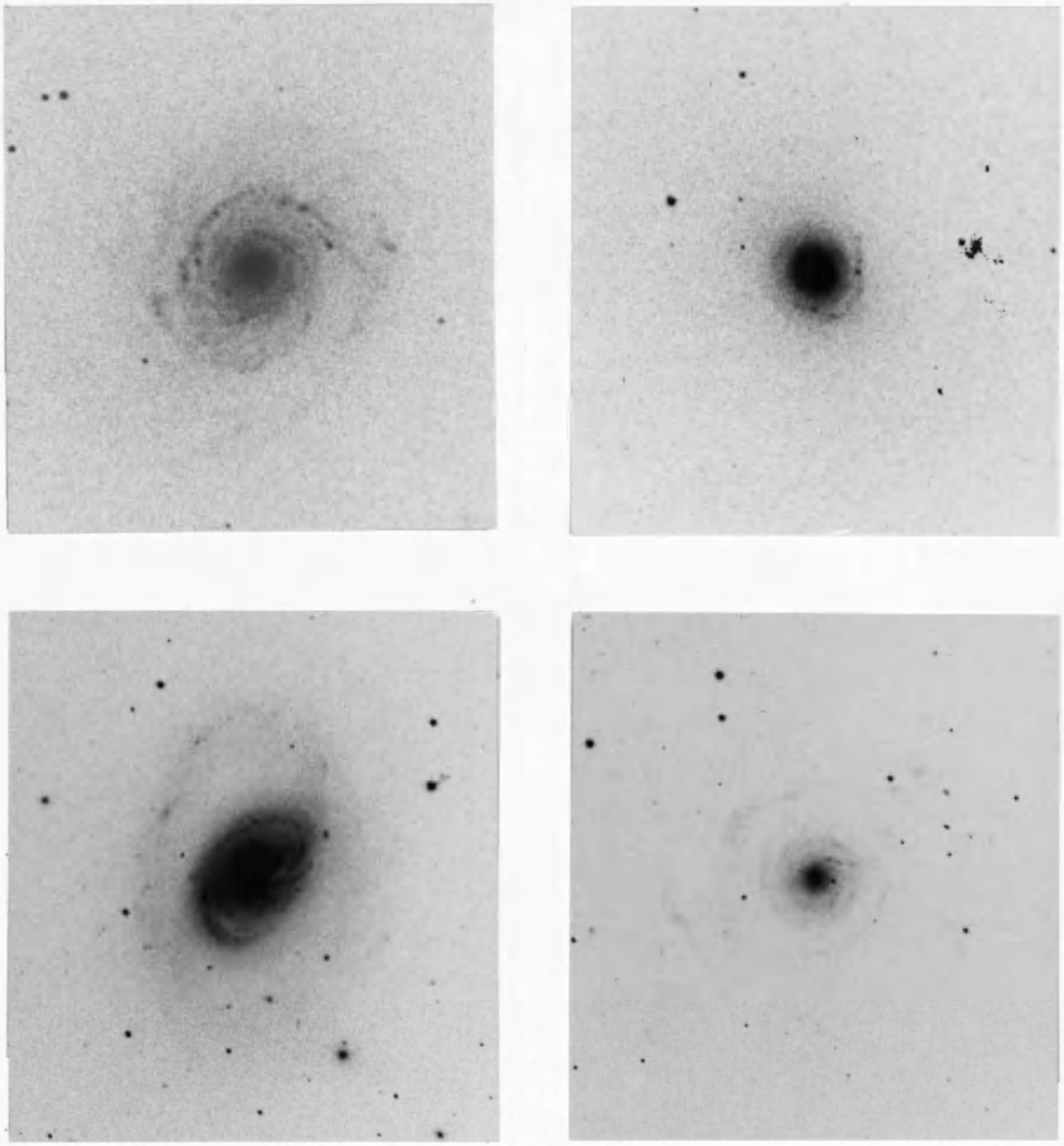

Figure 8.--Continued Prints from the long plates of the program spiral galaxies -- North is up and east is to the left. The scale is such that three inches corresponds to 512 pixels for all galaxies. Upper left = NGC 3147, upper right = NGC 3277, lower left = NGC 3368, lower right = NGC 3642.

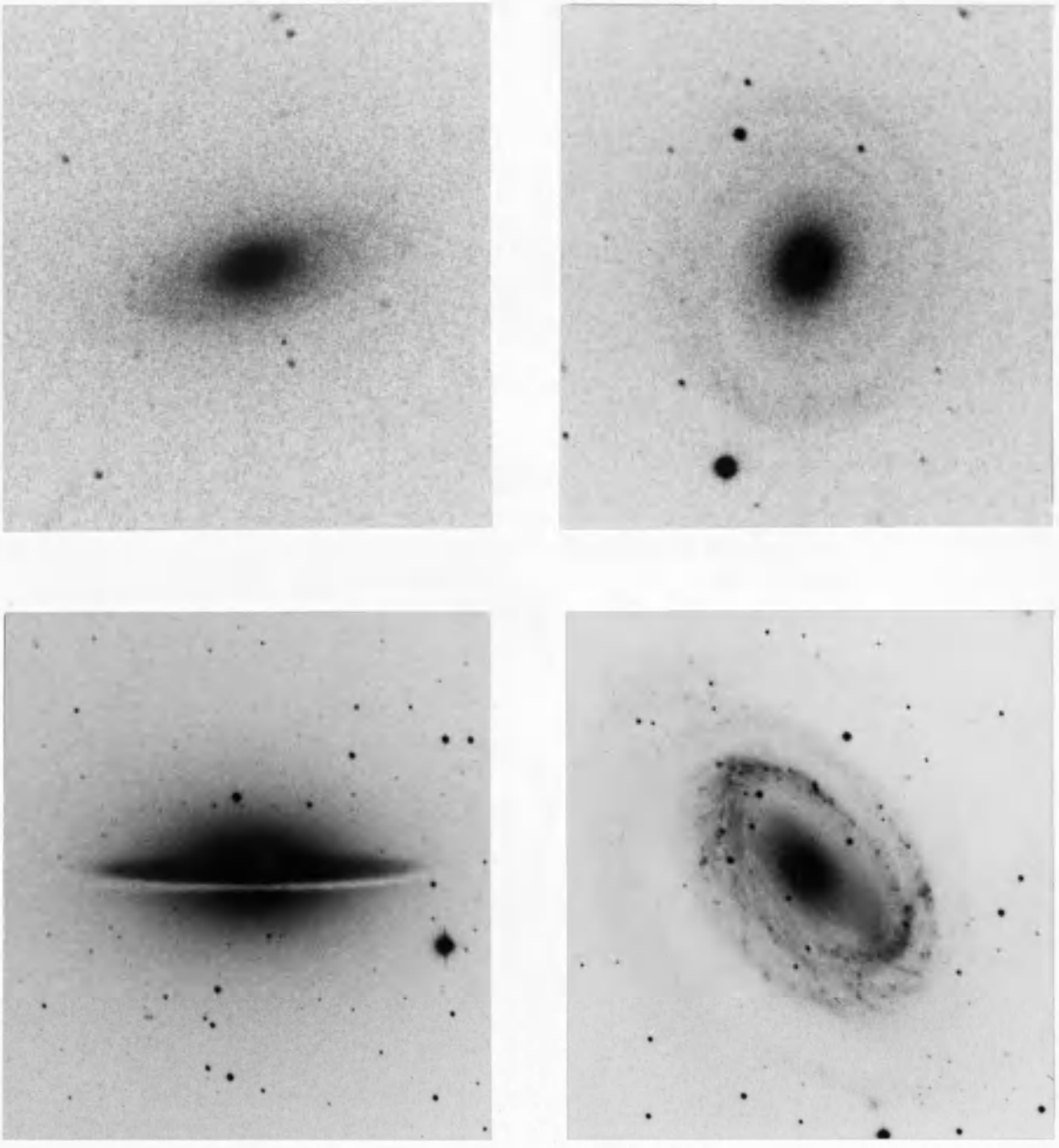

Figure 8.--Continued Prints from the long plates of the program spiral galaxies -- North is up and east is to the left. The scale is such that three inches corresponds to 512 pixels for all galaxies. Upper left = NGC 3898, upper right = NGC 4378, lower left = NGC 4594, lower right = NGC 4725.

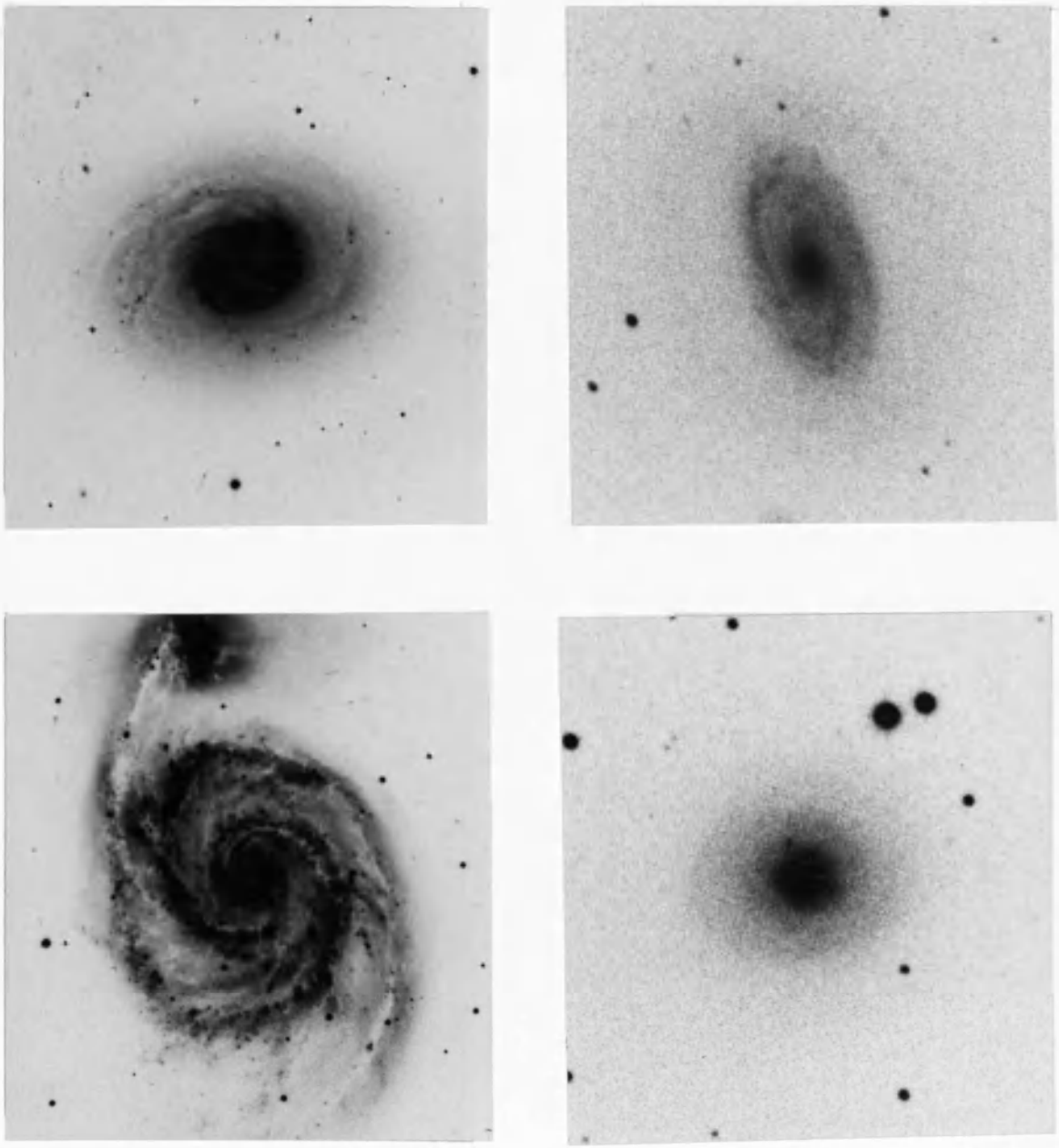

Figure 8.--Continued Prints from the long plates of the program spiral galaxies -- North is up and east is to the left. The scale is such that three inches corresponds to 512 pixels for all galaxies. Upper left = NGC 4736, upper right = NGC 4941, lower left = NGC 5194, lower right = NGC 6340.

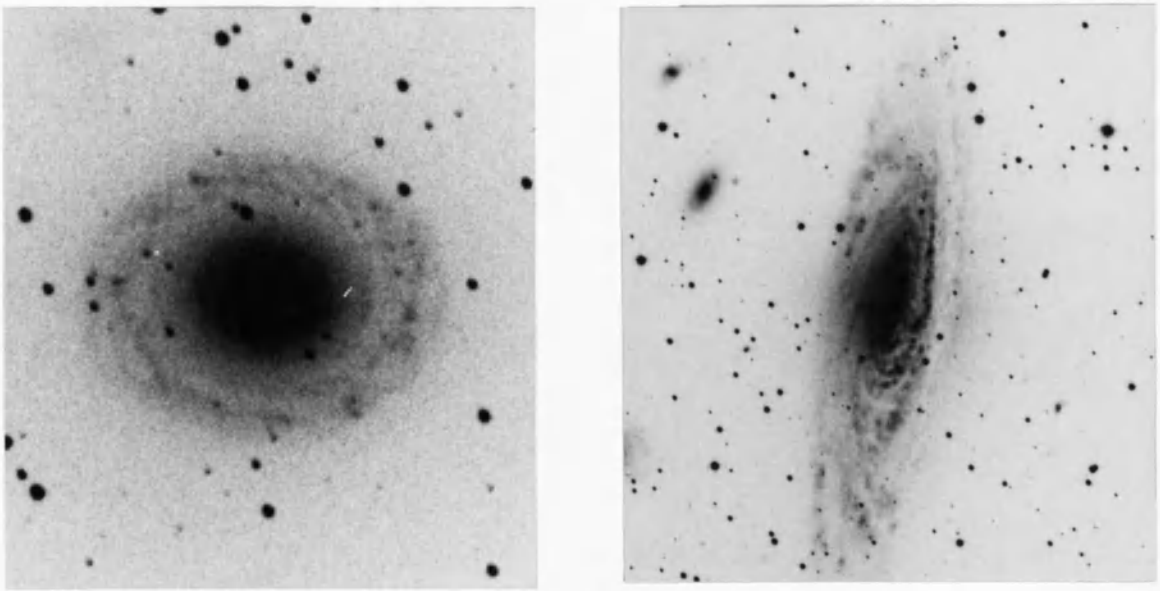

Figure 8.--Continued Prints from the long plates of the program spiral galaxies -- North is up and east is to the left. The scale is such that three inches corresponds to 512 pixels for all galaxies. Left = NGC 7217, right = NGC 7331.

Table 5. Plate Material

NGC	Date	Batch	Exposure (min.)	Plate no.
488	12/21/78	1G8	20	4936
	12/21/78	1G8	120	4935
	9/21/79	1E9	20	5390
	9/21/79	1E9	120	5389
628	12/26/78	1G8	20	4963
	12/26/78	1G8	80	4964
	9/22/79	1E9	19	5394
	9/22/79	1E9	120	5393
1058	12/24/78	1G8	90	4958
	9/23/79	1E9	15	5402
	9/23/79	1E9	120	5401
2268	12/21/78	1G8	20	4938
	12/21/78	1G8	120	4937
2336	12/22/78	1G8	20	4947
	12/22/78	1G8	120	4946
2344	12/23/78	1G8	20	4953
	12/23/78	1G8	120	4952
2655	12/23/78	1G8	20	4956
	12/23/78	1G8	90	4955
2681	12/23/78	1G8	20	4954
	12/21/78	1G8	90	4939
2775	12/26/78	1G8	120	4966
	4/ 1/79	1K8	15	5085
2841	12/26/78	1G8	120	4965
	4/ 1/79	1G8	15	5086
2855	3/31/79	1K8	15	5078
	3/31/79	1K8	120	5079
2967	12/24/78	1G8	120	4959
	4/ 2/79	1K8	15	5091
3147	4/ 4/79	1K8	15	5107
	4/ 4/79	1K8	100	5108
3277	12/24/78	1G8	90	4960
	4/ 4/79	1K8	15	5109
3368	4/ 2/79	1K8	15	5093
	4/ 2/79	1K8	120	5092
3379	3/31/79	1K8	15	5081
	3/31/79	1K8	120	5080
3642	12/23/78	1G8	90	4957
	4/ 4/79	1K8	15	5110
3898	4/ 3/79	1K8	15	5101
	4/ 3/79	1K8	100	5100
4378	4/ 3/79	1K8	15	5105
	4/ 3/79	1K8	120	5104
4486	4/ 3/79	1K8	15	5103
	4/ 3/79	1K8	100	5102

Table 5.--Continued

NGC	Date	Batch	Exposure (min.)	Plate no.
4594	4/ 2/79	1K8	114	5094
	4/ 4/79	1K8	15	5111
4725	4/ 1/79	1G8	100	5089
	4/ 2/79	1G8	15	5097
	4/ 4/79	1K8	15	5113
	4/ 4/79	1K8	120	5114
4736	3/31/79	1K8	100	5082
	4/ 2/79	1G8	15	5098
4941	4/ 2/79	1K8	15	5095
	4/ 2/79	1K8	120	5096
5194	3/31/79	1K8	110	5083
	4/ 2/79	1G8	15	5099
6340	4/ 1/79	1G8	110	5090
7217	9/23/79	1E9	15	5398
	9/21/79	1E9	120	5386
7331	9/21/79	1E9	20	5388
	9/21/79	1E9	120	5387
Praesepe	4/ 1/79	1K8	10	5084
Blank Field (1615+41)	4/ 4/79	1K8	100	5115

variations in exposure due to the telescope. The tests made with these plates will be described later.

In order to calibrate the plates some aperture photometry was obtained with the Kitt Peak National Observatory #1-36 inch telescope in an observing run in April 1979. A second run in September produced no further measurements because of bad weather. The choice had been made to observe in the B bandpass because the majority of photometry in the literature is in this band or can be converted to it in a rather straightforward way. Therefore, the small amount of calibrating photometry was no drawback. The photometric measurements were made with a 1P21 photomultiplier tube through apertures of two sizes. In all cases the galaxy was centered in the aperture visually before each observation. The aperture sizes and beam profiles were measured by scanning a bright star slowly across the field. The measurements, made in B and V, were reduced in the usual manner, using 33 standard star observations to correct for extinction and to transform to the standard BV system. The reduced values are listed in Table 6.

The preliminary reduction of the surface photometry consists of the steps required to derive a set of luminosity profiles from the plate material for each galaxy. This begins with the digitization of the plates. The plates were scanned on the Kitt Peak National Observatory PDS microdensitometer. A 40 micron square aperture, corresponding to 1.15 arcseconds on an edge, was used. Since the reductions were to be done using a Grinnell Video Display which stores a 512 by 512 picture, it was decided to limit all scans to this number of steps. For this reason, each galaxy plate was scanned twice, once with a step-size large

Table 6. Photoelectric Aperture Photometry

NGC	Aperture (arcsecs)	V	B-V
2655	36.5	11.30	0.94
2681	10.0	12.10	0.85
	36.5	11.37	0.81
2775	36.5	11.49	0.94
2841	10.0	12.20	1.05
	36.5	11.00	0.98
3147	10.0	12.99	1.05
	36.5	11.89	0.94
3277	36.5	12.42	0.82
3368	36.5	10.95	1.01
3379	10.0	11.90	1.04
	36.5	10.64	0.98
3642	10.0	14.04	0.82
	36.5	12.71	0.78
3898	10.0	12.60	0.99
	36.5	11.71	0.96
4378	10.0	13.49	1.02
	36.5	12.35	0.97
4486	36.5	10.70	0.99
4594	36.5	10.12	1.04
4725	10.0	12.44	1.01
	36.5	11.38	0.98
4736	10.0	10.68	0.90
	36.5	9.41	0.87
4941	36.5	13.05	0.97
5194	10.0	12.55	0.89
	36.5	10.92	0.78
6340	10.0	13.47	1.01
	36.5	12.32	0.95

enough to ensure an accurate determination of the sky intensity and once with a step-size small enough to ensure adequate resolution within the galaxy. The large step-size was chosen such that the picture extended further from the galaxy than twice the radius of the 25 Bμ isophote as listed in de Vaucouleurs, de Vaucouleurs, and Corwin (1976). The smaller step-size was generally one-half of the larger step-size, and the most commonly used values were 20 and 40 microns or 40 and 80 microns. All pictures were centered on the nucleus of the galaxy. The spot plates were scanned with 70 micron steps in one direction and 175 micron steps in the other in order to fit the 3 by 7 spot pattern into a 512 by 512 picture.

All of the subsequent reductions, including the conversion from densities to intensities, the determination and subtraction of the sky, the absolute calibration, and the measurement of a series of radial profiles, were done with a Nova 800 minicomputer and a Grinnell Video Display terminal. Programs for carrying out these operations were written specifically for this application in the Forth language. Pictures were stored on magnetic tape during several stages of the reduction.

Each spot plate picture was first analyzed to determine the densities of the spots. The local fog around each spot was determined from the mean of 240 pixels. Then the mean and standard deviation of the density were computed from 640 pixels within each spot. The local fog for each spot was subtracted from each mean density yielding a list of 21 density values for each spot plate. Densities of the spots generally ranged from about 0.05 to 3.50. The relative intensities of

the spots were determined by means of a photoelectric calibration unit which attaches to the spot sensitometer. Repeated measurements indicated that the values determined with this device were accurate to better than 1%. The set of intensities and densities were then fit to the function:

$$\text{Log } I = P_0 + P_1 D + P_2 D^2 + P_3 D^3 + P_4 D^4 + P_5 \log (1-10^{-D}).$$

The parameters, P_0 through P_5, defined by this function, were solved for in a least squares manner. A plot of typical spot measurements and the fit to them is shown in Figure 9. A look-up table was then calculated such that each of the 2048 density values written by the PDS was given a corresponding intensity. These numbers were scaled such that the densest pixel in the center of the galaxy had an intensity of 32000, close to the maximum allowed single precision integer in the 16-bit minicomputer. This usually produced an intensity value for the sky of about 1000. Then each picture was transformed by means of this table into an intensity picture, the background fog being subtracted first. No rescaling was done between the large step-size and small step-size pictures for each galaxy.

The next step was to subtract the sky. This was done by sampling the intensity in 100 ten pixel by ten pixel square areas around the outer edge of the large step-size picture. Care was taken to exclude stars by removing data from areas with large variations in intensity. These intensities were then combined to determine a fit to the function:

$$I_{sky} = I_0 + I_x X + I_y Y$$

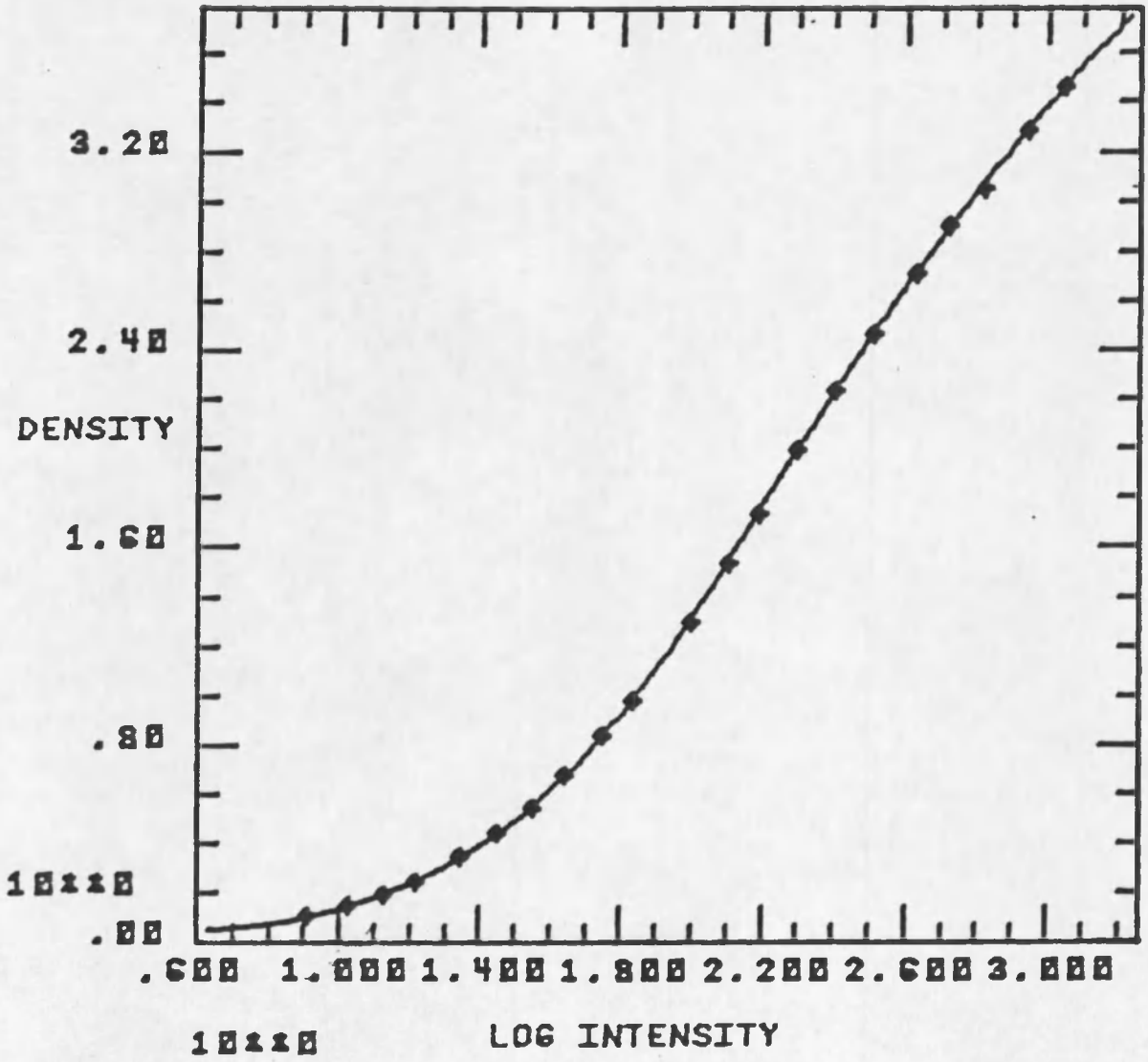

Figure 9. A typical characteristic curve for the plates obtained in this study -- The squares are measurements of individual spots. The line is the function defined in the text.

where I_0 is the value of the sky in the (0,0) pixel, I_x is the gradient in the horizontal direction, and I_y is the gradient in the vertical direction. In almost all cases, the total variation of the sky from one corner to another was less than or on the order of 1% of the mean value. Possible radial variations will be discussed later. These sky parameters were then scaled to the small step-size picture and, for each pixel, a value of sky intensity was computed and subtracted.

The absolute calibration was the next step in the reduction procedure. The literature was searched for photoelectric aperture photometry in the B band through apertures smaller than 200 arcseconds. Almost all of the photometry was found through references in de Vaucouleurs et al. (1976). The photoelectric measurements obtained by the author and listed in Table 2 were combined with this compilation. The result was a list of from two to eight measurements through different apertures for each galaxy. For two galaxies only one calibrating measurement was available, and for one, NGC 2344, no photometry was found. A wide range of aperture sizes was sought both because of the increased accuracy of the zero point determination and because consistency between large and small apertures rules out large systematic errors in the density to intensity conversion.

The calibration was determined in the following way. First, the center of the galaxy was located using an iterative center of gravity technique. Then, for each aperture size for which a magnitude had been found, the calibration constant, Δm, was calculated. This constant is defined by:

$$\Delta m = m(r) + 2.5 \log I(r)$$

where m(r) is the photoelectric B magnitude in an aperture with radius r and I(r) is the total intensity within a radius r from the center of the galaxy as measured on the digitized plate. In order to calculate I(r), a scheme was devised to accurately account for pixels which fall partially within the relevant radius. The means and standard deviations of all calibration constants for each galaxy were calculated. The standard deviations, number of measurements, and differences between the magnitudes in the smallest and largest apertures for each galaxy are listed in Table 7. It can be seen that, in general, the zero points are quite well determined, usually to 0.10 magnitude or better. We consider this quite satisfactory considering the heterogeneous origins and possible centering uncertainties in the calibrating photometry.

The one exception to this calibration procedure was NGC 2344. Since no aperture photometry was found for this galaxy, the zero point was determined from the sky brightness as measured from plates exposed before and after the exposure on NGC 2344. This zero point calibration is certainly more uncertain, perhaps by as much as 0.2 or 0.3 magnitudes.

Only the short exposure plates of each galaxy were calibrated in the manner described above. It was decided to measure a series of luminosity profiles from each picture, long and short, and then to combine them by adding or subtracting a constant to the long exposure profiles to make them fit the short exposure ones. The luminosity profiles are a series of radial measurements of surface brightness, spaced ten degrees apart in angle around the galaxy. The radial spacing of the points and the aperture size in which the measurements were made varied with distance from the center. This was done in order to obtain both

Table 7. Precision of Zero-Point Determinations

NGC	Std. dev.	Number of determ.	Range of magnitudes
488	.16	7	2.35
628	.25	3	3.85
1058		1	
2268	.04	2	1.52
2336		1	
2344		0	
2655	.07	2	0.66
2681	.09	6	1.66
2775	.15	4	1.00
2841	.08	8	2.75
2855	.31	3	2.31
2967	.01	2	0.12
3147	.10	4	2.29
3277	.09	6	0.74
3368	.03	8	2.75
3379	.10	8	2.33
3642	.09	2	1.37
3898	.12	3	1.77
4378	.11	4	1.21
4486	.12	9	1.47
4594	.03	2	0.89
4725	.11	2	1.09
4736	.10	6	1.61
4941		1	
5194	.11	6	1.91
6340	.03	2	0.30
7217	.01	3	0.83
7331	.06	4	2.24

good spatial resolution near the center of the galaxy and to extend the measurements to low surface brightness levels in the outer parts of the galaxy. Table 8 lists the radial positions and aperture sizes used. All linear sizes are in pixels, and in the column giving the aperture sizes, nS indicates a square aperture with edge n while mR indicates a circular aperture with radius m. After the luminosity profiles were measured for both the long and short plates of a galaxy, they were combined. This was done by taking the mean difference in magnitude between all points from 20 Bμ to 22 Bμ in the short profile and the corresponding points in the long profile. This difference was applied as an additive constant to the long profile. In order to remove possible saturation effects at high surface brightnesses, all points from the short profile with brightnesses $\leq$20 Bμ were substituted into the long profile at the corresponding locations. Finally, the profiles were edited so that any point affected by a foreground star was removed from the data. The final profiles are a 36 by 72 point (2592 points) array of surface brightness measurements.

It is desirable to perform two tests on the data to ensure its photometric accuracy. First, we consider the possible existence of radial gradients in the sky background. In order to investigate this, one long exposure plate of a field chosen at random was obtained. This plate was scanned with step sizes of 20, 40, and 80 microns and converted to intensities in a manner identical to the galaxy exposures.

The sky was fit to measurements of the picture with 80 micron steps, then scaled down and subtracted from the 40 micron picture. Similarly, the sky was fit to the 40 micron picture, and then subtracted

Table 8. Aperture Radii and Positions

Point no.	Galactocentric radius (pixels)	Aperture size	Point no.	Galactocentric radius (pixels)	Aperture size
1	0.0	1. S	37	70.0	5. R
2	1.0	1. S	38	75.0	5. R
3	2.0	1. S	39	80.0	5. R
4	3.0	1. S	40	85.0	5. R
5	4.0	1. S	41	90.0	5. R
6	5.0	1. S	42	95.0	5. R
7	6.0	1. S	43	100.0	5. R
8	7.0	1. S	44	105.0	5. R
9	8.0	1. S	45	110.0	5. R
10	9.0	1. S	46	115.0	5. R
11	10.0	1. S	47	120.0	5. R
12	11.0	2. S	48	125.0	5. R
13	13.0	2. S	49	130.0	5. R
14	15.0	2. S	51	140.0	5. R
15	17.0	2. S	52	145.0	5. R
16	19.0	2. S	52	145.0	5. R
17	21.0	2. S	53	150.0	5. R
18	23.0	2. S	54	155.0	5. R
19	25.0	2. S	55	160-0	5. R
20	27.0	2. S	56	165.0	5. R
21	29.0	2. S	57	170.0	5. R
22	31.0	2. S	58	175.0	5. R
23	32.5	2.5 R	59	180.0	5. R
24	35.0	2.5 R	60	185.0	5. R
25	37.5	2.5 R	61	190.0	5. R
26	40.0	2.5 R	62	195.0	5. R
27	42.5	2.5 R	63	200.0	5. R
28	45.0	2.5 R	64	205.0	5. R
29	47.5	2.5 R	65	210.0	5. R
30	50.0	2.5 R	66	215.0	5. R
31	52.5	2.5 R	67	220.0	5. R
32	55.0	2.5 R	68	225.0	5. R
33	57.5	2.5 R	69	230.0	5. R
34	60.0	2.5 R	70	235.0	5. R
35	62.5	2.5 R	71	240.0	5. R
36	65.0	5. R	72	245.0	5. R

from the picture with 20 micron steps. In each sky-subtracted picture, the intensity was measured in 2000 pixels near the center, taking care not to include any stars. If there were no radial variations, it is expected that the mean value in these pixels should be zero. In fact, the averages were 1.4% of the mean sky brightness in the 40 micron step-size picture and 0.6% of the sky in the 20 micron step-size picture. Thus, there is evidence for a small radial gradient. The effect of such a gradient is twofold. First, the sky subtraction procedure will leave a small unsubtracted residual with an amplitude of up to 1.4% of the sky brightness at the center of the plate. Second, the calibration procedure will be affected by both this excess sky contribution and the presumably similar gradient superposed on the light distribution of the galaxy. In practice, however, it is expected that both of these effects are negligible in comparison with the random errors contributed by photon statistics on the plate. Note that one might worry about the effect of such a systematic error when larger apertures are used, but this occurs only toward the outer periphery of the picture where the gradient is reduced in magnitude. Therefore, we ignore the effects of radial variations in the sky and in the overall sensitivity of the plate.

The second check on the data is a comparison of the surface brightness measurements with those published by other observers. Two of the galaxies for which we obtained plate material, NGC 3379 and NGC 4486, were observed specifically for that reason. Figures 3 and 4 show the difference between our measured surface brightnesses and those of other observers, plotted as a function of surface brightness. In

Figure 10, our measurements of NGC 3379 are compared with those of de Vaucouleurs and Capaccioli (1979), Burkhead and Kalinowski (1974), and Burstein (1979d). It can be seen that the agreement between all these sources and the measurements made in this study is good, with few differences greater than 0.1 magnitude at levels brighter than about 25 Bμ. Figure 11 shows our measurements of NGC 4486 compared with those of de Vaucouleurs and Nieto (1978, 1979) and Young et al. (1978). In this case, there appears to be a zero point offset with respect to the measurements of de Vaucouleurs and Nieto. The average discrepancy, 0.08 Bμ is shown by a dotted line in this figure. Again, we claim that at surface brightnesses above about 25 Bμ, our photometry is accurate to about 0.1 magnitude, aside from the accuracy of the zero point determination.

The problem of presenting such a large body of data is a considerable one. We have 2592 photometric measurements for each of 28 galaxies. To tabulate so many numbers is clearly impossible. nstead, we have produced an "elliptically averaged" profile for each galaxy. To do this, an ellipse, centered on the nucelus of the galaxy, was fit to an outer isophote. Then the 36 radial profiles were co-added, each one being stretched or shrunk according to the radius of the ellipse at that angle relative to the major axis. The result of this procedure would be a high signal-to-noise average profile of the galaxy as seen face-on but for one effect. Since the bulges tend to be more spherical than the disks, the apparent eccentricities of the bulges are less than those of the disks. Thus, the bulge is stretched along its minor axis and this elliptically averaged profile is slightly incorrect near the

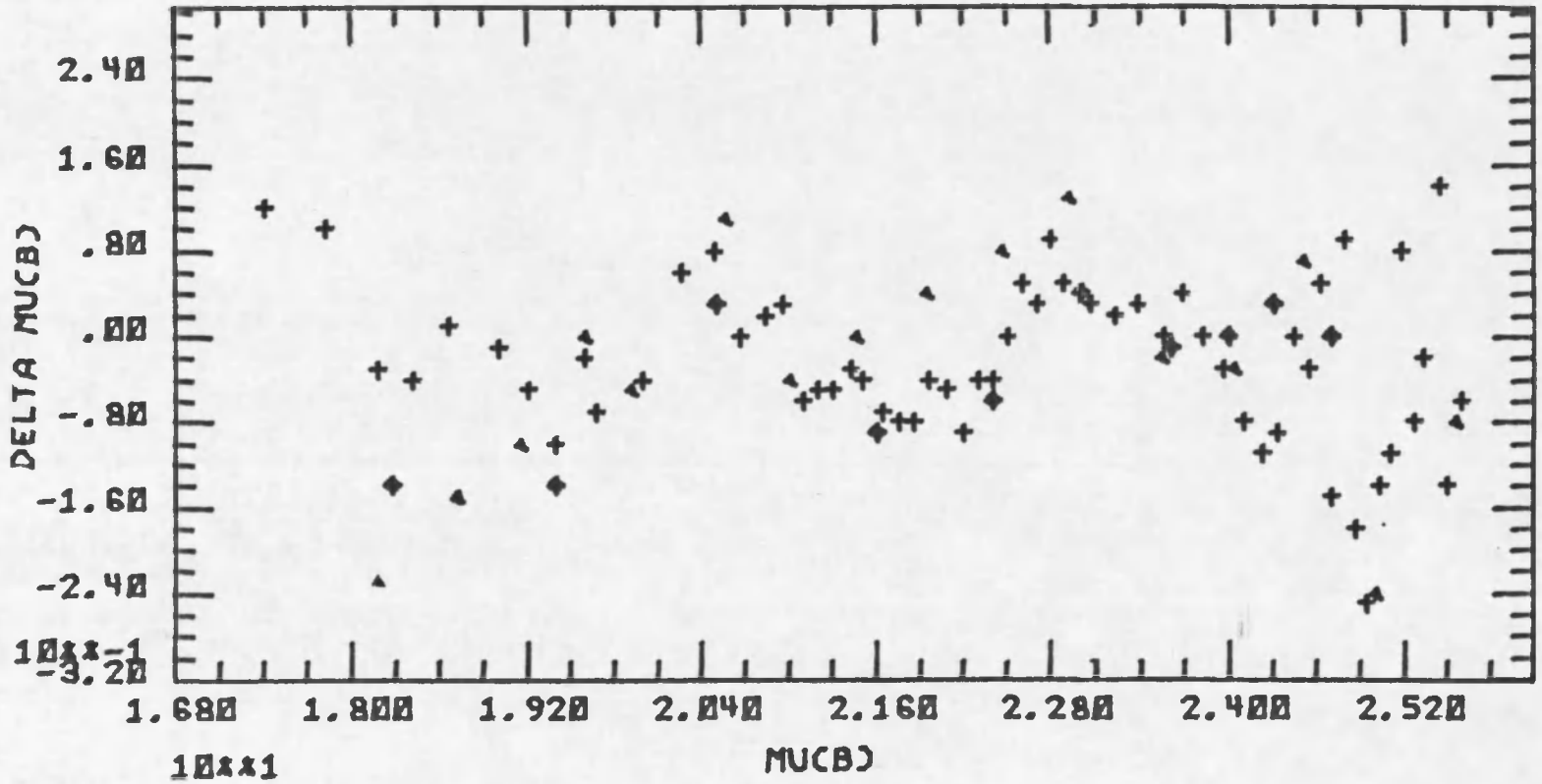

Figure 10. A comparison of surface brightness measurements of NGC 3379 made in this study with those of other authors -- The vertical scale is the difference between our measurements and those of deVaucouleurs and Capaccioli (1979)--crosses, Burkhead and Kalinowski (1974)--diamonds, and Burstein (1979b)--triangles. The horizontal scale is our measured surface brightness.

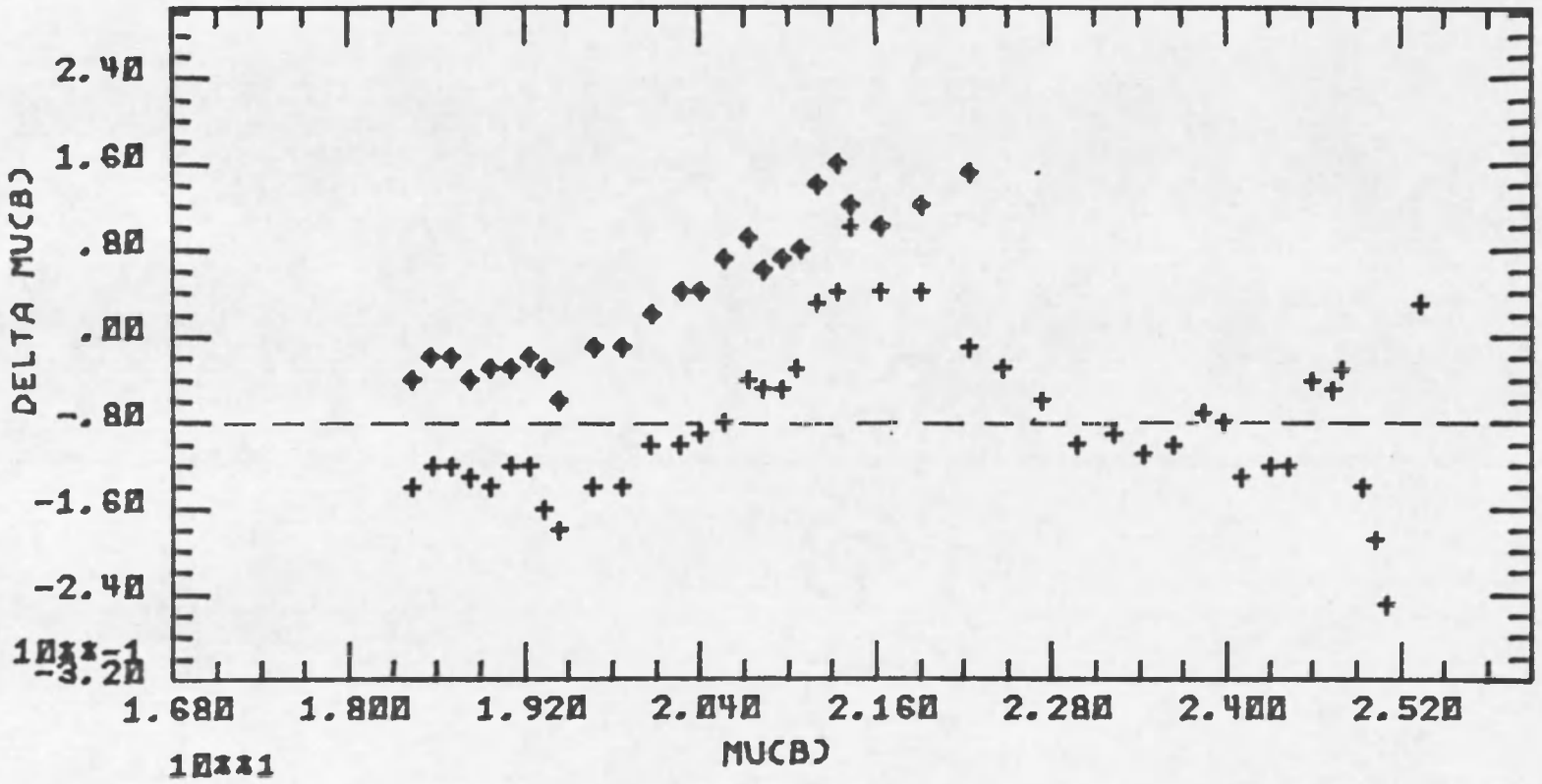

Figure 11. A comparison of surface brightness measurements of NGC 4486 made in this study with those of other authors -- The vertical scale is the difference between our measurements and those of deVaucouleurs and Nieto (1978, 1979)--crosses, and Young et al. (1978)--diamonds. The horizontal scale is our measured surface brightness. The dashed line represents the zero point offset of 0.08 magnitudes per square arcsecond between our numbers and those of deVaucouleurs and Nieto.

center where the bulge dominates. This effect is a function of inclination of the galaxy, as it can be seen that in a galaxy exactly face-on, this error vanishes. Even with this error, however, the elliptically averaged profiles are useful for determining the radial shape of the disks. Figure 12 shows the elliptically averaged profiles for 25 of the 26 galaxies and the numbers are listed in Table 9. For NGC 4594, the minor axis is shown because the galaxy is close to edge-on.

Decomposition of the Profiles

As discussed at the beginning of this chapter, previous workers (Kormendy 1977c, Burstein 1979b) have carefully considered the subject of separating luminosity profiles into bulge and disk contributions. The major conceptual problem inherent to all methods devised is that one must assume the fitting functions. Neither the de Vaucouleurs law nor the exponential disk have any basis in physics (in fact, flat rotation curves suggest an r^{-1} mass falloff in the disk), but have been found empirically to fit the data. The question arises when we cannot produce a sum of these two functions to fit the observed profile. Is this evidence for a third component, or does it suggest that we are using the wrong fitting function for one of the components? If this latter is the case, how can we distinguish a disk with a hole in the middle from a bulge which falls off faster than expected in its outer parts? Obviously, the information one gets out of such a decomposition is dependent upon the assumptions one puts in.

Once the fitting functions have been chosen, the next problem is how to derive the best fit to the data. This is where Kormendy's

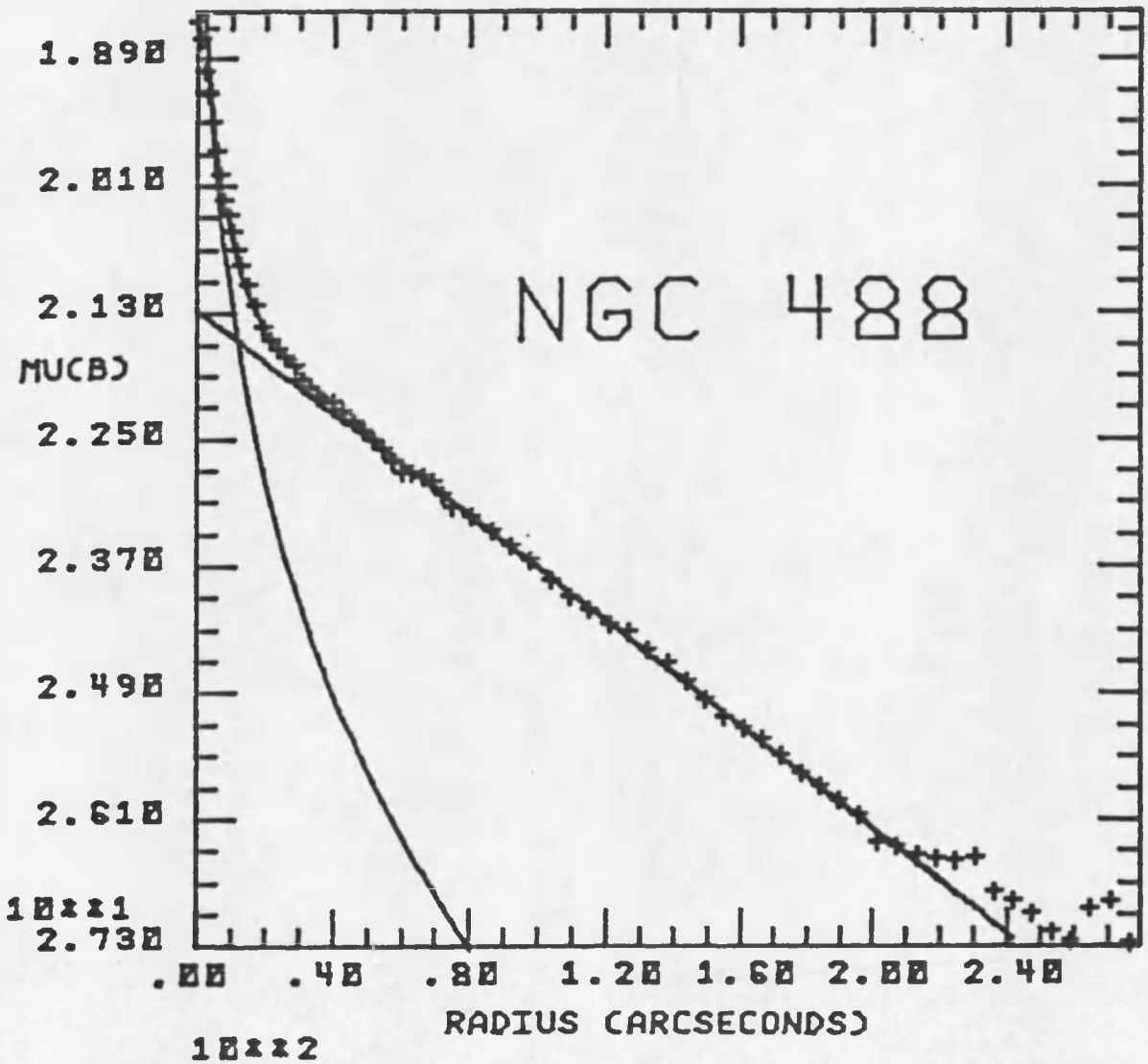

Figure 12. Elliptically averaged major axis profiles -- Surface brightness in magnitudes per square arcsecond in the B band versus radius in arcseconds is plotted for NGC 488. Bulge and disk fits and their sum are shown.

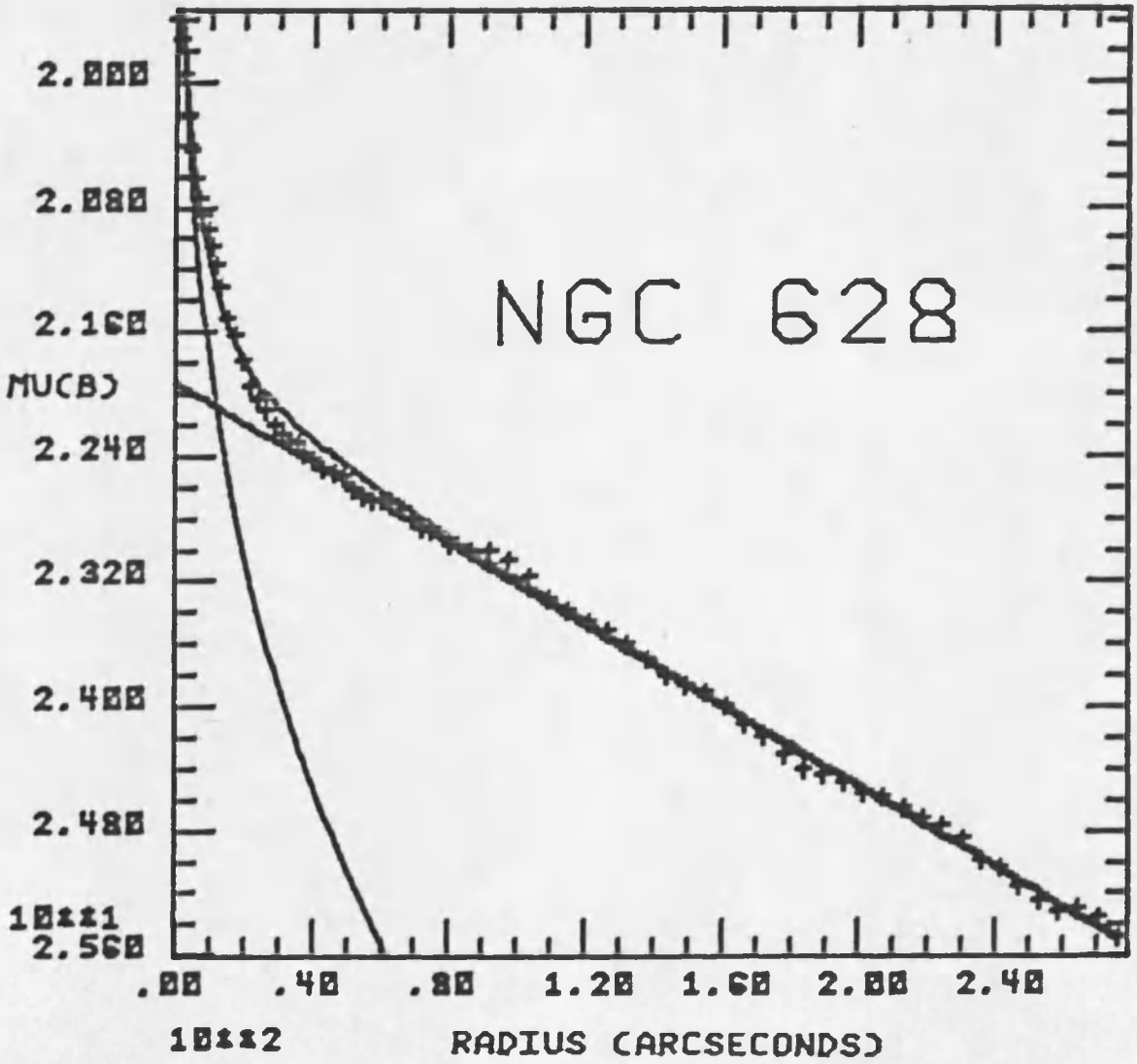

Figure 12.--Continued Elliptically averaged major axis profiles -- Surface brightness in magnitudes per square arcsecond in the B band versus radius in arcseconds is plotted for NGC 628. Bulge and disk fits and their sum are shown.

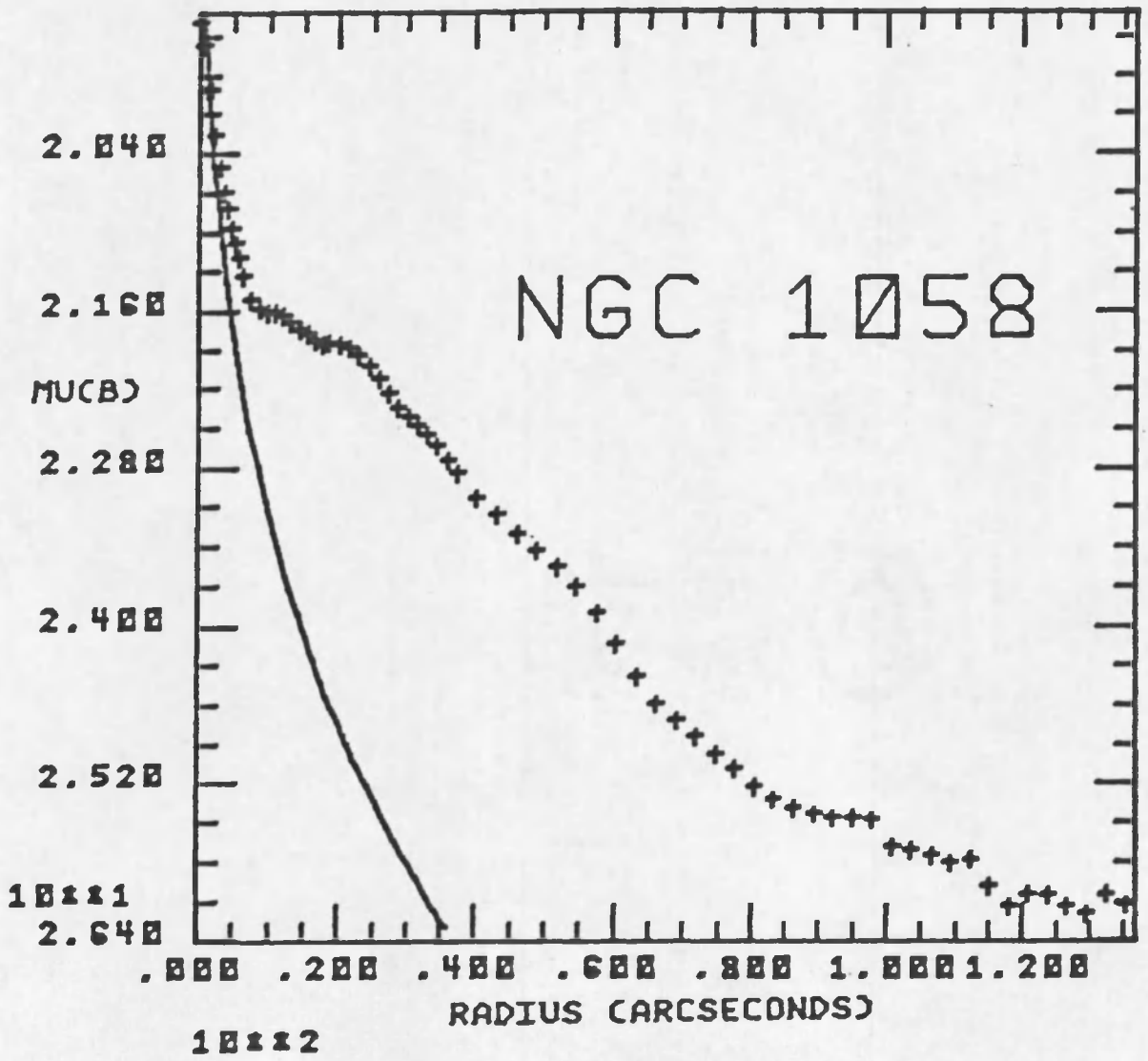

Figure 12.--Continued Elliptically averaged major axis profiles -- Surface brightness in magnitudes per square arcsecond in the B band versus radius in arcseconds is plotted for NGC 1058. Bulge fit is shown.

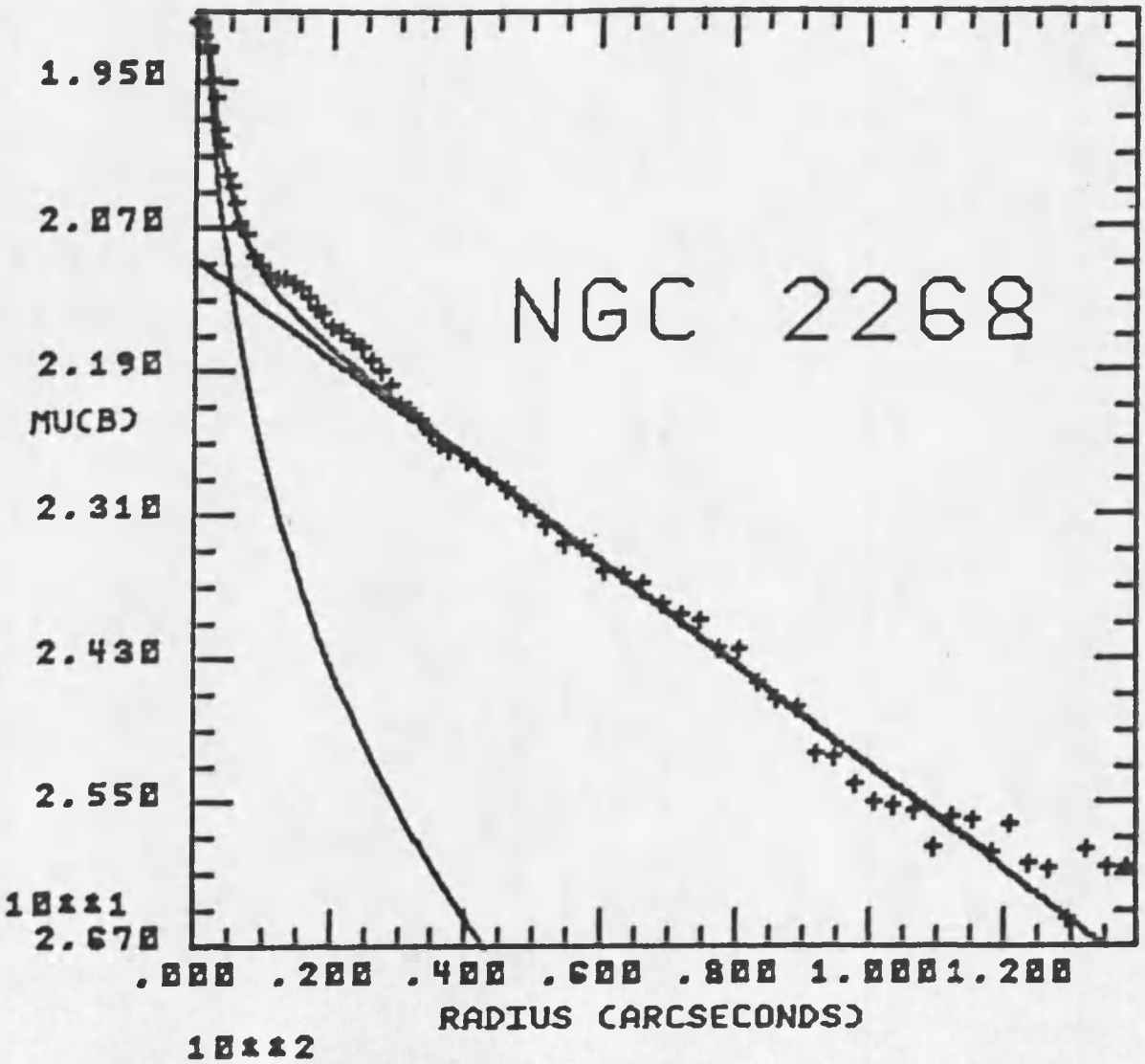

Figure 12.--Continued Elliptically averaged major axis profiles -- Surface brightness in magnitudes per square arcsecond in the B band versus radius in arcseconds is plotted for NGC 2268. Bulge and disk fits and their sum are shown.

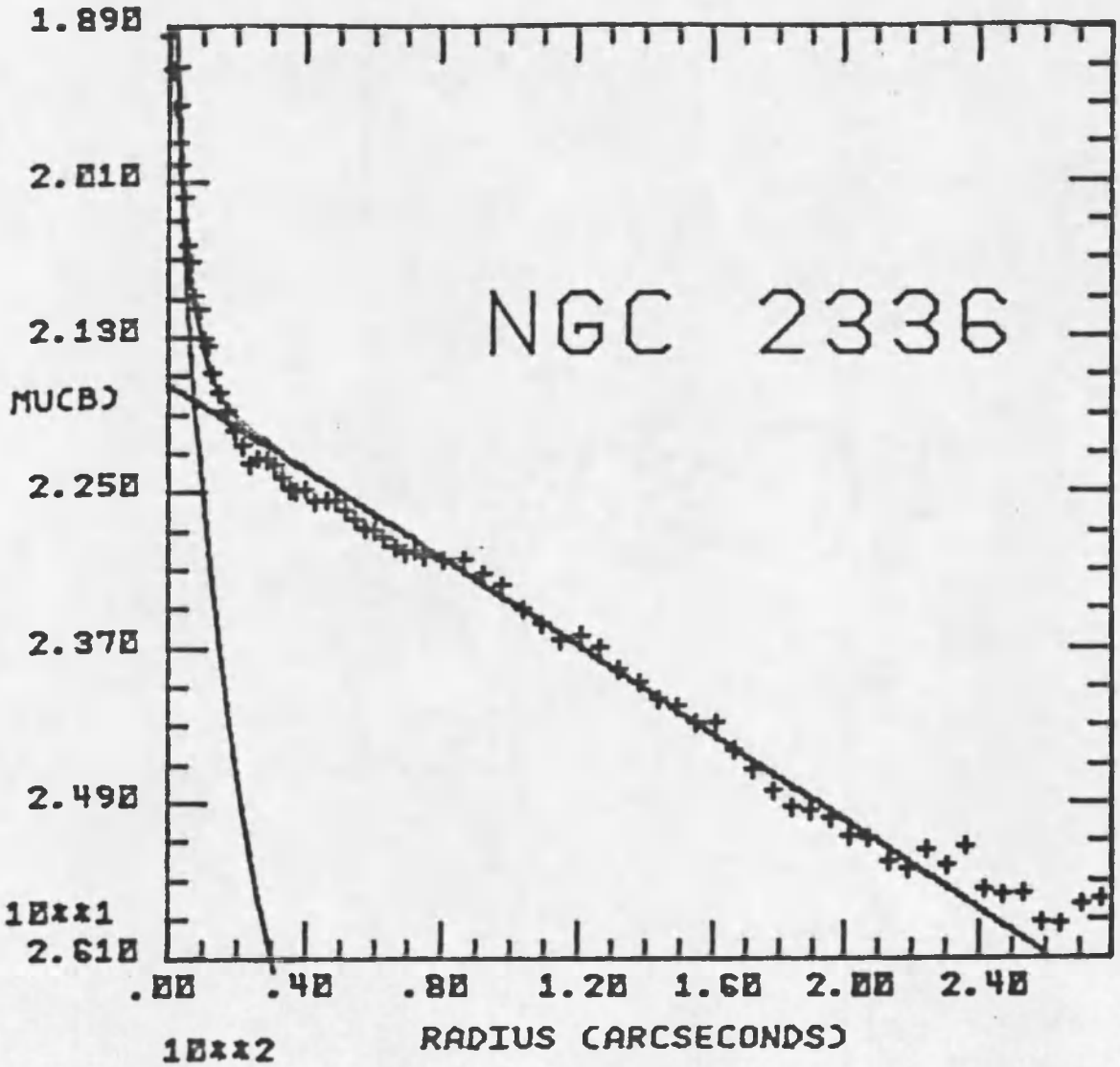

Figure 12.--Continued Elliptically averaged major axis profiles -- Surface brightness in magnitudes per square arcsecond in the B band versus radius in arcseconds is plotted for NGC 2336. Bulge and disk fits and their sum are shown.

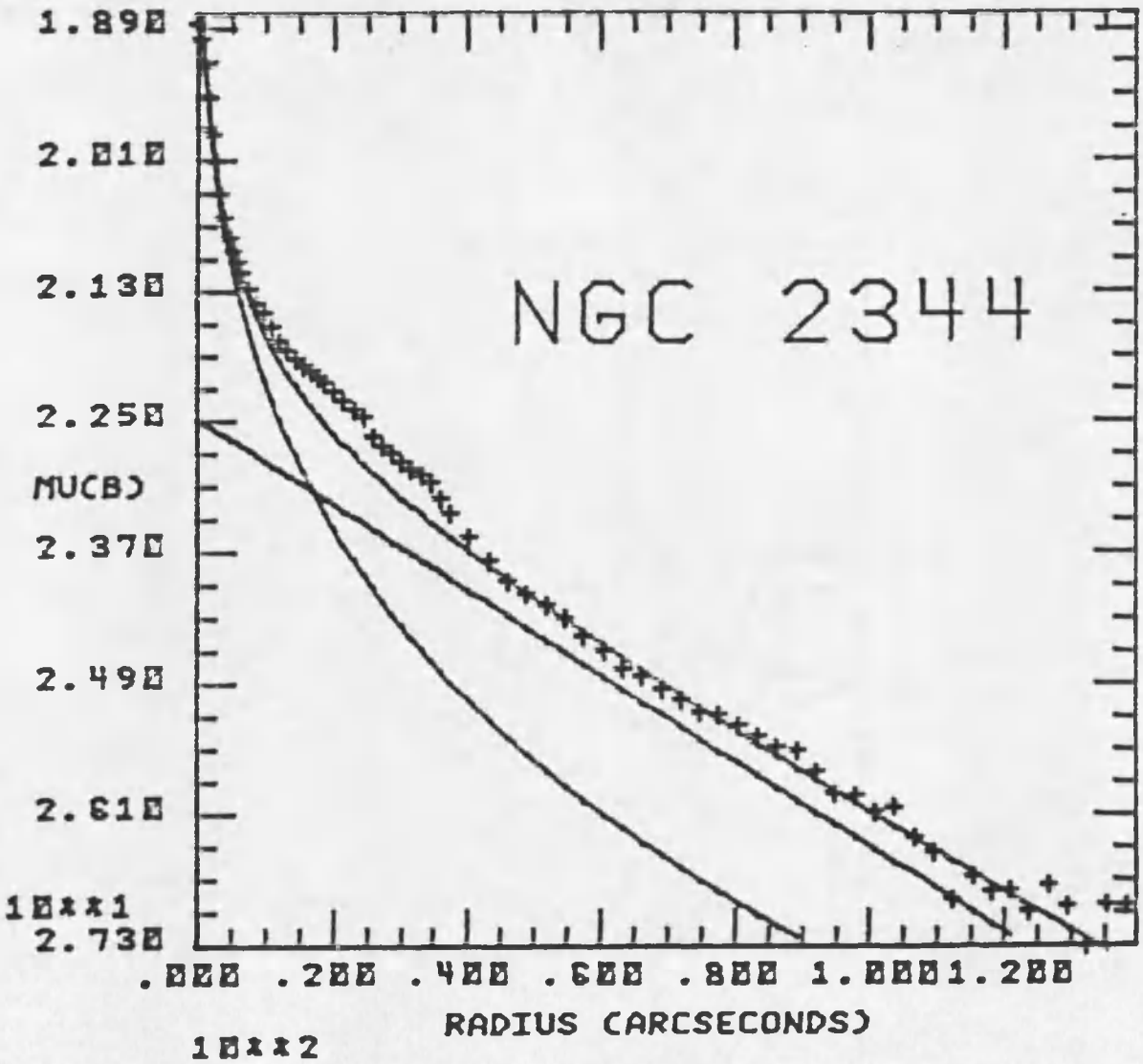

Figure 12.--Continued Elliptically averaged major axis profiles -- Surface brightness in magnitudes per square arcsecond in the B band versus radius in arcseconds is plotted for NGC 2344. Bulge and disk sits and their sum are shown.

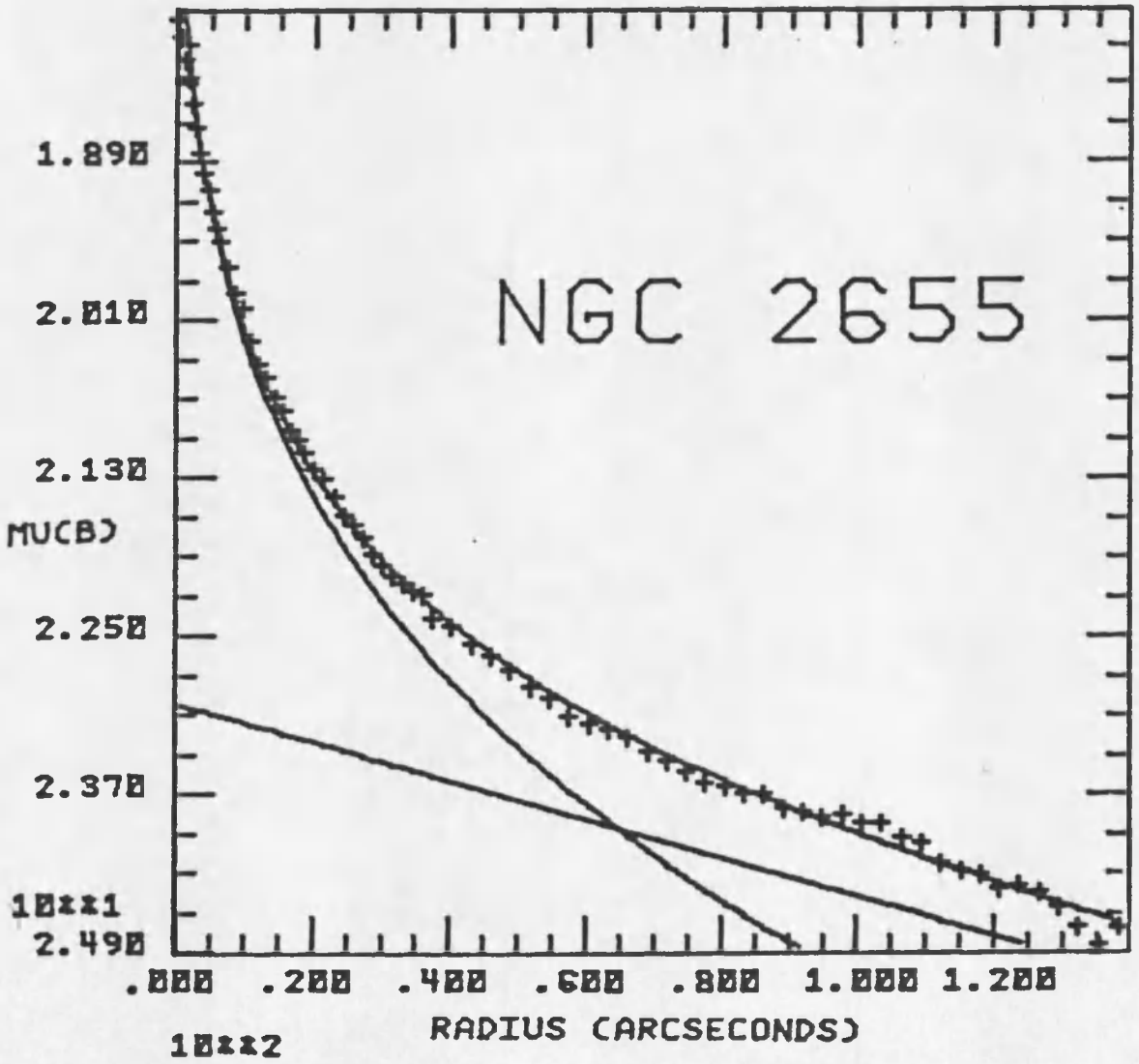

Figure 12.--Continued Elliptically averaged major axis profiles -- Surface brightness in magnitudes per square arcsecond in the B band versus radius in arcseconds is plotted for NGC 2655. Bulge and disk fits and their sum are shown.

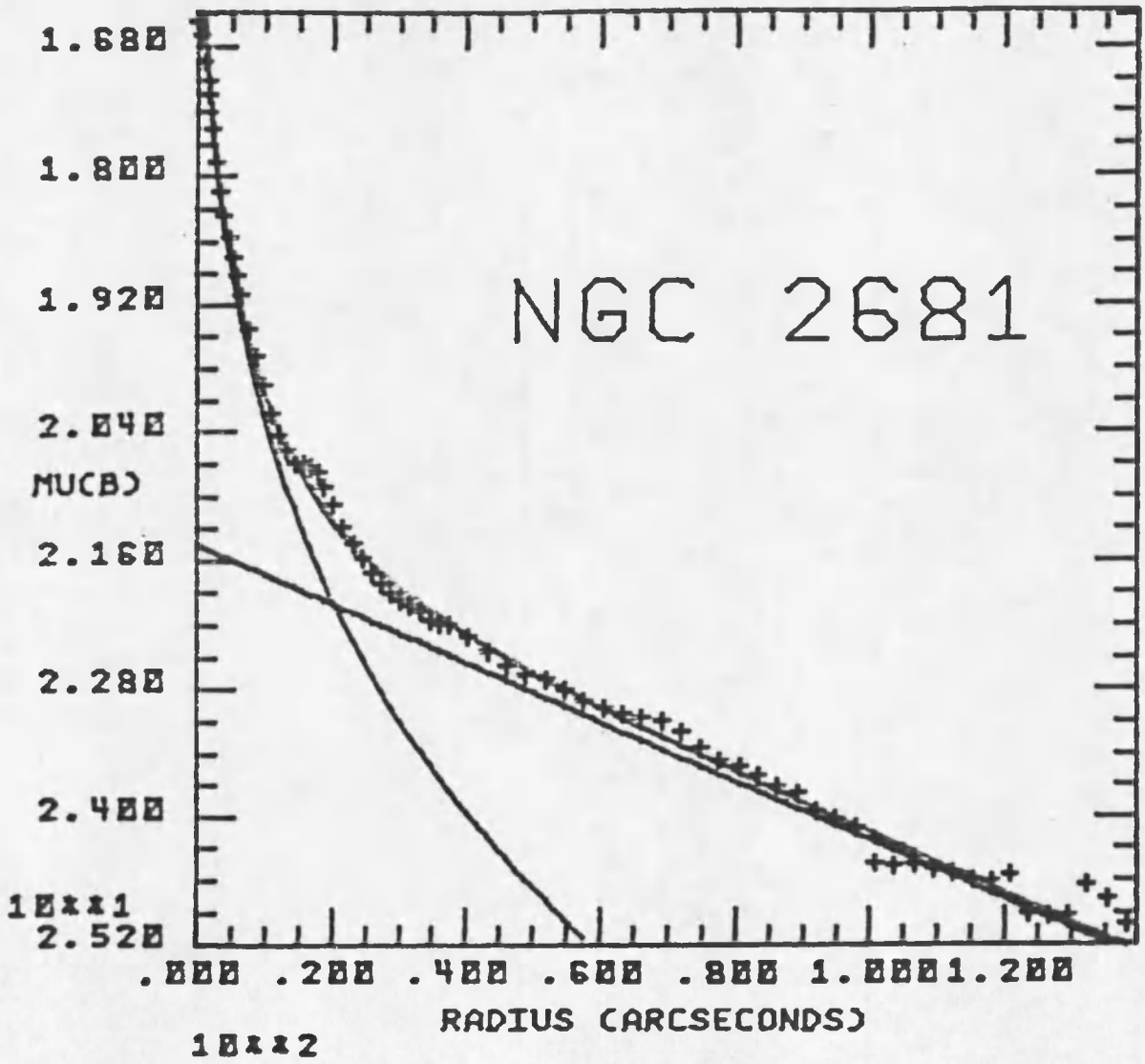

Figure 12.--Continued Elliptically averaged major axis profiles -- Surface brightness in magnitudes per square arcsecond in the B band versus radius in arcseconds is plotted for NGC 2681. Bulge and disk fits and their sum are shown.

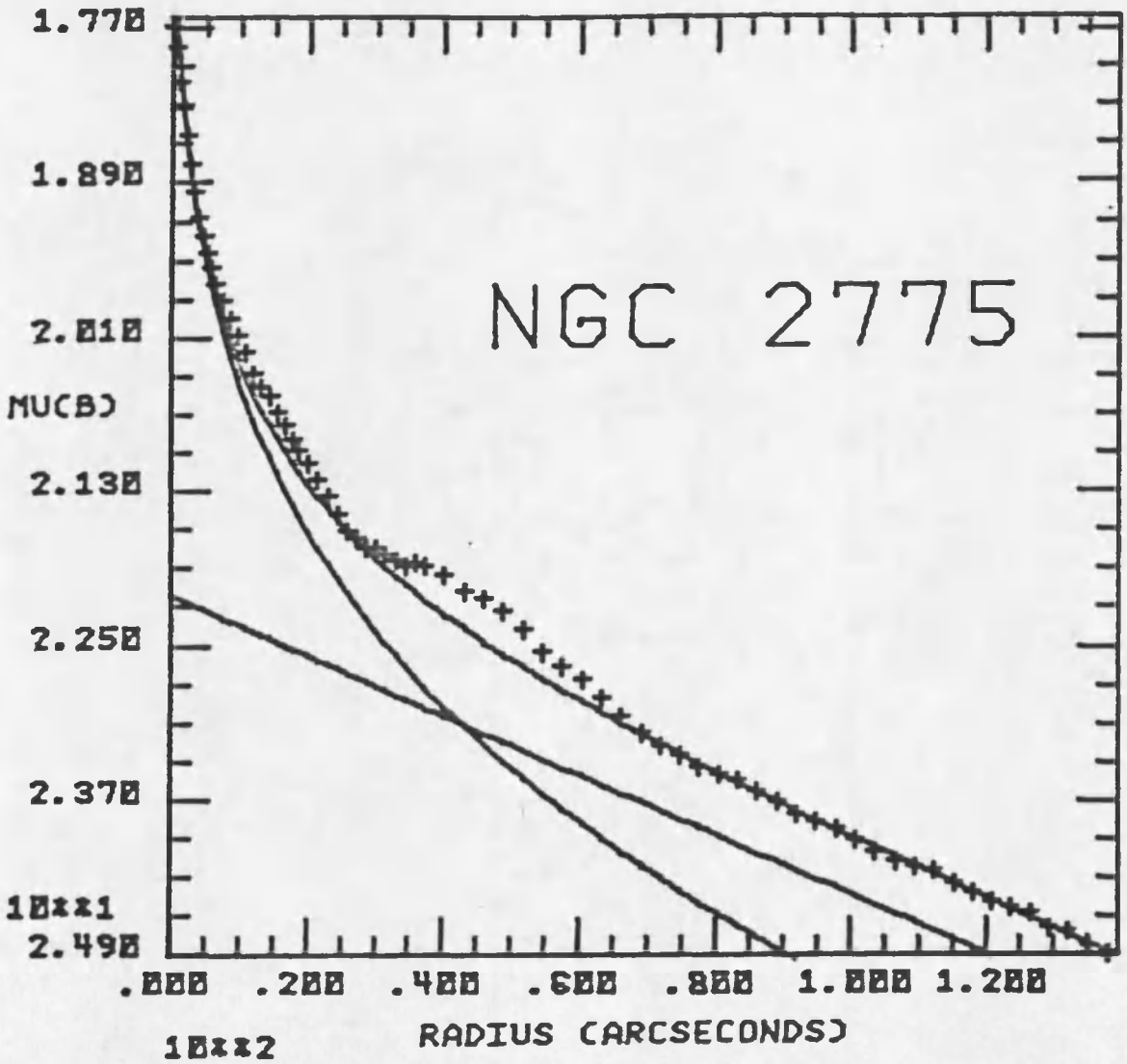

Figure 12.--Continued Elliptically averaged major axis profiles -- Surface brightness in magnitudes per square arcsecond in the B band versus radius in arcseconds is plotted for NGC 2775. Bulge and disk fits and their sum are shown.

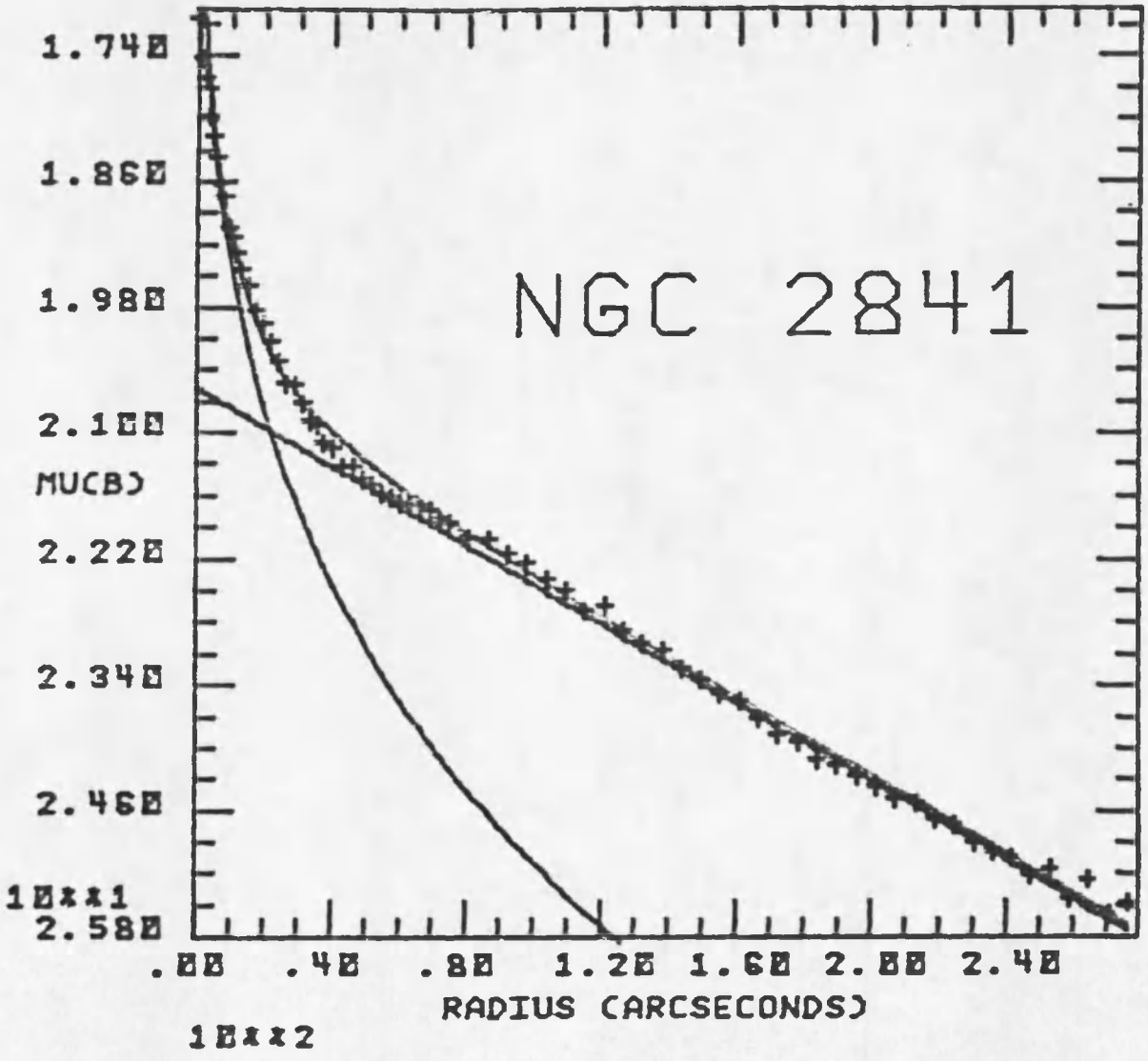

Figure 12.--Continued Elliptically averaged major axis profiles -- Surface brightness in magnitudes per square arcsecond in the B band versus radius in arcseconds is plotted for NGC 2841. Bulge and disk fits and their sum are shown.

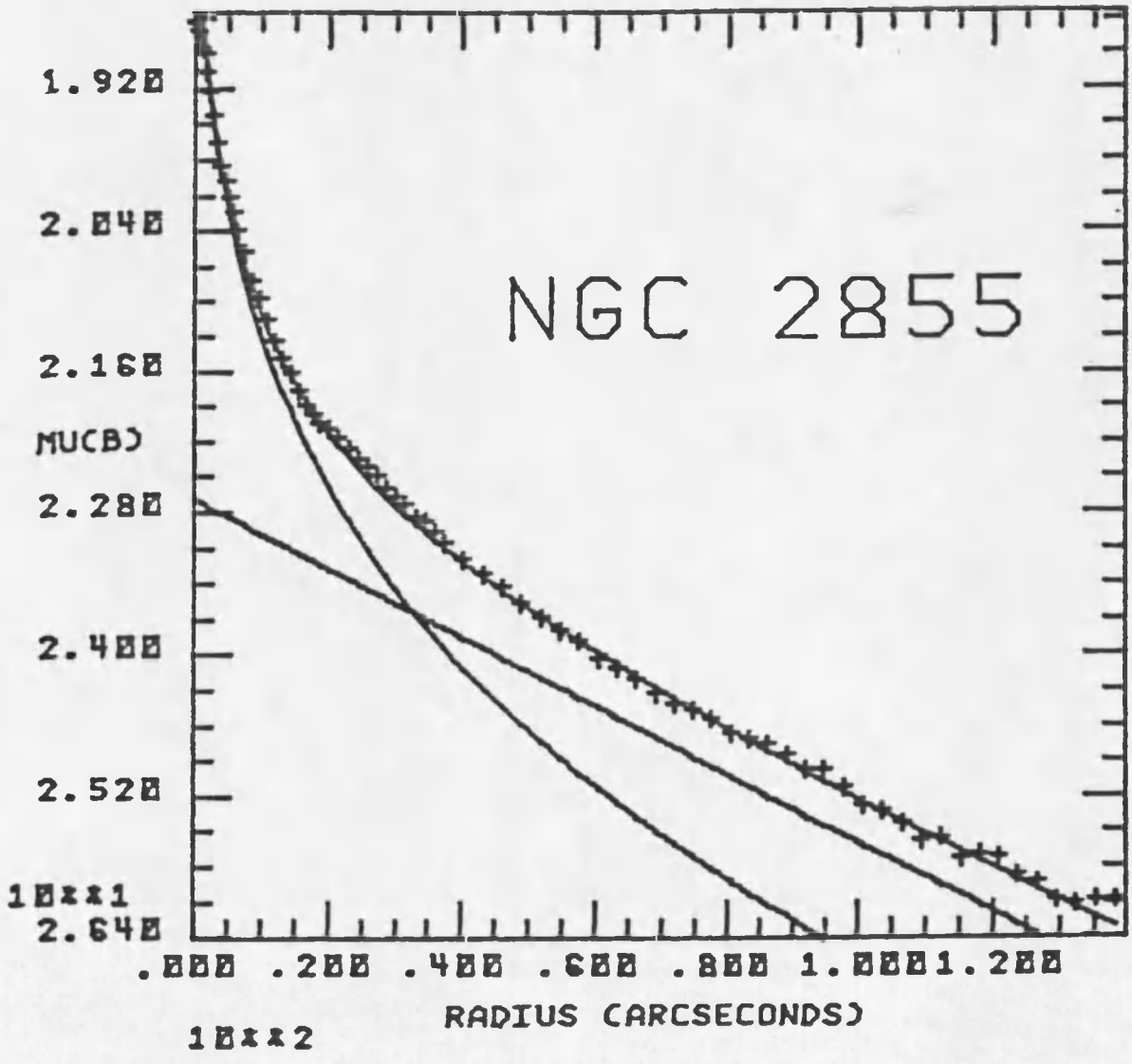

Figure 12.--Continued Elliptically averaged major axis profiles -- Surface brightness in magnitudes per square arcsecond in the B band versus radius in arcseconds is plotted for NGC 2855. Bulge and disk fits and their sum are shown.

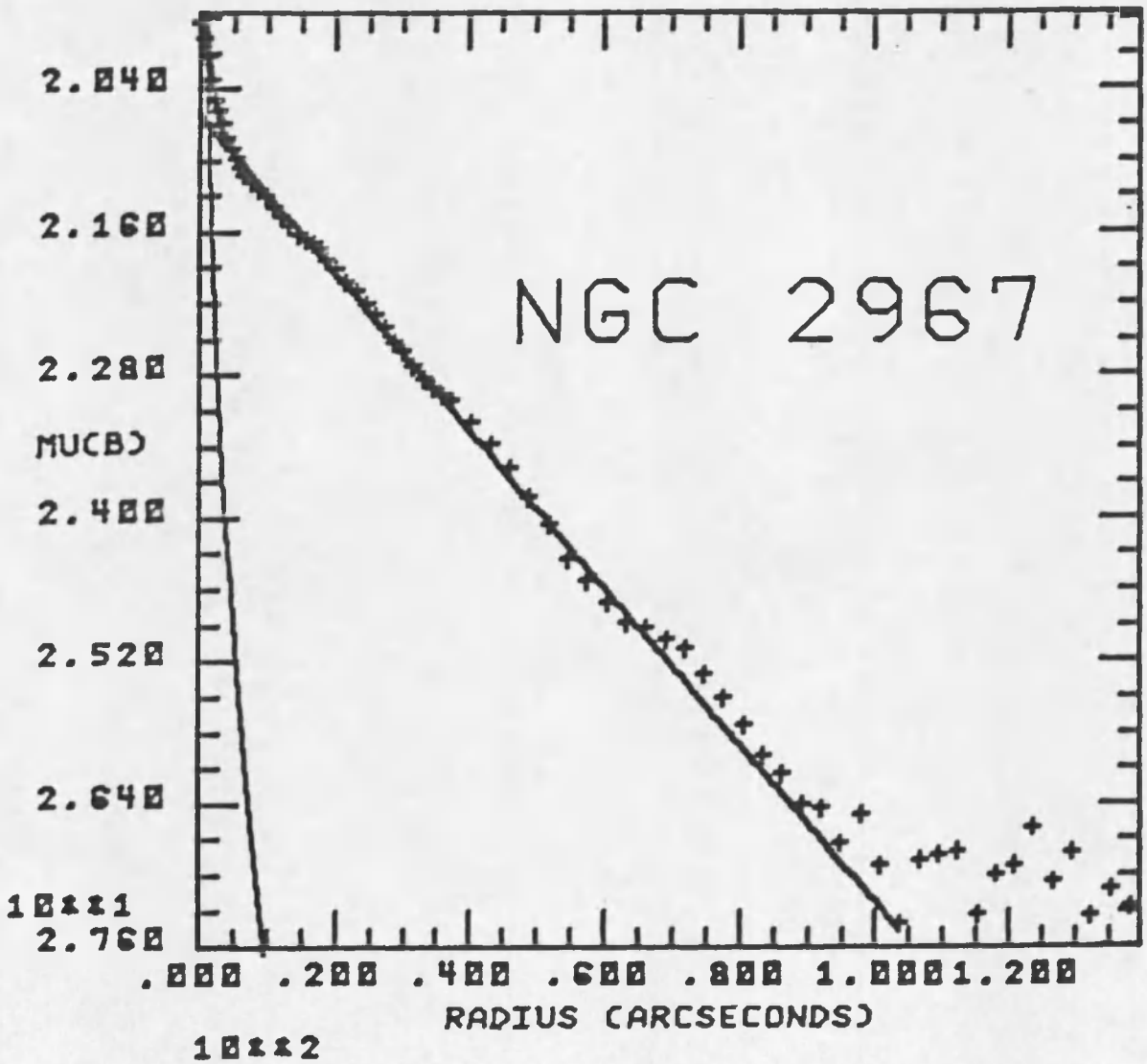

Figure 12.--Continued Elliptically averaged major axis profiles -- Surface brightness in magnitudes per square arcsecond in the B band versus radius in arcseconds is plotted for NGC 2967. Bulge and disk fits and their sum are shown.

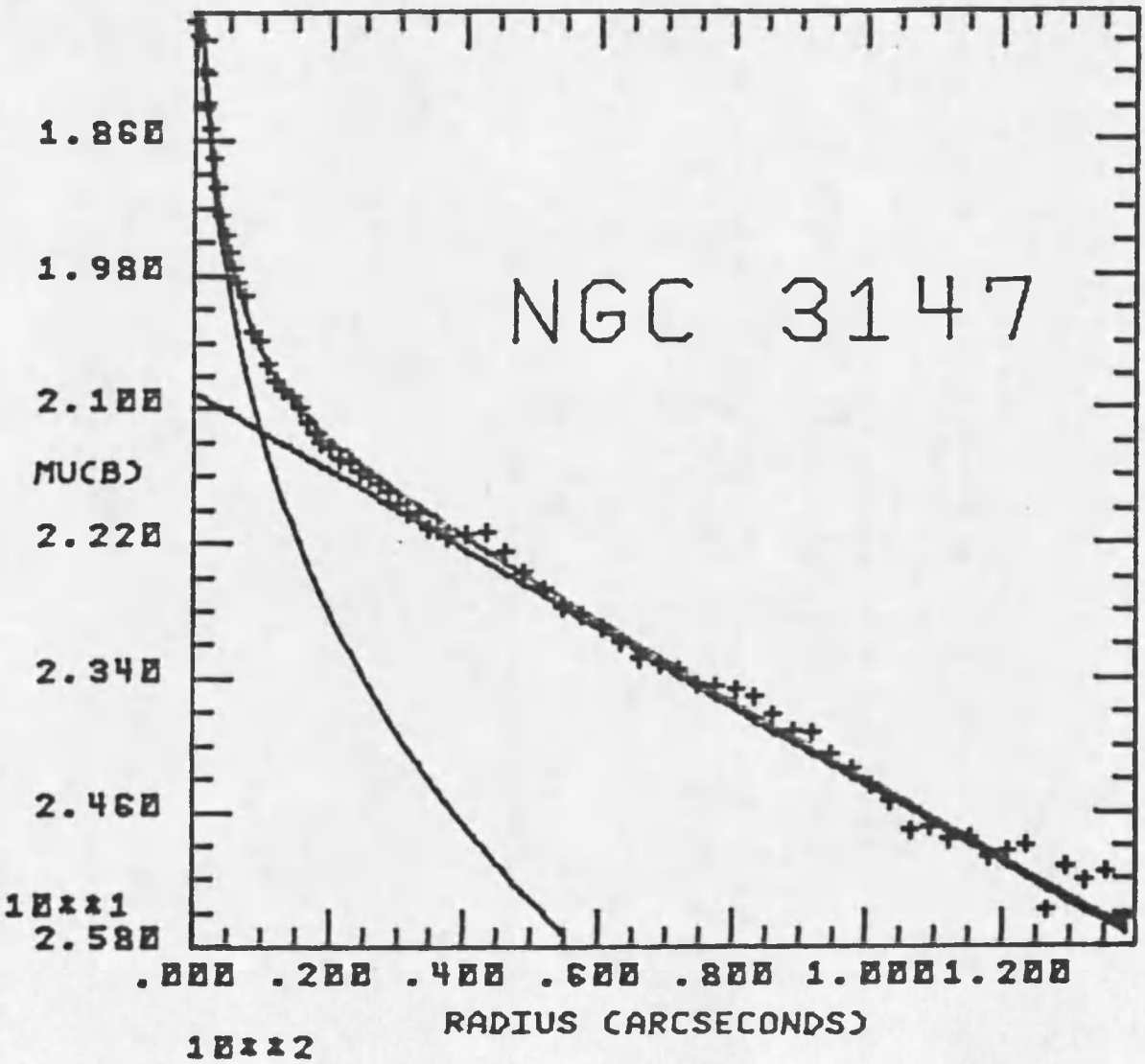

Figure 12.--Continued Elliptically averaged major axis profiles -- Surface brightness in magnitudes per square arcsecond in the B band versus radius in arcseconds is plotted for NGC 3147. Bulge and disk fits and their sum are shown.

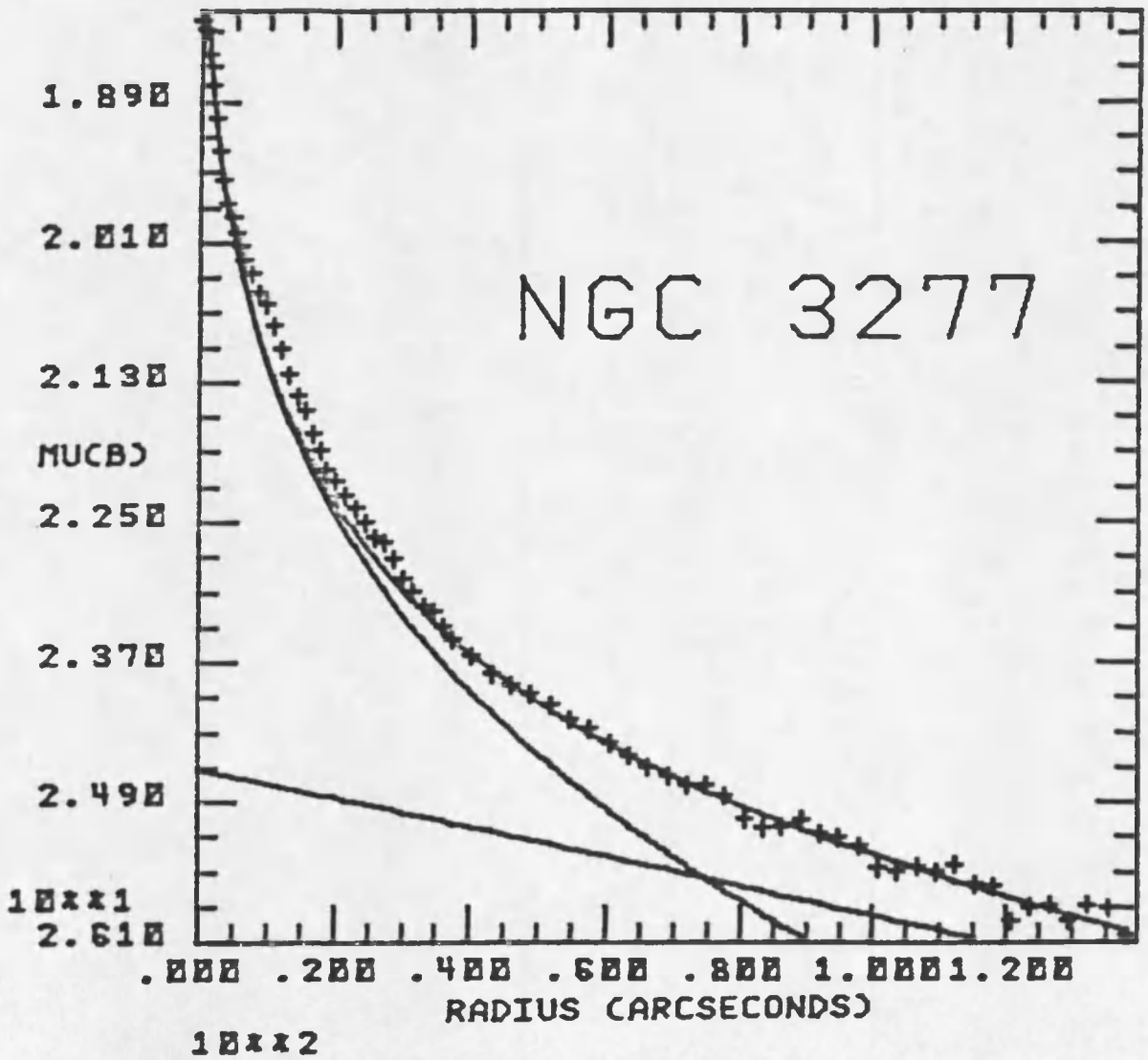

Figure 12.--Continued Elliptically averaged major axis profiles -- Surface brightness in magnitudes per square arcsecond in the B band versus radius in arcseconds is plotted for NGC 3277. Bulge and disk fits and their sum are shown.

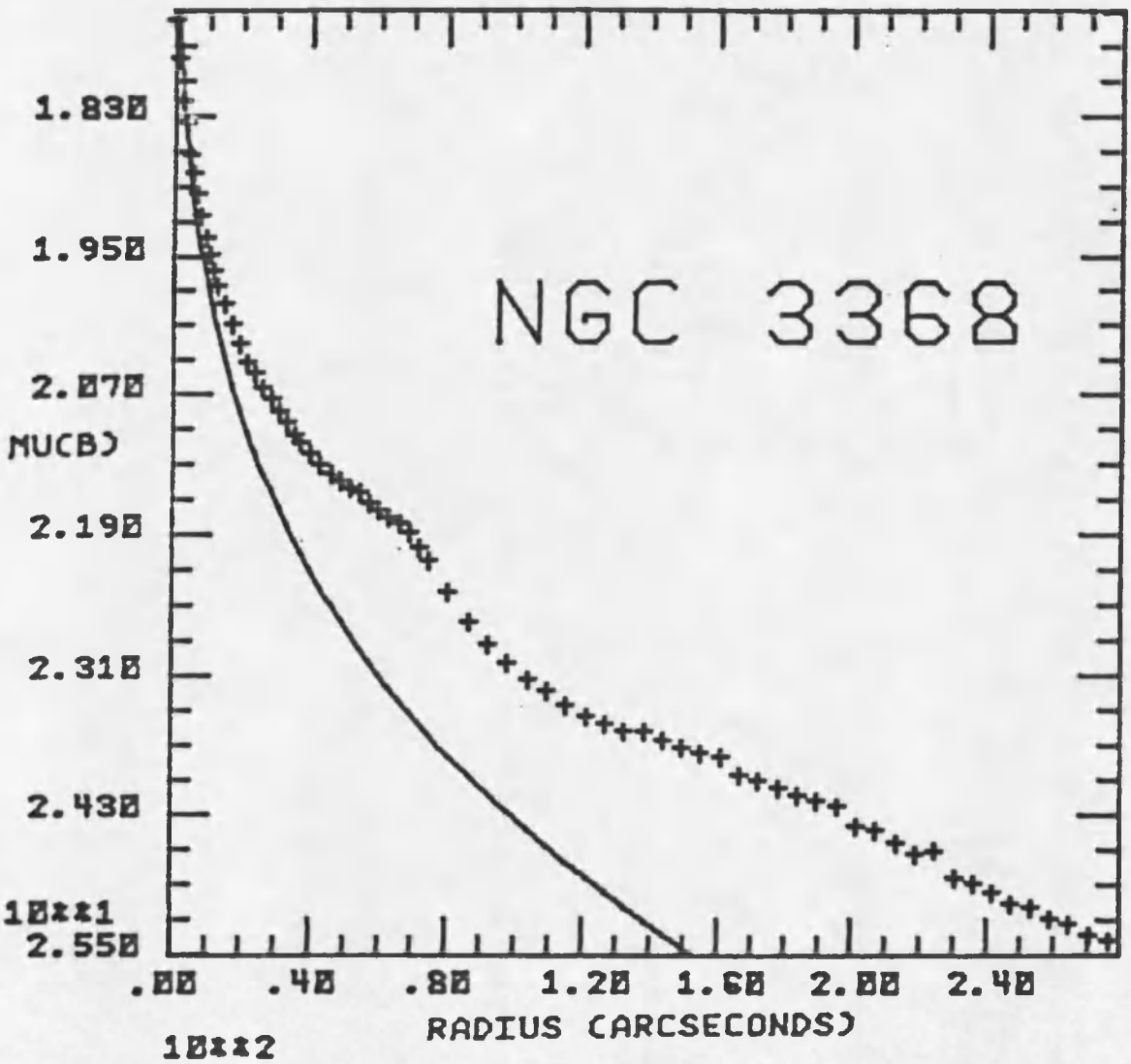

Figure 12.--Continued Elliptically averaged major axis profiles -- Surface brightness in magnitudes per square arcsecond in the B band versus radius in arcseconds is plotted for NGC 3368. Bulge fit is shown.

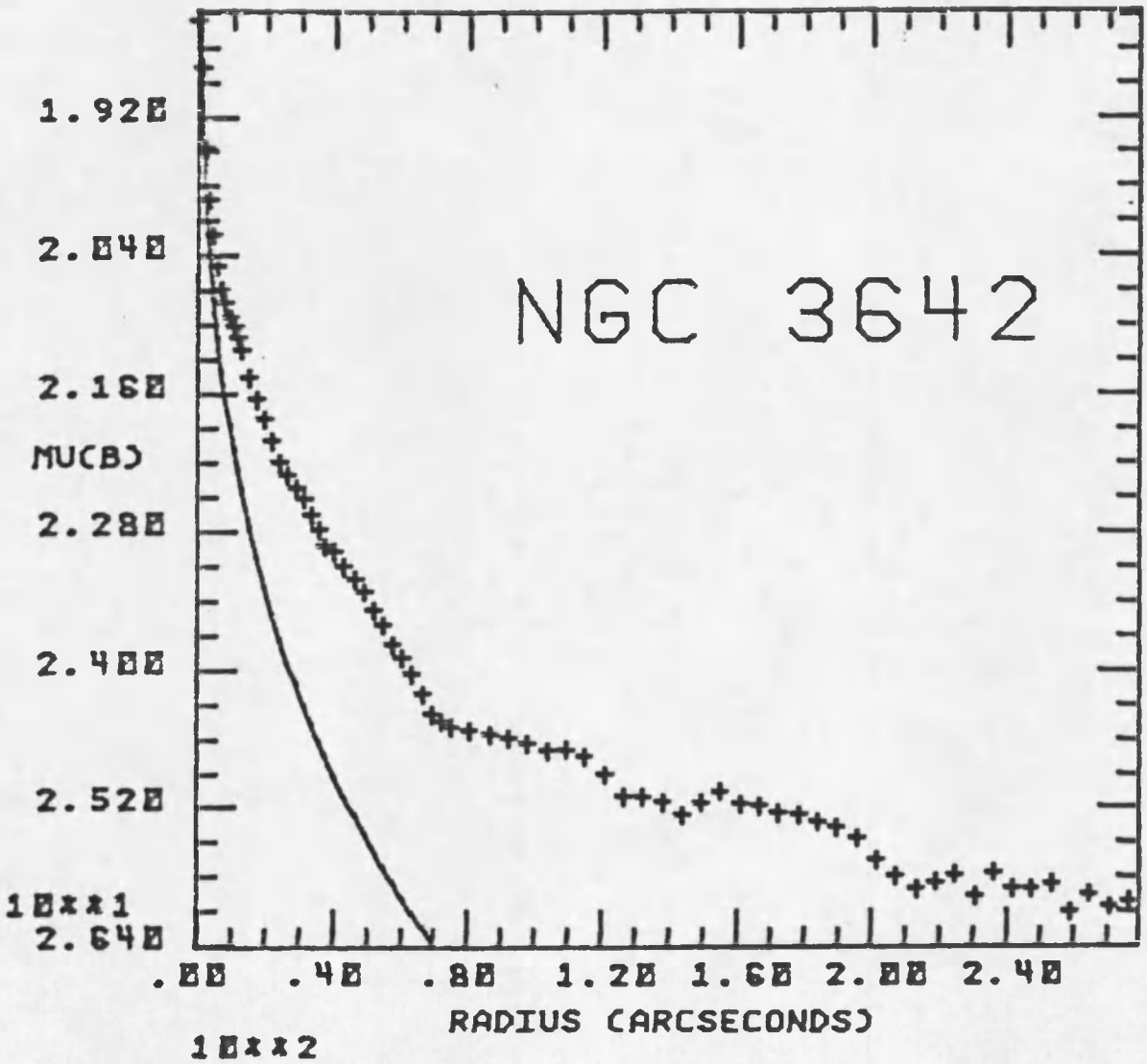

Figure 12.--Continued Elliptically averaged major axis profiles -- Surface brightness in magnitudes per square arcsecond in the B band versus radius in arcseconds is plotted for NGC 3642. Bulge fit is shown.

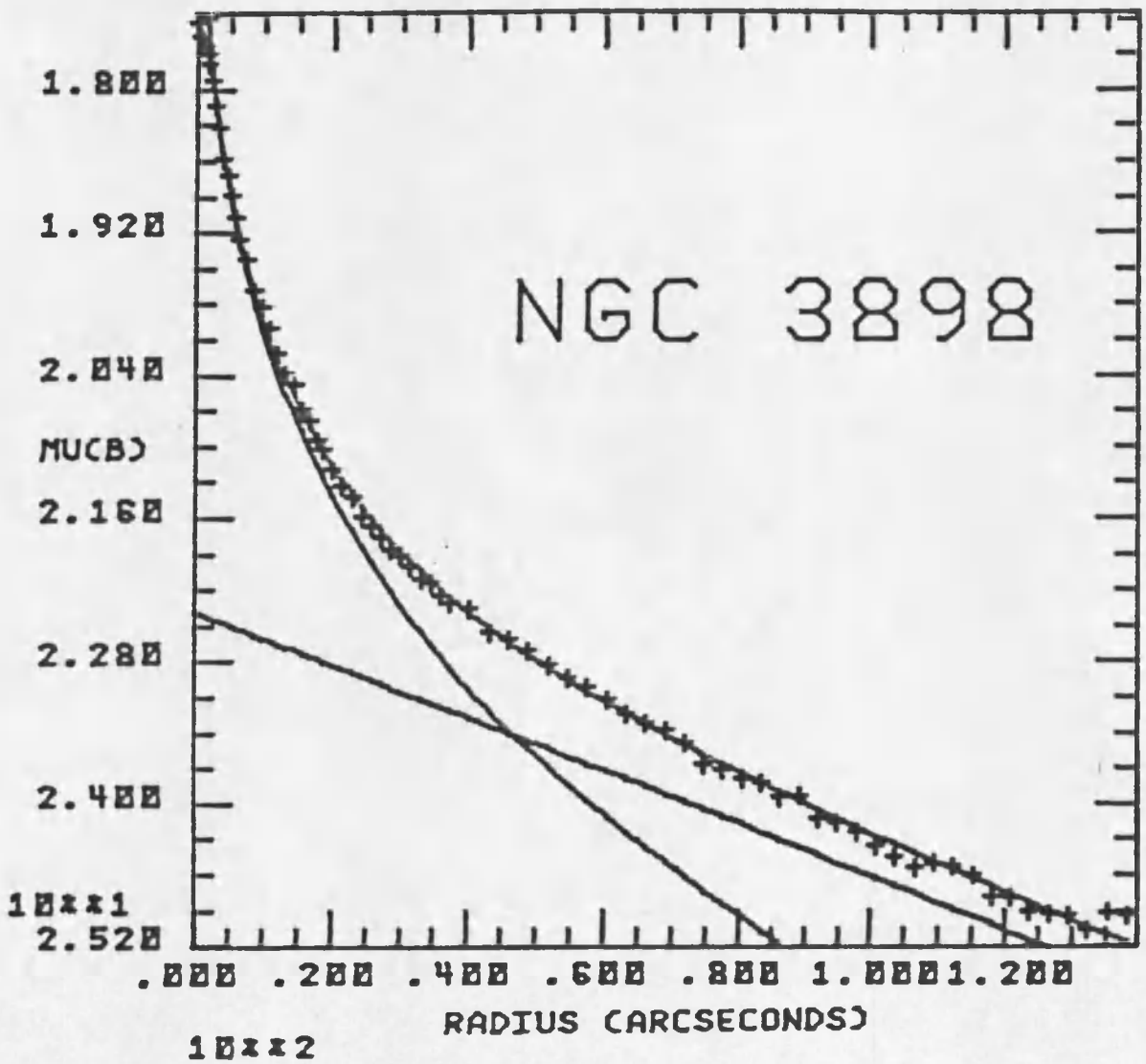

Figure 12.--Continued Elliptically averaged major axis profiles -- Surface brightness in magnitudes per square arcsecond in the B band versus radius in arcseconds is plotted for NGC 3898. Bulge and disk fits and their sum are shown.

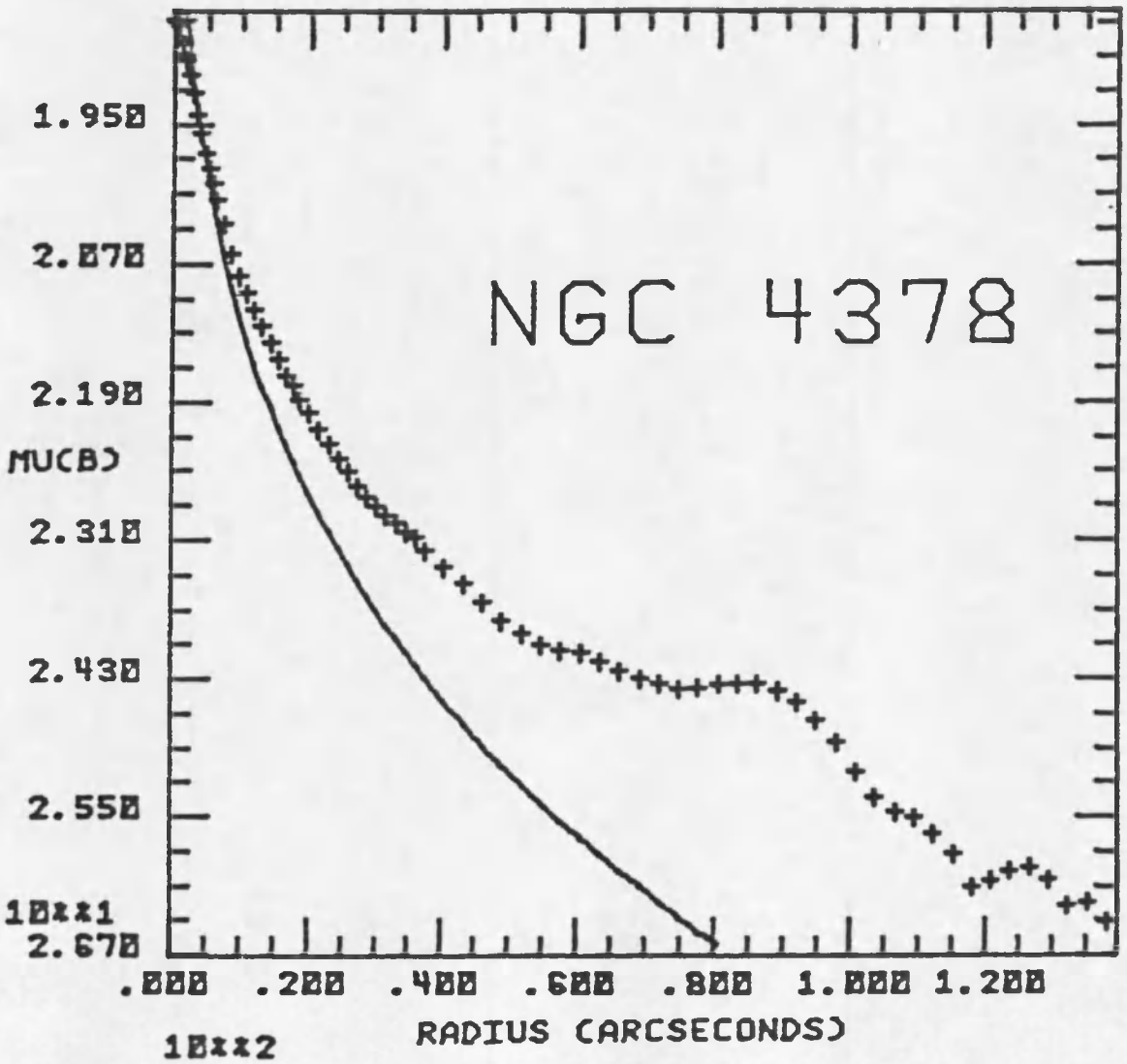

Figure 12.--Continued Elliptically averaged major axis profiles -- Surface brightness in magnitudes per square arcsecond in the B band versus radius in arcseconds is plotted for NGC 4378. Bulge fit is shown.

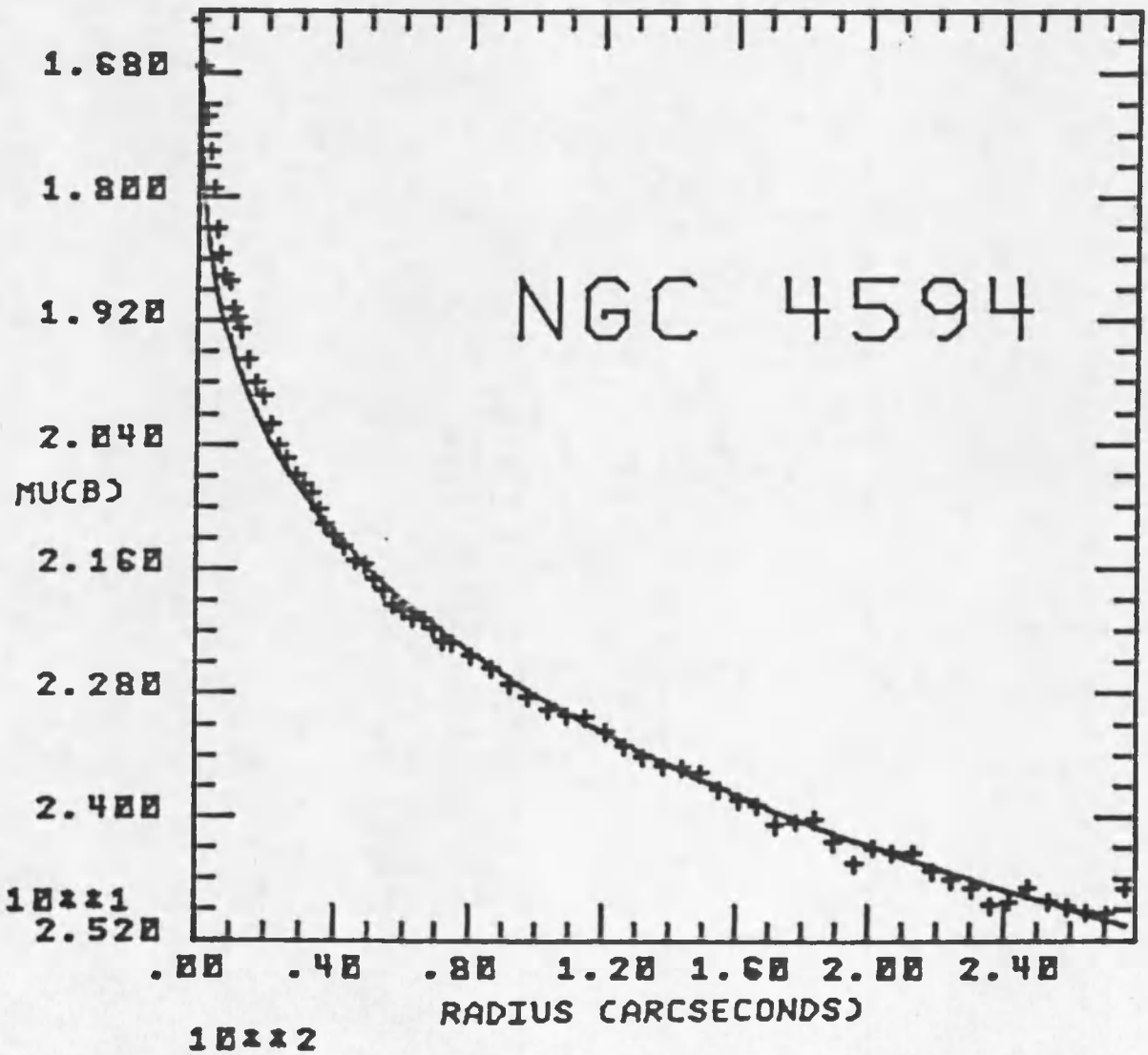

Figure 12.--Continued Elliptically averaged major axis profiles -- Surface brightness in magnitudes per square arcsecond in the B band versus radius in arcseconds is plotted for the north half of the minor axis of NGC 4594. Bulge fit is shown.

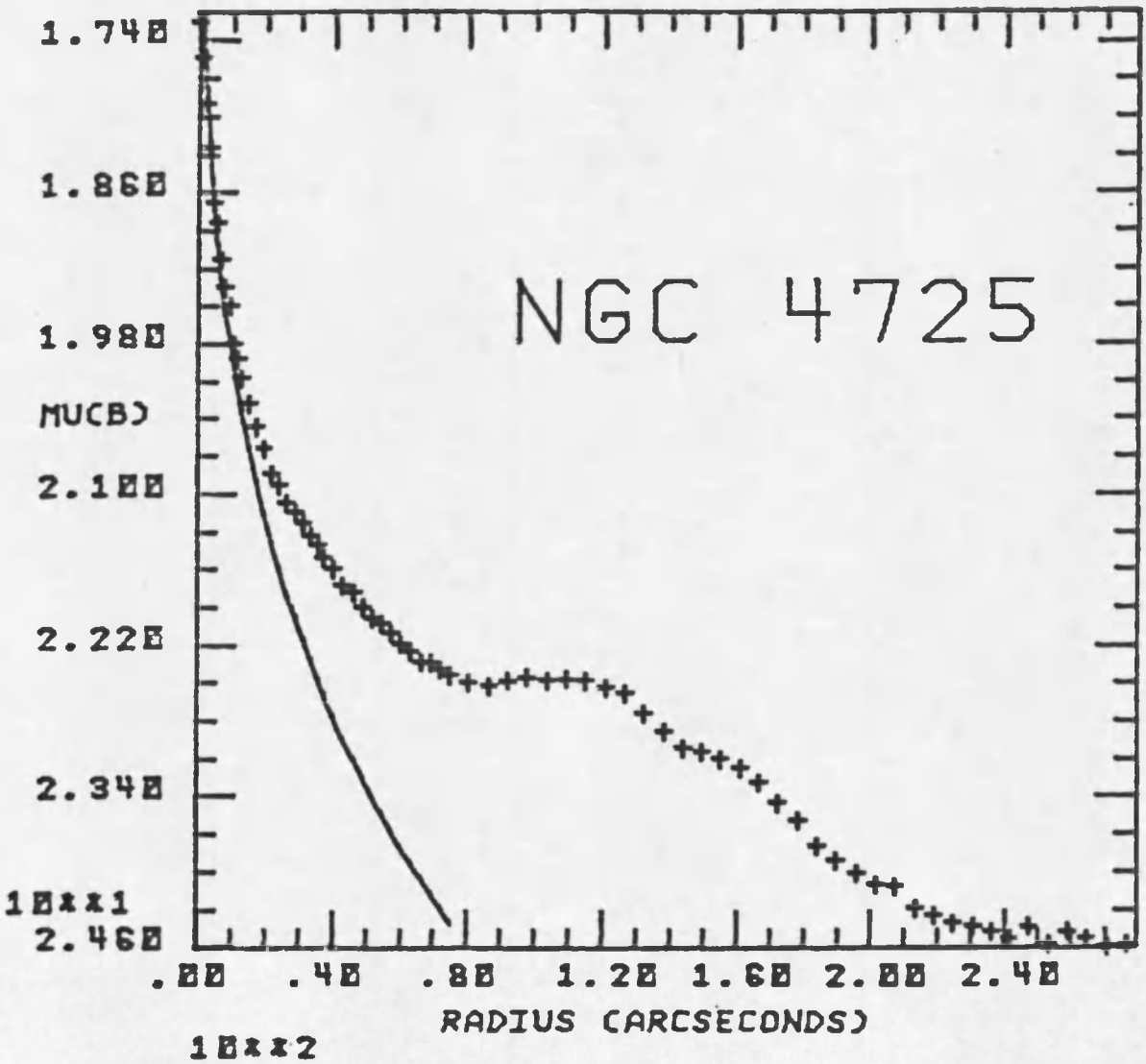

Figure 12.--Continued Elliptically averaged major axis profiles -- Surface brightness in magnitudes per square arcsecond in the B band versus radius in arcseconds is plotted for NGC 4725. Bulge fit is shown.

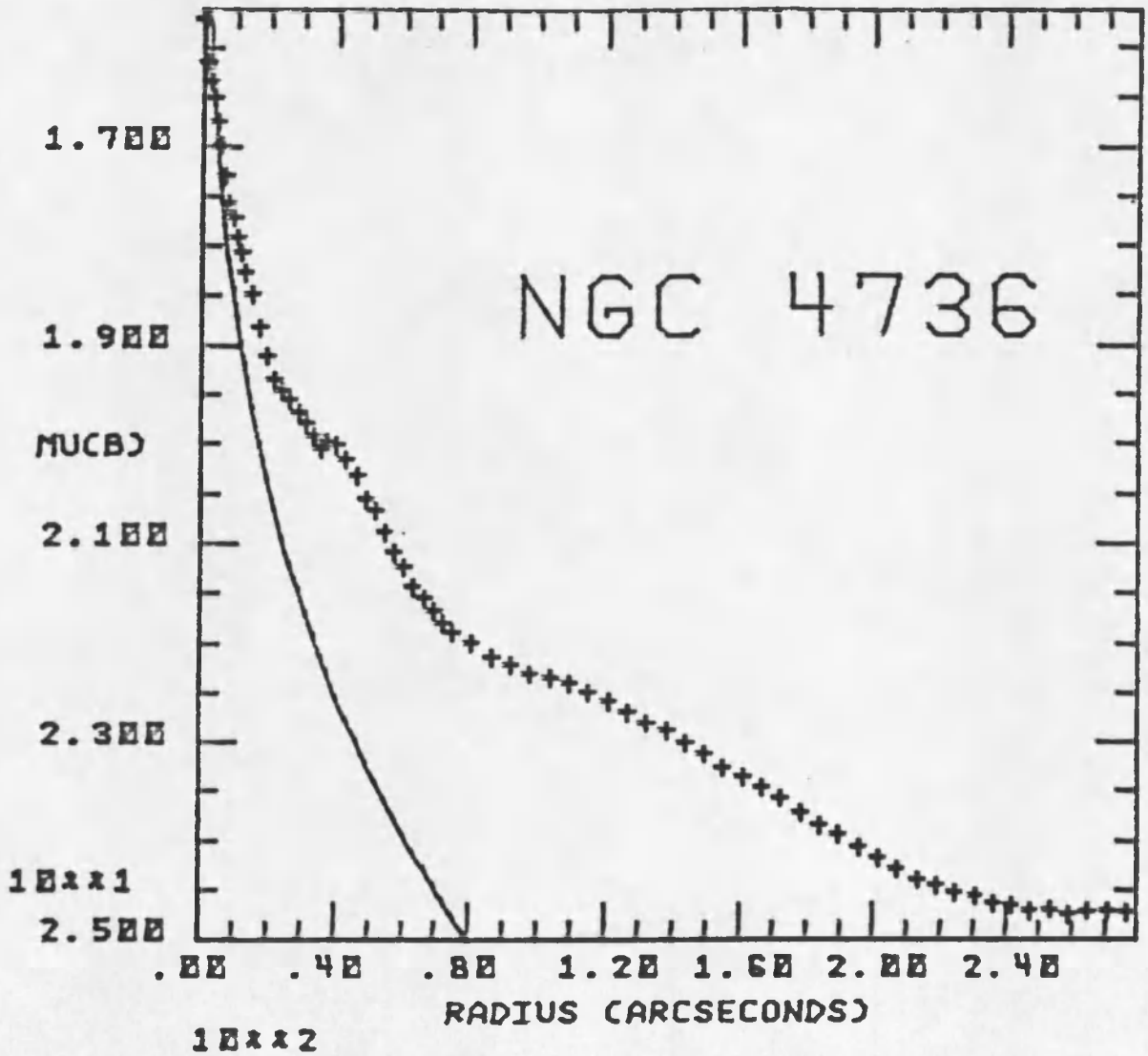

Figure 12.--Continued Elliptically averaged major axis profiles -- Surface brightness in magnitudes per square arcsecond in the B band versus radius in arcseconds is plotted for NGC 4736. Bulge fit is shown.

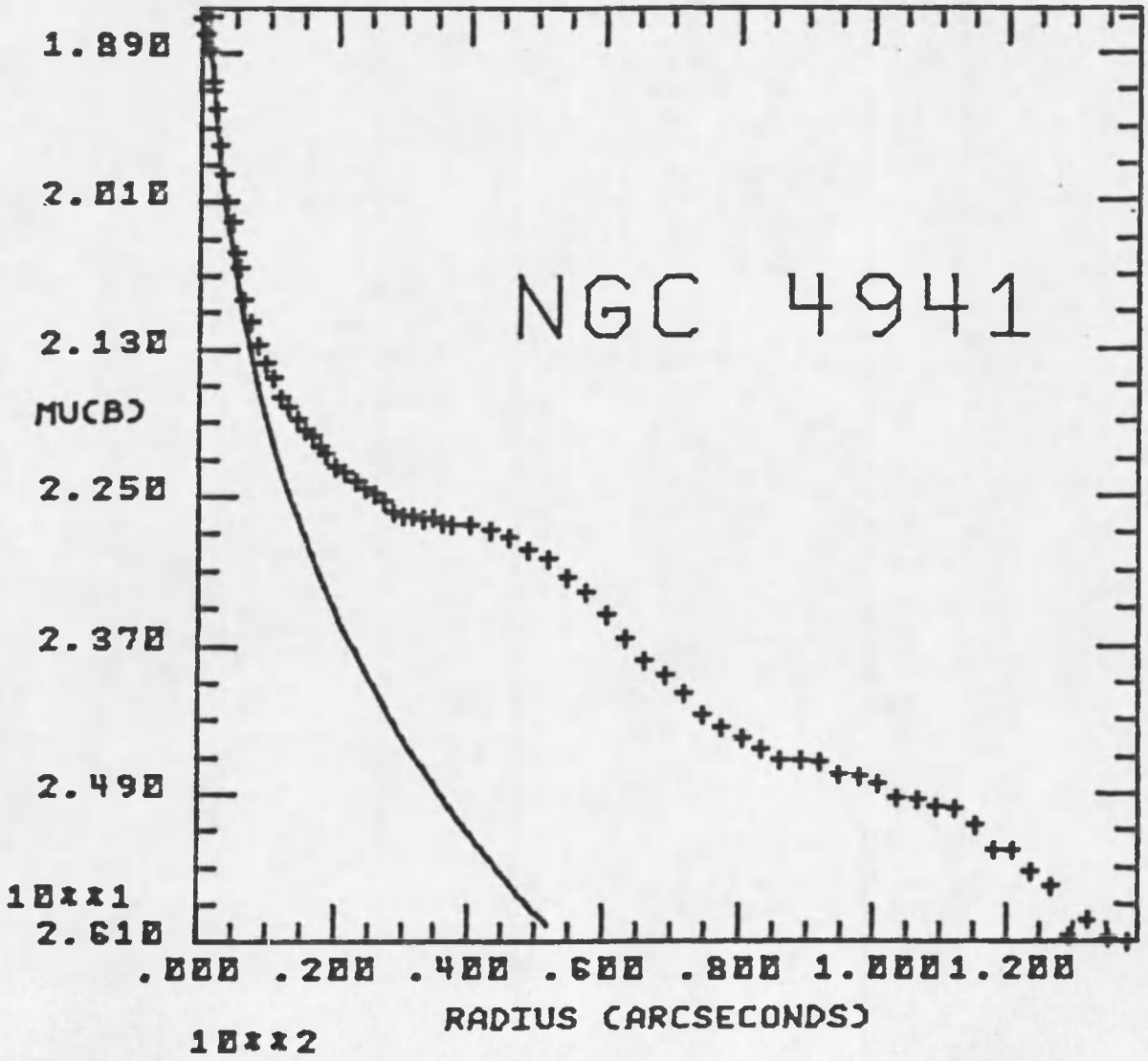

Figure 12.--Continued Elliptically averaged major axis profiles -- Surface brightness in magnitudes per square arcsecond in the B band versus radius in arcseconds is plotted for NGC 4941. Bulge fit is shown.

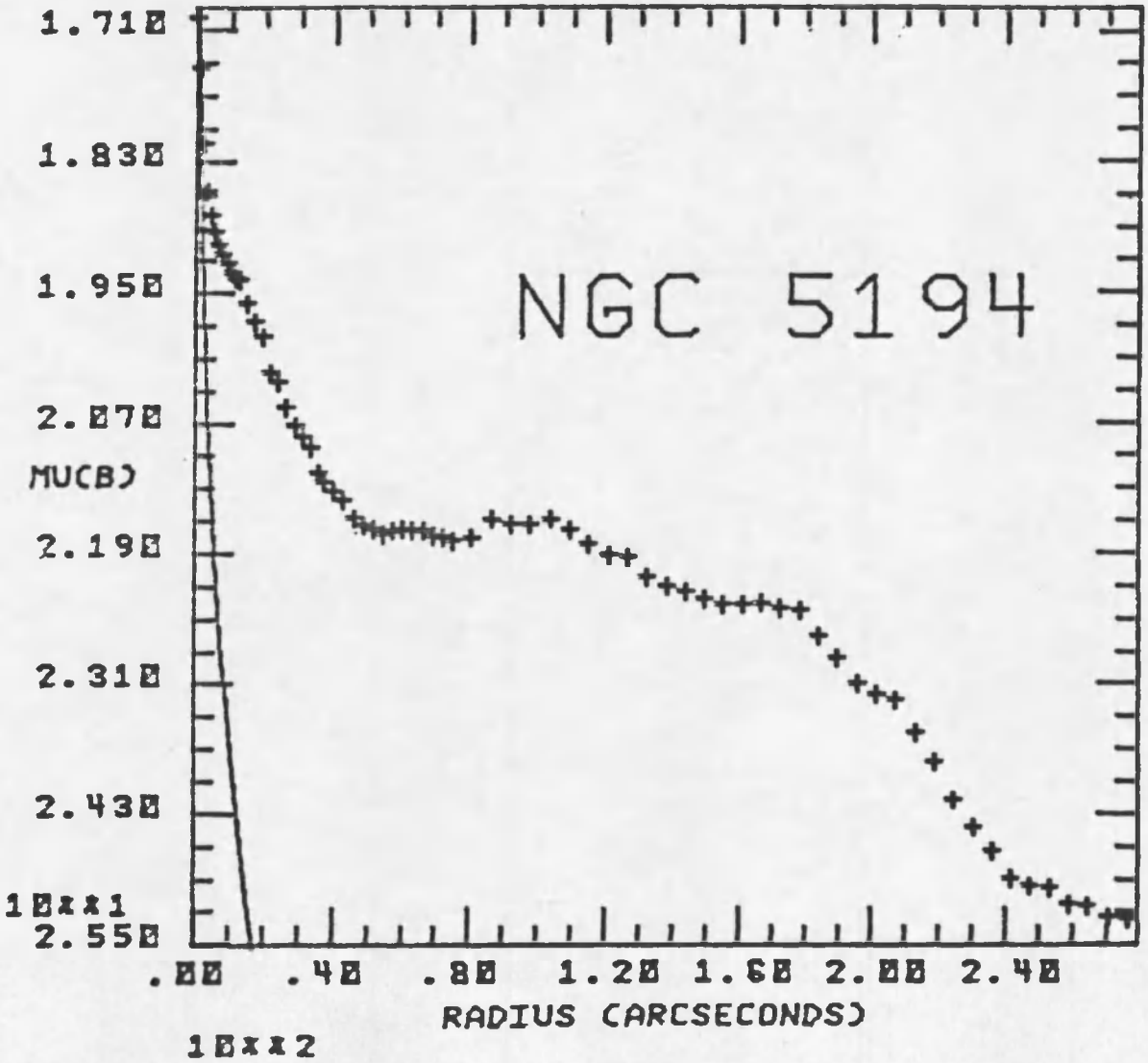

Figure 12.--Continued Elliptically averaged major axis profiles -- Surface brightness in magnitudes per square arcsecond in the B band versus radius in arcseconds is plotted for NGC 5194. Bulge fit is shown.

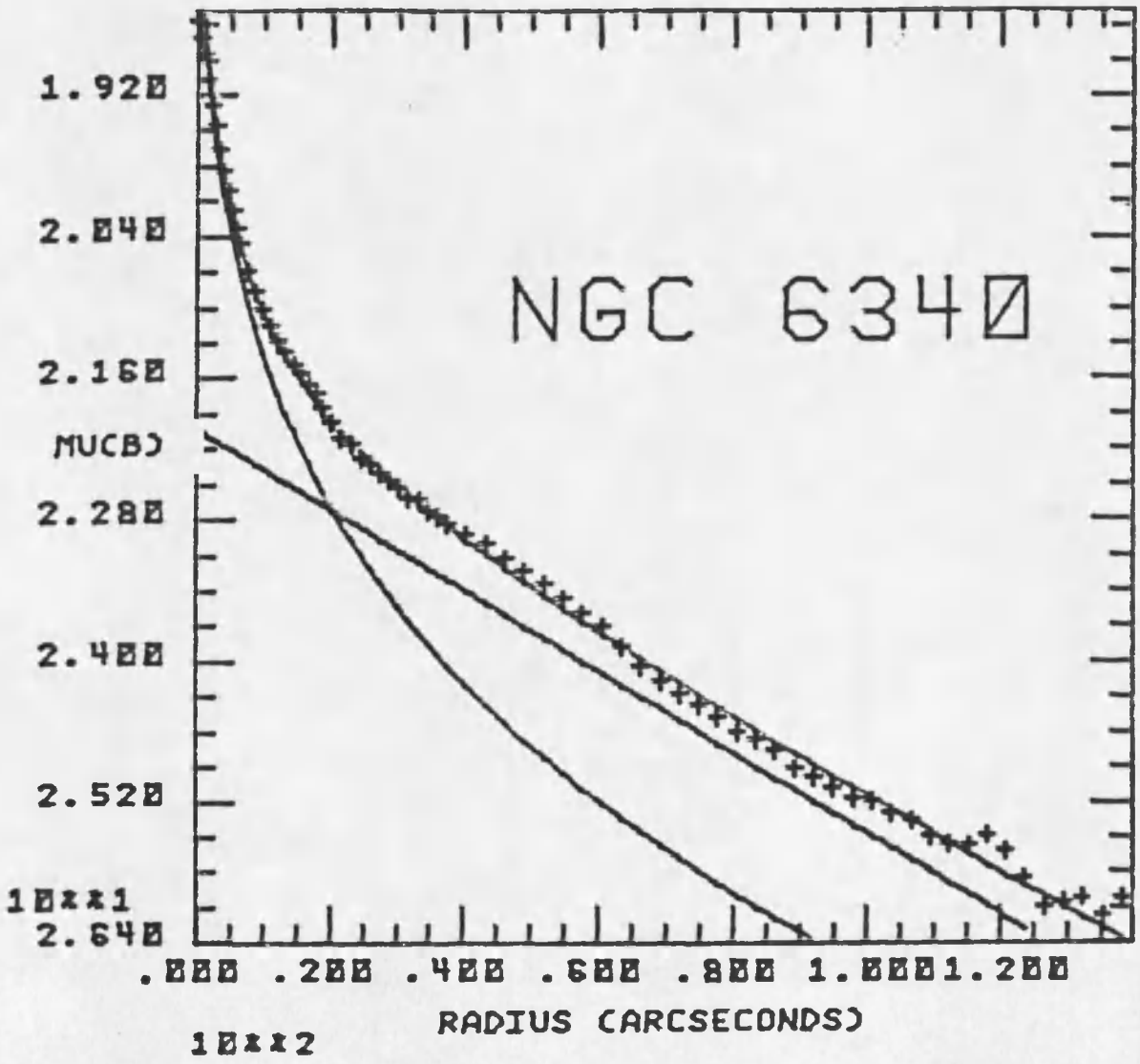

Figure 12.--Continued Elliptically averaged major axis profiles -- Surface brightness in magnitudes per square arcsecond in the B band versus radius in arcseconds is plotted for NGC 6340. Bulge and disk fits and their sum are shown.

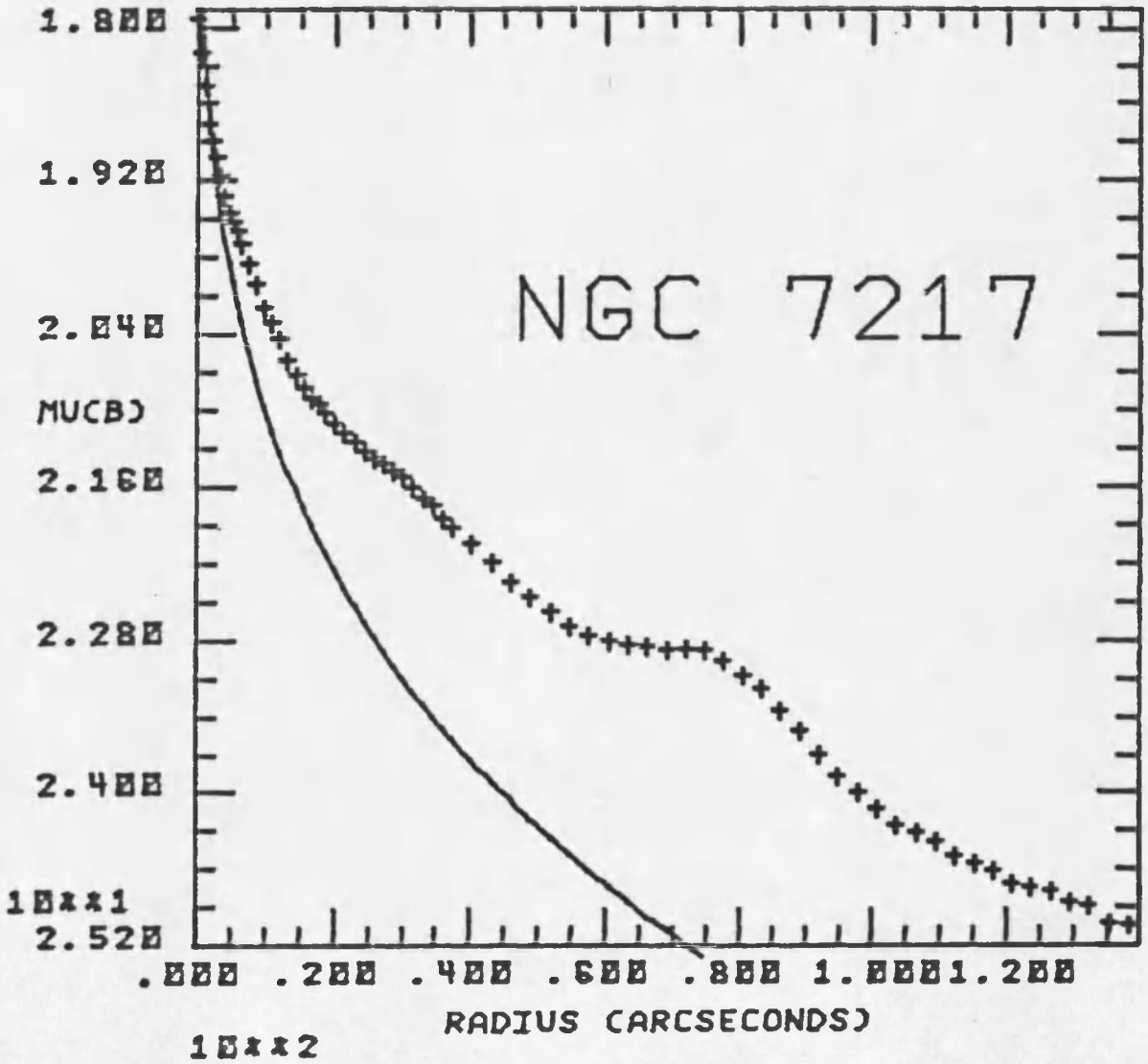

Figure 12.--Continued Elliptically averaged major axis profiles -- Surface brightness in magnitudes per square arcsecond in the B band versus radius in arcseconds is plotted for NGC 7217. Bulge fit is shown.

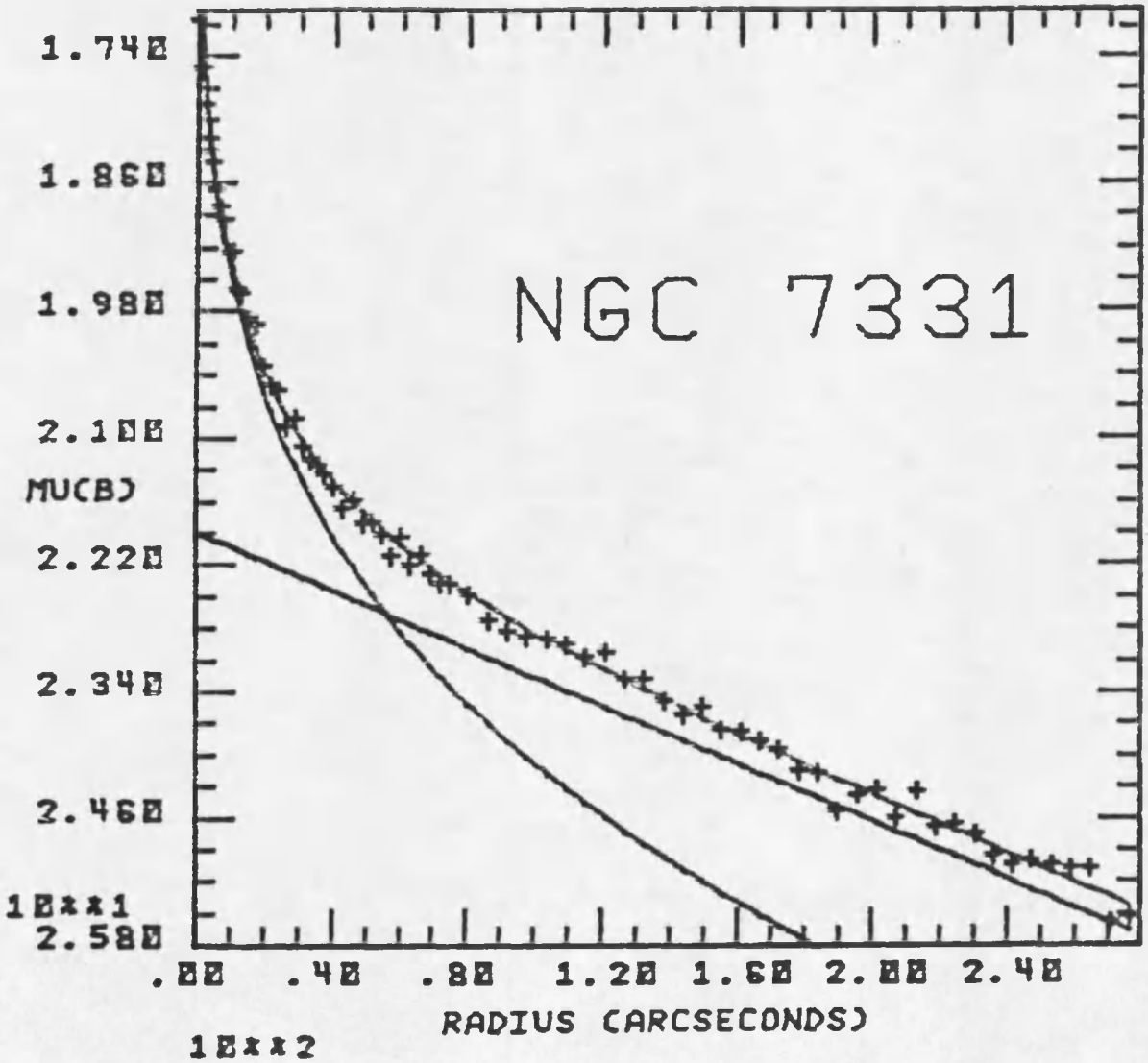

Figure 12.--Continued Elliptically averaged major axis profiles -- Surface brightness in magnitudes per square arcsecond in the B band versus radius in arcseconds is plotted for NGC 7331. Bulge and disk fits and their sum are shown.

Table 9. Elliptically Averaged Major Axis Profiles

Point no.	Surface brightness	Point no.	Surface brightness	Point no.	Surface brightness
NGC 488--1 pixel = 1.151 arcseconds:					
1	18.51	25	22.20	49	24.94
2	18.69	26	22.31	50	25.11
3	19.00	27	22.41	51	25.22
4	19.22	28	22.49	52	25.33
5	19.48	29	22.58	53	25.49
6	19.75	30	22.69	54	25.66
7	19.97	31	22.81	55	25.78
8	20.22	32	22.80	56	25.92
9	20.37	33	22.83	57	26.04
10	20.52	34	22.89	58	26.31
11	20.68	35	23.00	59	26.35
12	20.82	36	23.14	60	26.43
13	21.01	37	23.21	61	26.47
14	21.22	38	23.35	62	26.48
15	21.42	39	23.48	63	26.44
16	21.54	40	23.63	64	26.78
17	21.63	41	23.81	65	26.86
18	21.69	42	23.97	66	26.98
19	21.78	43	24.09	67	27.16
20	21.92	44	24.23	68	27.24
21	21.99	45	24.31	69	26.94
22	22.08	46	24.47	70	26.86
23	22.11	47	24.61	71	27.27
24	22.12	48	24.78	72	26.75
NGC 628--1 pixel = 1.151 arcseconds:					
1	19.59	25	22.48	49	23.84
2	19.72	26	22.49	50	23.89
3	19.95	27	22.52	51	23.98
4	20.21	28	22.60	52	24.09
5	20.42	29	22.65	53	24.18
6	20.61	30	22.67	54	24.30
7	20.73	31	22.68	55	24.39
8	20.84	32	22.68	56	24.42
9	20.94	33	22.73	57	24.47
10	21.05	34	22.79	58	24.54
11	21.17	35	22.85	59	24.57
12	21.31	36	22.86	60	24.64
13	21.50	37	22.96	61	24.71
14	21.61	38	23.00	62	24.75
15	21.77	39	23.00	63	24.84
16	21.94	40	23.05	64	24.98

Table 9.--Continued Elliptically Averaged Major Axis Profiles

Point no.	Surface brightness	Point no.	Surface brightness	Point no.	Surface brightness
17	22.02	41	23.16	65	25.03
18	22.09	42	23.30	66	25.15
19	22.19	43	23.37	67	25.24
20	22.25	44	23.44	68	25.31
21	22.30	45	23.50	69	25.29
22	22.31	46	23.58	70	25.35
23	22.38	47	23.68	71	25.48
24	22.42	48	23.78	72	25.60
NGC 1058--1 pixel = 0.575 arcseconds:					
1	19.37	25	21.88	49	24.97
2	19.55	26	21.94	50	25.08
3	19.90	27	22.01	51	25.22
4	19.90	28	22.11	52	25.32
5	20.25	29	22.22	53	25.38
6	20.50	30	22.34	54	25.42
7	20.69	31	22.40	55	25.46
8	20.82	32	22.47	56	25.46
9	20.96	33	22.54	57	25.47
10	21.07	34	22.62	58	25.68
11	21.19	35	22.73	59	25.70
12	21.33	36	22.84	60	25.75
13	21.51	37	23.03	61	25.80
14	21.58	38	23.15	62	25.77
15	21.60	39	23.30	63	25.98
16	21.60	40	23.43	64	26.14
17	21.63	41	23.54	65	26.04
18	21.68	42	23.71	66	26.05
19	21.74	43	23.89	67	26.13
20	21.77	44	24.13	68	26.19
21	21.82	45	24.37	69	26.04
22	21.85	46	24.59	70	26.12
23	21.84	47	24.71	71	26.28
24	21.85	48	24.84		
NGC 2268--1 pixel = 0.575 arcseconds:					
1	18.98	25	21.57	49	23.97
2	19.01	26	21.64	50	24.21
3	19.11	27	21.69	51	24.22
4	19.23	28	21.81	52	24.50
5	19.46	29	21.90	53	24.63
6	19.62	30	22.02	54	24.70
7	19.88	31	22.16	55	25.09

Table 9.--Continued Elliptically Averaged Major Axis Profiles

Point no.	Surface brightness	Point no.	Surface brightness	Point no.	Surface brightness
8	20.01	32	22.21	56	25.11
9	20.25	33	22.30	57	25.35
10	20.35	34	22.41	58	25.50
11	20.49	35	22.50	59	25.53
12	20.65	36	22.55	60	25.57
13	20.75	37	22.64	61	25.88
14	20.93	38	22.75	62	25.61
15	21.00	39	22.89	63	25.65
16	21.07	40	23.03	64	25.92
17	21.10	41	23.18	65	25.67
18	21.10	42	23.34	66	26.01
19	21.15	43	23.37	67	26.06
20	21.19	44	23.57	68	26.47
21	21.28	45	23.60	69	25.89
22	21.36	46	23.67	70	26.05
23	21.41	47	23.83	71	26.04
24	21.51	48	23.93	72	26.01
NGC 2336--1 pixel = 1.151 arcseconds:					
1	18.95	25	22.57	49	24.14
2	19.22	26	22.55	50	24.27
3	19.52	27	22.56	51	24.27
4	19.96	28	22.64	52	24.48
5	20.22	29	22.71	53	24.64
6	20.58	30	22.77	54	24.81
7	20.71	31	22.79	55	24.93
8	20.97	32	22.84	56	24.96
9	21.08	33	22.91	57	25.01
10	21.30	34	22.96	58	25.16
11	21.35	35	22.94	59	25.17
12	21.57	36	22.99	60	25.35
13	21.73	37	23.02	61	25.41
14	21.87	38	23.02	62	25.25
15	22.01	39	23.13	63	25.39
16	22.13	40	23.22	64	25.23
17	22.27	41	23.39	65	25.57
18	22.23	42	23.51	66	25.60
19	22.25	43	23.63	67	25.59
20	22.29	44	23.60	68	25.82
21	22.39	45	23.69	69	25.84
22	22.47	46	23.86	70	25.67
23	22.49	47	23.95	71	25.63
24	22.46	48	24.09	72	25.89

Table 9.--Continued Elliptically Averaged Major Axis Profiles

Point no.	Surface brightness	Point no.	Surface brightness	Point no.	Surface brightness
NGC 2344--1 pixel = 0.575 arcseconds:					
1	18.83	25	22.29	49	25.14
2	18.98	26	22.37	50	25.17
3	19.22	27	22.45	51	25.26
4	19.51	28	22.63	52	25.36
5	19.85	29	22.71	53	25.46
6	20.09	30	22.78	54	25.50
7	20.39	31	22.87	55	25.70
8	20.61	32	22.92	56	25.90
9	20.80	33	22.98	57	25.91
10	20.92	34	23.05	58	26.06
11	21.02	35	23.20	59	26.01
12	21.12	36	23.33	60	26.30
13	21.26	37	23.54	61	26.43
14	21.40	38	23.77	62	26.87
15	21.49	39	23.94	63	26.64
16	21.62	40	24.06	64	26.79
17	21.74	41	24.16	65	26.78
18	21.83	42	24.28	66	26.99
19	21.91	43	24.45	67	26.72
20	21.98	44	24.58	68	26.93
21	22.04	45	24.75	69	27.29
22	22.08	46	24.81	70	26.92
23	22.13	47	24.93	71	26.93
24	22.21	48	25.03	72	27.35
NGC 2655--1 pixel = 0.575 arcseconds:					
1	17.81	25	21.30	49	23.52
2	17.94	26	21.43	50	23.60
3	18.11	27	21.57	51	23.62
4	18.26	28	21.65	52	23.68
5	18.45	29	21.74	53	23.68
6	18.63	30	21.86	54	23.79
7	18.82	31	21.96	55	23.82
8	18.98	32	22.03	56	23.87
9	19.11	33	22.09	57	23.84
10	19.28	34	22.14	58	23.91
11	19.40	35	22.18	59	23.90
12	19.50	36	22.35	60	24.02
13	19.69	37	22.41	61	24.07
14	19.89	38	22.56	62	24.21
15	20.00	39	22.63	63	24.27
16	20.25	40	22.75	64	24.29

Table 9.--Continued Elliptically Averaged Major Axis Profiles

Point no.	Surface brightness	Point no.	Surface brightness	Point no.	Surface brightness
17	20.43	41	22.87	65	24.41
18	20.52	42	22.96	66	24.37
19	20.68	43	23.09	67	24.44
20	20.77	44	23.16	68	24.55
21	20.93	45	23.20	69	24.70
22	21.00	46	23.25	70	24.83
23	21.09	47	23.37	71	24.70
24	21.22	48	23.42	72	25.08
NGC 2681--1 pixel = 0.575 arcseconds:					
1	16.55	25	21.29	49	23.34
2	16.68	26	21.43	50	23.45
3	16.92	27	21.57	51	23.50
4	17.22	28	21.71	52	23.60
5	17.55	29	21.81	53	23.70
6	17.86	30	21.90	54	23.76
7	18.13	31	21.97	55	23.93
8	18.35	32	22.02	56	24.01
9	18.56	33	22.05	57	24.10
10	18.74	34	22.15	58	24.42
11	18.92	35	22.19	59	24.44
12	19.10	36	22.19	60	24.43
13	19.42	37	22.30	61	24.48
14	19.67	38	22.44	62	24.51
15	19.95	39	22.57	63	24.59
16	20.22	40	22.66	64	24.61
17	20.43	41	22.70	65	24.52
18	20.56	42	22.80	66	24.90
19	20.68	43	22.89	67	24.92
20	20.69	44	22.97	68	24.92
21	20.72	45	23.02	69	24.63
22	20.78	46	23.05	70	24.76
23	20.90	47	23.08	71	25.01
24	21.07	48	23.19	72	24.85
NGC 2775--1 pixel = 0.575 arcseconds:					
1	17.67	25	21.20	49	23.34
2	17.84	26	21.33	50	23.42
3	18.11	27	21.47	51	23.49
4	18.31	28	21.59	52	23.53
5	18.53	29	21.66	53	23.62
6	18.76	30	21.72	54	23.71
7	18.97	31	21.72	55	23.80

Table 9.--Continued Elliptically Averaged Major Axis Profiles

Point no.	Surface brightness	Point no.	Surface brightness	Point no.	Surface brightness
8	19.16	32	21.79	56	23.85
9	19.31	33	21.82	57	23.92
10	19.44	34	21.86	58	24.00
11	19.55	35	21.84	59	24.10
12	19.68	36	21.87	60	24.18
13	19.81	37	21.93	61	24.21
14	19.95	38	22.07	62	24.24
15	20.07	39	22.13	63	24.34
16	20.20	40	22.22	64	24.42
17	20.37	41	22.37	65	24.49
18	20.47	42	22.53	66	24.53
19	20.55	43	22.66	67	24.57
20	20.67	44	22.75	68	24.68
21	20.77	45	22.89	69	24.71
22	20.89	46	23.03	70	24.83
23	20.97	47	23.16	71	24.87
24	21.07	48	23.26	72	24.89
NGC 2841--1 pixel = 1.151 arcseconds:					
1	17.03	25	21.30	49	23.33
2	17.41	26	21.31	50	23.46
3	17.59	27	21.42	51	23.54
4	17.95	28	21.47	52	23.71
5	18.15	29	21.57	53	23.86
6	18.35	30	21.60	54	23.92
7	18.61	31	21.65	55	24.11
8	18.74	32	21.67	56	24.16
9	19.03	33	21.70	57	24.26
10	19.11	34	21.72	58	24.36
11	19.28	35	21.81	59	24.49
12	19.43	36	21.85	60	24.52
13	19.59	37	21.98	61	24.68
14	19.82	38	22.01	62	24.73
15	19.95	39	22.13	63	24.90
16	20.12	40	22.22	64	24.98
17	20.31	41	22.38	65	25.04
18	20.51	42	22.47	66	25.22
19	20.54	43	22.68	67	25.14
20	20.71	44	22.62	68	25.43
21	20.87	45	22.87	69	25.25
22	20.91	46	22.98	70	25.56
23	21.08	47	23.06	71	25.47
24	21.13	48	23.22	72	25.60

Table 9.--Continued Elliptically Averaged Major Axis Profiles

Point no.	Surface brightness	Point no.	Surface brightness	Point no.	Surface brightness
NGC 2855--1 pixel = 0.575 arcseconds:					
1	18.62	25	22.16	49	24.45
2	18.71	26	22.25	50	24.54
3	18.85	27	22.34	51	24.66
4	19.05	28	22.40	52	24.70
5	19.21	29	22.48	53	24.75
6	19.42	30	22.58	54	24.83
7	19.64	31	22.67	55	24.96
8	19.84	32	22.72	56	24.96
9	19.96	33	22.83	57	25.11
10	20.10	34	22.87	58	25.27
11	20.23	35	22.95	59	25.30
12	20.38	36	23.04	60	25.42
13	20.57	37	23.17	61	25.57
14	20.81	38	23.30	62	25.54
15	20.96	39	23.41	63	25.73
16	21.15	40	23.55	64	25.67
17	21.33	41	23.67	65	25.71
18	21.49	42	23.77	66	25.86
19	21.61	43	23.88	67	25.93
20	21.76	44	24.02	68	26.08
21	21.88	45	24.11	69	26.10
22	21.96	46	24.19	70	26.07
23	22.04	47	24.32	71	26.08
24	22.08	48	24.40	72	26.05
NGC 2967--1 pixel = 0.575 arcseconds:					
1	19.83	25	22.02	49	25.30
2	19.97	26	22.10	50	25.50
3	20.13	27	22.20	51	25.72
4	20.32	28	22.30	52	25.99
5	20.48	29	22.39	53	26.14
6	20.59	30	22.51	54	26.41
7	20.69	31	22.60	55	26.44
8	20.80	32	22.73	56	26.72
9	20.90	33	22.82	57	26.48
10	20.98	34	22.90	58	26.91
11	21.06	35	22.97	59	27.40
12	21.11	36	23.02	60	26.86
13	21.18	37	23.19	61	26.82
14	21.24	38	23.38	62	26.78
15	21.30	39	23.58	63	27.32
16	21.39	40	23.82	64	26.99
17	21.46	41	24.05	65	26.91

Table 9.--Continued Elliptically Averaged Major Axis Profiles

Point no.	Surface brightness	Point no.	Surface brightness	Point no.	Surface brightness
18	21.55	42	24.34	66	26.59
19	21.62	43	24.52	67	27.05
20	21.66	44	24.70	68	26.81
21	21.69	45	24.87	69	27.34
22	21.75	46	24.91	70	27.11
23	21.83	47	25.02	71	27.26
24	21.91	48	25.08	72	26.79
NGC 3147--1 pixel = 0.575 arcseconds:					
1	17.52	25	21.43	49	23.43
2	17.66	26	21.47	50	23.46
3	17.96	27	21.55	51	23.48
4	18.25	28	21.60	52	23.55
5	18.48	29	21.66	53	23.71
6	18.75	30	21.72	54	23.86
7	19.01	31	21.85	55	23.87
8	19.26	32	21.92	56	24.07
9	19.43	33	21.91	57	24.20
10	19.57	34	22.05	58	24.34
11	19.72	35	22.07	59	24.49
12	19.85	36	22.13	60	24.75
13	19.97	37	22.11	61	24.72
14	20.29	38	22.08	62	24.84
15	20.37	39	22.26	63	24.82
16	20.58	40	22.44	64	24.99
17	20.73	41	22.59	65	24.93
18	20.81	42	22.75	66	24.89
19	20.87	43	22.82	67	25.48
20	20.98	44	22.93	68	25.08
21	21.11	45	23.06	69	25.21
22	21.21	46	23.20	70	25.13
23	21.29	47	23.26	71	25.55
24	21.33	48	23.30	72	25.79
NGC 3277--1 pixel = 0.575 arcseconds:					
1	18.19	25	22.26	49	24.75
2	18.26	26	22.38	50	24.84
3	18.48	27	22.49	51	25.04
4	18.75	28	22.63	52	25.11
5	19.03	29	22.67	53	25.10
6	19.30	30	22.81	54	25.04
7	19.57	31	22.98	55	25.17
8	19.76	32	23.09	56	25.20

Table 9.--Continued Elliptically Averaged Major Axis Profiles

Point no.	Surface brightness	Point no.	Surface brightness	Point no.	Surface brightness
9	19.87	33	23.21	57	25.28
10	20.01	34	23.26	58	25.46
11	20.12	35	23.38	59	25.49
12	20.24	36	23.50	60	25.44
13	20.35	37	23.64	61	25.48
14	20.52	38	23.79	62	25.42
15	20.62	39	23.88	63	25.60
16	20.80	40	23.97	64	25.62
17	21.00	41	24.06	65	25.90
18	21.23	42	24.18	66	25.78
19	21.40	43	24.27	67	25.77
20	21.54	44	24.38	68	25.91
21	21.74	45	24.49	69	25.77
22	21.88	46	24.58	70	25.81
23	22.05	47	24.67	71	26.03
24	22.15	48	24.74	72	25.95
NGC 3368--1 pixel = 1.151 arcseconds:					
1	17.47	25	21.30	49	23.70
2	17.80	26	21.37	50	23.75
3	18.16	27	21.44	51	23.79
4	18.35	28	21.50	52	23.95
5	18.63	29	21.53	53	23.99
6	18.78	30	21.62	54	24.06
7	18.96	31	21.68	55	24.12
8	19.15	32	21.75	56	24.16
9	19.34	33	21.81	57	24.22
10	19.48	34	21.87	58	24.39
11	19.62	35	22.00	59	24.43
12	19.75	36	22.12	60	24.52
13	19.91	37	22.39	61	24.63
14	20.07	38	22.64	62	24.60
15	20.25	39	22.82	63	24.84
16	20.40	40	22.99	64	24.88
17	20.50	41	23.13	65	24.96
18	20.62	42	23.22	66	25.06
19	20.73	43	23.35	67	25.09
20	20.84	44	23.44	68	25.18
21	20.93	45	23.50	69	25.22
22	21.05	46	23.57	70	25.32
23	21.10	47	23.57	71	25.36
24	21.19	48	23.65	72	25.55

Table 9.--Continued Elliptically Averaged Major Axis Profiles

Point no.	Surface brightness	Point no.	Surface brightness	Point no.	Surface brightness
NGC 3642--1 pixel = 1.151 arcseconds:					
1	18.35	25	23.08	49	25.13
2	18.76	26	23.19	50	25.04
3	19.46	27	23.31	51	25.14
4	19.90	28	23.47	52	25.16
5	20.20	29	23.60	53	25.23
6	20.47	30	23.77	54	25.24
7	20.68	31	23.88	55	25.30
8	20.80	32	24.03	56	25.34
9	20.91	33	24.20	57	25.45
10	21.00	34	24.38	58	25.64
11	21.09	35	24.43	59	25.77
12	21.21	36	24.48	60	25.89
13	21.44	37	24.51	61	25.82
14	21.63	38	24.54	62	25.76
15	21.80	39	24.57	63	25.95
16	22.00	40	24.62	64	25.74
17	22.19	41	24.68	65	25.89
18	22.30	42	24.67	66	25.89
19	22.40	43	24.73	67	25.85
20	22.50	44	24.89	68	26.10
21	22.64	45	25.08	69	25.94
22	22.77	46	25.08	70	26.05
23	22.91	47	25.13	71	26.00
24	22.96	48	25.24	72	26.14
NGC 3898--1 pixel = 0.575 arcseconds:					
1	17.42	25	21.32	49	23.66
2	17.54	26	21.42	50	23.72
3	17.62	27	21.58	51	23.79
4	17.78	28	21.66	52	23.83
5	17.92	29	21.75	53	23.93
6	18.12	30	21.87	54	23.92
7	18.31	31	21.91	55	24.13
8	18.58	32	22.00	56	24.15
9	18.70	33	22.11	57	24.24
10	18.87	34	22.13	58	24.35
11	19.06	35	22.24	59	24.44
12	19.24	36	22.30	60	24.53
13	19.41	37	22.36	61	24.49
14	19.68	38	22.55	62	24.53
15	19.81	39	22.62	63	24.59
16	20.00	40	22.70	64	24.78

Table 9.--Continued Elliptically Averaged Major Axis Profiles

Point no.	Surface brightness	Point no.	Surface brightness	Point no.	Surface brightness
17	20.20	41	22.83	65	24.79
18	20.38	42	22.93	66	24.90
19	20.47	43	23.00	67	24.92
20	20.68	44	23.11	68	24.93
21	20.78	45	23.23	69	25.06
22	20.94	46	23.32	70	24.91
23	21.01	47	23.38	71	24.94
24	21.18	48	23.48	72	25.12
NGC 4378--1 pixel = 0.575 arcseconds:					
1	18.58	25	22.12	49	24.37
2	18.62	26	22.25	50	24.36
3	18.78	27	22.38	51	24.33
4	18.93	28	22.50	52	24.32
5	19.05	29	22.62	53	24.33
6	19.22	30	22.71	54	24.39
7	19.40	31	22.79	55	24.50
8	19.58	32	22.88	56	24.65
9	19.74	33	22.94	57	24.84
10	19.87	34	23.02	58	25.10
11	20.00	35	23.06	59	25.32
12	20.15	36	23.18	60	25.45
13	20.36	37	23.32	61	25.49
14	20.61	38	23.46	62	25.64
15	20.81	39	23.62	63	25.82
16	20.94	40	23.79	64	26.11
17	21.09	41	23.89	65	26.04
18	21.23	42	23.99	66	25.96
19	21.38	43	24.05	67	25.93
20	21.52	44	24.06	68	26.04
21	21.67	45	24.14	69	26.26
22	21.74	46	24.22	70	26.23
23	21.87	47	24.28	71	26.41
24	21.99	48	24.33	72	26.71
NGC 4594, north half of minor axis--1 pixel = 1.151 arcseconds:					
1	16.28	25	21.37	49	23.57
2	16.73	26	21.51	50	23.73
3	17.21	27	21.55	51	23.83
4	17.55	28	21.68	52	23.88
5	17.92	29	21.79	53	24.08
6	18.30	30	21.94	54	24.03
7	18.54	31	21.98	55	23.99
8	18.75	32	22.05	56	24.23

Table 9.--Continued Elliptically Averaged Major Axis Profiles

Point no.	Surface brightness	Point no.	Surface brightness	Point no.	Surface brightness
9	18.80	33	22.07	57	24.45
10	19.08	34	22.16	58	24.29
11	19.16	35	22.29	59	24.34
12	19.27	36	22.30	60	24.34
13	19.56	37	22.43	61	24.51
14	19.79	38	22.55	62	24.59
15	19.91	39	22.70	63	24.69
16	20.20	40	22.84	64	24.85
17	20.40	41	22.94	65	24.81
18	20.54	42	23.01	66	24.67
19	20.69	43	23.02	67	24.80
20	20.77	44	23.16	68	24.86
21	20.85	45	23.30	69	24.91
22	21.03	46	23.41	70	24.94
23	21.15	47	23.49	71	24.69
24	21.27	48	23.52	72	24.77
NGC 4725--1 pixel = 1.151 arcseconds:					
1	17.23	25	21.71	49	23.03
2	17.52	26	21.77	50	23.09
3	17.89	27	21.89	51	23.15
4	18.23	28	21.97	52	23.28
5	18.66	29	22.02	53	23.43
6	18.82	30	22.09	54	23.58
7	19.11	31	22.18	55	23.79
8	19.33	32	22.24	56	23.89
9	19.48	33	22.31	57	24.00
10	19.78	34	22.32	58	24.10
11	19.90	35	22.37	59	24.11
12	20.06	36	22.43	60	24.27
13	20.26	37	22.48	61	24.34
14	20.45	38	22.51	62	24.39
15	20.62	39	22.47	63	24.42
16	20.82	40	22.44	64	24.47
17	20.92	41	22.47	65	24.52
18	21.06	42	22.45	66	24.42
19	21.13	43	22.46	67	24.57
20	21.21	44	22.52	68	24.47
21	21.32	45	22.57	69	24.53
22	21.39	46	22.73	70	24.58
23	21.50	47	22.86	71	24.56
24	21.58	48	23.00	72	24.66

Table 9.--Continued Elliptically Averaged Major Axis Profiles

Point no.	Surface brightness	Point no.	Surface brightness	Point no.	Surface brightness
NGC 4736--1 pixel = 1.151 arcseconds:					
1	15.69	25	20.14	49	23.11
2	16.13	27	20.30	50	23.26
3	16.33	27	20.54	51	23.34
4	16.49	28	20.66	52	23.46
5	16.72	29	20.87	53	23.56
6	16.97	30	21.08	54	23.71
7	17.27	31	21.23	55	23.83
8	17.56	32	21.42	56	23.93
9	17.70	33	21.53	57	24.05
10	17.90	34	21.66	58	24.16
11	18.06	35	21.78	59	24.29
12	18.25	36	21.88	60	24.38
13	18.48	37	21.99	61	24.45
14	18.81	38	22.13	62	24.53
15	19.10	39	22.20	63	24.56
16	19.33	40	22.29	64	24.62
17	19.44	41	22.35	65	24.65
18	19.54	42	22.39	66	24.70
19	19.66	43	22.49	67	24.69
20	19.78	44	22.58	68	24.73
21	19.89	45	22.68	69	24.71
22	20.03	46	22.79	70	24.70
23	19.96	47	22.88	71	24.72
24	20.00	48	22.99	72	24.81
NGC 4941--1 pixel = 0.575 arcseconds:					
1	18.61	25	22.30	49	24.25
2	18.74	26	22.37	50	24.35
3	18.86	27	22.42	51	24.45
4	19.12	28	22.47	52	24.53
5	19.34	29	22.53	53	24.63
6	19.64	30	22.61	54	24.62
7	19.87	31	22.64	55	24.63
8	20.09	32	22.64	56	24.73
9	20.26	33	22.68	57	24.75
10	20.50	34	22.66	58	24.81
11	20.63	35	22.70	59	24.93
12	20.88	36	22.72	60	24.94
13	21.07	37	22.72	61	25.01
14	21.26	38	22.77	62	25.03
15	21.40	39	22.83	63	25.16
16	21.53	40	22.92	64	25.35
17	21.69	41	23.00	65	25.35

Table 9.--Continued Elliptically Averaged Major Axis Profiles

Point no.	Surface brightness	Point no.	Surface brightness	Point no.	Surface brightness
18	21.77	42	23.14	66	25.54
19	21.87	43	23.26	67	25.65
20	21.95	44	23.44	68	26.05
21	21.99	45	23.63	69	25.92
22	22.08	46	23.82	70	26.06
23	22.15	47	23.94	71	26.10
24	22.24	48	24.07	72	26.31
NGC 5194--1 pixel = 1.151 arcseconds:					
1	16.96	25	21.40	49	22.33
2	17.43	26	21.57	50	22.37
3	18.12	27	21.64	51	22.37
4	18.55	28	21.67	52	22.35
5	18.77	29	21.72	53	22.40
6	18.93	30	21.69	54	22.42
7	19.05	31	21.67	55	22.65
8	19.13	32	21.67	56	22.85
9	19.21	33	21.68	57	23.09
10	19.29	34	21.73	58	23.19
11	19.34	35	21.75	59	23.24
12	19.36	36	21.78	60	23.55
13	19.58	37	21.74	61	23.82
14	19.75	38	21.57	62	24.16
15	19.89	39	21.63	63	24.42
16	20.22	40	21.62	64	24.65
17	20.30	41	21.59	65	24.89
18	20.54	42	21.68	66	24.96
19	20.71	43	21.82	67	24.98
20	20.82	44	21.91	68	25.12
21	20.91	45	21.93	69	25.14
22	21.14	46	22.11	70	25.25
23	21.23	47	22.19	71	25.25
24	21.30	48	22.25	72	25.18
NGC 6340--1 pixel = 0.575 arcseconds:					
1	18.55	25	22.10	49	24.35
2	18.70	26	22.14	50	24.47
3	18.84	27	22.27	51	24.59
4	19.06	28	22.31	52	24.65
5	19.27	29	22.39	53	24.75
6	19.45	30	22.45	54	24.90
7	19.64	31	22.52	55	24.97
8	19.83	32	22.61	56	25.07

Table 9.--Continued Elliptically Averaged Major Axis Profiles

Point no.	Surface brightness	Point no.	Surface brightness	Point no.	Surface brightness
9	20.00	33	22.62	57	25.16
10	20.17	34	22.73	58	25.17
11	20.33	35	22.77	59	25.28
12	20.45	36	22.83	60	25.35
13	20.68	37	22.91	61	25.49
14	20.86	38	23.00	62	25.55
15	21.01	39	23.12	63	25.56
16	21.15	40	23.23	64	25.47
17	21.28	41	23.34	65	25.60
18	21.36	42	23.47	66	25.84
19	21.47	43	23.59	67	26.09
20	21.55	44	23.69	68	26.04
21	21.63	45	23.86	69	26.01
22	21.71	46	24.03	70	26.16
23	21.84	47	24.15	71	26.00
24	21.97	48	24.26	72	26.00
NGC 7217--1 pixel = 0.575 arcseconds:					
1	17.92	25	21.17	49	22.87
2	18.20	26	21.25	50	22.96
3	18.45	27	21.32	51	23.07
4	18.75	28	21.37	52	23.18
5	18.89	29	21.42	53	23.34
6	19.01	30	21.48	54	23.51
7	19.15	31	21.52	55	23.69
8	19.31	32	21.59	56	23.86
9	19.44	33	21.68	57	24.00
10	19.52	34	21.75	58	24.12
11	19.58	35	21.85	59	24.25
12	19.68	36	21.92	60	24.31
13	19.84	37	22.05	61	24.38
14	19.99	38	22.19	62	24.49
15	20.19	39	22.34	63	24.56
16	20.30	40	22.46	64	24.60
17	20.43	41	22.58	65	24.71
18	20.59	42	22.69	66	24.74
19	20.71	43	22.76	67	24.77
20	20.82	44	22.81	68	24.85
21	20.89	45	22.84	69	24.88
22	20.95	46	22.85	70	25.02
23	21.01	47	22.87	71	25.04
24	21.10	48	22.86	72	24.98

Table 9.--Continued Elliptically Averaged Major Axis Profiles

Point no.	Surface brightness	Point no.	Surface brightness	Point no.	Surface brightness
NGC 7331--1 pixel = 1.151 arcseconds:					
1	17.03	25	21.65	49	23.51
2	17.51	26	21.57	50	23.74
3	17.85	27	21.80	51	23.76
4	18.17	28	21.78	52	23.85
5	18.41	29	21.90	53	23.93
6	18.65	30	22.10	54	24.14
7	18.82	31	21.91	55	24.15
8	18.93	32	22.20	56	24.51
9	19.24	33	22.09	57	24.36
10	19.23	34	22.28	58	24.30
11	19.59	35	22.36	59	24.59
12	19.62	36	22.36	60	24.32
13	19.86	37	22.47	61	24.68
14	19.92	38	22.70	62	24.64
15	20.31	39	22.81	63	24.75
16	20.49	40	22.87	64	24.94
17	20.53	41	22.88	65	25.04
18	20.88	42	22.92	66	24.99
19	20.80	43	23.05	67	25.04
20	21.07	44	23.00	68	25.08
21	21.19	45	23.27	69	25.07
22	21.24	46	23.27	70	25.57
23	21.32	47	23.46	71	25.52
24	21.45	48	23.61	72	25.49

iterative scheme represents a great step forward. The procedure is as follows. First, two ranges of radii are chosen, one in which the disk clearly dominates the profile, and one in which the bulge is contributing most of the light. Then, the disk fitting function is fit by least squares to the data within the disk-dominated fitting range. This calculated disk contribution is then subtracted from the observed data points at all radii and these corrected data are fit to the bulge fitting function in the range dominated by bulge light. This fit is then subtracted from the original observed profile, and the process is repeated until it converges, usually after several iterations.

This technique has several advantages over the obvious alternative methods. First, it successfully accounts for the contribution of the component which does not dominate in each range. Second, since no information is derived from the range in which neither component strongly dominates, a comparison of the observed data there with the sum of the two calculated components indicates with what success the fitting functions can be extrapolated. Third, the iterative technique allows different fitting ranges to be used for the two components. This is in contrast to a non-linear least squares fit of the data to the sum of the two fitting functions.

In view of the fact that profiles have been derived here at a number of different position angles around each galaxy, a new method, based on the iterative scheme, was invented to make use of as much information as possible. As in previous studies, the decision was made to use a de Vaucouleurs law for the bulge and a radial exponential for the disk. In terms of magnitudes the de Vaucouleurs law is given by:

$$\mu = \mu_e + 8.325\ ((r/r_e)^{1/4} - 1)$$

where r_e is the effective radius inside of which half of the light is contained and μ_e is the surface brightness at r_e. The exponential disk is given by:

$$\mu = \mu_o + 1.0857\ r/r_o$$

where r_o is the scale length of the exponential and μ_o is the central surface brightness in magnitudes per square arcsecond.

Now each radial profile at a different angle could be decomposed independent of all the rest, but we know that all the disk fits and bulge fits must join at the center, at r = 0. This constraint implies that μ_e and μ_o must be the same for all profiles from each galaxy. Thus, if all the profiles are used to derive the best values for μ_e and μ_o, we can then apply the iterative technique to each profile separately, holding the scale surface brightnesses at the determined values and solving only for the scale length of each component. These scale lengths as a function of angle represent ellipses, one for the disk and one for the bulge. The values can be fit to ellipses, using the relation:

$$r = \sqrt{r_{maj}^2\ \cos^2(\theta - \theta_o) + r_{min}^2\ \sin^2(\theta - \theta_o)}$$

where r_{maj} and r_{min} are the major and minor axis scale lengths and θ_o is the position angle of the major axis on the sky. From this fit, then, the face-on (major axis) scale lengths of the disk and bulge, the inclination of the galaxy (assuming the disk to be thin and round), and the apparent flattening of the bulge can be determined. The

inclination of the disk and the apparent flattening of the bulge are expected to be much more accurately determined than could be achieved by merely measuring ratios of apparent radii because much more information has been utilized.

This procedure has been followed for each of the galaxies which appears to have an exponential disk. Specifically, the elliptically averaged major axis profiles have been iteratively decomposed to find the disk central surface brightness and the bulge effective surface brightness for each galaxy. The disk profile, bulge profile, and sum for each galaxy are shown on the plot of elliptically averaged major axis profile for each galaxy (Figure 12). Then, each single radial profile was combined with the profile 180° around the galaxy, and the 18 resulting profiles were iteratively decomposed, holding the scale surface brightnesses at the values previously determined. This procedure yields the parameters listed in Table 10. The disk central surface brightness, now called $B(0)_c$ has been corrected for galactic extinction using the A_B values given in de Vaucouleurs et al. (1976) and for the inclination of the disk:

$$B(0)_c = \mu_o - A_B + 2.5 \log(\cos i).$$

The disk scale length, r_o, is given in kpc, using the distances given in Chapter I. For those galaxies not included in the table in Chapter I, the distances used are given in the last column of Table 11. The bulge effective surface brightnesses have been corrected for galactic absorption only, and the mean bulge scale lengths $\langle r_e \rangle$, are the geometric means of the major and minor axis scale lengths in kpc.

Table 10. Parameters of Decomposed Spiral Galaxies

NGC	$B(0)_c$	r_0 (kpc)	B_e	r_e (kpc)	Inclination	$(b/a)_{B,TRUE}$	P.A.
488	21.32	7.71	20.15	1.09	39.8	0.72	7.5
628	21.70	5.07	23.23	1.51	10.6		5.8
2268	21.07	5.10	20.92	0.92	55.3	0.89	65.9
2336	21.86	12.58	18.86	0.40	56.9	0.80	172.5
2344	22.28	2.35	23.06	1.51	36.9		154.7
2655	22.48	8.91	21.55	3.40	33.8		16.7
2681	21.25	3.13	19.42	0.59	21.6		160.5
2775	22.21	3.54	22.45	2.29	44.4	0.80	163.3
2841	21.26	5.40	20.10	0.94	65.1	0.63	149.6
2855	22.71	4.95	22.46	1.54	44.3	0.70	128.4
2967	20.48	2.57	17.39	0.06	25.8		136.4
3147	20.75	6.25	20.74	1.72	35.9		144.4
3898	23.14	4.83	20.89	1.06	66.6	0.67	109.5
4594			23.40	14.18		0.71	
6340	21.73	5.16	22.62	3.83	24.2		138.7
7331	22.67	8.61	21.32	2.55	72.0	0.46	170.8

Table 11. Derived Overall Parameters of Program Spirals

NGC	M_B	B/D	$(M_O^T)_c$	$(B/D)_c$	
488	-20.00	0.21	-21.44	0.36	
628	-17.63	0.08	-19.05	0.37	
1058	-15.82	0.10	-16.96	0.54	D = 10.2 mpc
2268	-18.87	0.14	-19.98	0.56	
2336	-19.14	0.06	-20.78	0.28	
2344	-16.77	0.28	-17.71	0.73	
2655	-21.07	1.24	-21.30	4.21	
2681	-19.40	0.69	-19.82	2.13	
2775	-19.32	1.22	-19.61	3.28	
2841	-19.74	0.32	-20.67	0.74	
2855	-19.52	1.19	-19.87	2.65	
2967	-16.62	0.04	-18.97	0.13	D = 30.2 mpc
3147	-20.41	0.28	-21.36	0.72	
3277	-18.81	1.51	-18.98	6.03	
3368	-19.23	0.77	-19.81	1.71	
3642	-18.84	0.16	-19.32	1.78	
3898	-19.21	1.39	-19.45	3.98	
4378	-20.79				
4594	-22.63				
4725	-19.74	0.23	-20.72	0.68	
4736	-18.35	0.28	-19.26	0.76	
4941	-16.67	0.08	-18.92	0.14	D = 15.7 mpc
5194	-15.88	0.01	-19.58	0.03	
6340	-20.26	0.88	-20.65	2.33	
7217	-19.50	0.39	-20.39	0.79	
7331	-20.67	1.10	-20.79	8.24	D = 17.0 mpc

Inclinations are determined by the formula:

$$i = \cos^{-1} (b/a)_D$$

where $(b/a)_D$ is the ratio of the minor to major axis of the disk, as determined by the ellipse which has been fit to the scale lengths. The column labeled $(b/a)_{B,TRUE}$ shows the true bulge flattening, determined by:

$$(b/a)_{B,TRUE} = \sqrt{\frac{(b/a)^2_{B,OBS} - 1}{\cos^2 i} + 1}$$

The position angles listed in the table correspond to both the bulge and the disk when they agree and only to the disk when they do not. The angles are measured north through east. No $(b/a)_{B,TRUE}$ was calculated for those galaxies in which the position angles of the bulge and disk disagreed (NGC's 2344, 2655, 2681, 3147, and 6340) or when the galaxy was almost face-on (NGC 628) or the bulge too small (NGC 2967). NGC 4594 has also been included in this table although the procedure applied to this almost edge-on galaxy was different. In this case, only the minor axis was fit to a de Vaucouleurs law at radii large enough that the disk is expected to be insignificant. The bulge flattening comes from a fit to an outer isophote.

Total bulge absolute magnitudes and bulge-to-disk ratios can be obtained by merely integrating the de Vaucouleurs law bulges and exponential disks for each galaxy, but one further correction is necessary. Because we are interested in bulge-to-disk <u>mass</u> ratios, both for comparison of spiral parameters with SO parameters and for investigation of intrinsic morphological structure, we must correct the disk

parameters for the color of the disk. The stellar population of the disk is younger, and therefore bluer and brighter, than an older population of equal mass. The adopted correction comes from Larson and Tinsley (1978) who calculated the UBV colors for a series of models with varying age, star formation rate, and initial mass function. Their findings indicate that the B magnitude of a blue disk must be faded by $4((B-V)_{bulge} - (B-V)_{disk})$ in order to convert a bulge-to-disk luminosity ratio to a bulge-to-disk mass ratio. Coincidentally, the same factor determines the amount the disk has been extincted by dust absorption. Thus, the correction applied compensates for both effects. The correction is determined by assuming that all bulges have the same color, B-V = 0.90. The contribution of the bulge to the total face-on B-V (from de Vaucouleurs et al. 1976) is calculated from this value and the uncorrected bulge-to-disk ratio for each galaxy. The remainder can be interpreted in terms of the face-on B-V for the disk. The correction is then calculated from the formula given above. The corrections range from 0.6 to 2.2 magnitudes and are fairly sensitive to the total face-on B-V values.

After the disk magnitudes have been corrected they are used to calculate new total magnitudes and bulge-to-disk ratios. Table 11 lists the bulge absolute magnitudes, the uncorrected bulge-to-disk ratios, the corrected total magnitudes, and the corrected bulge-to-disk ratios.

The galaxies which have disks whose profiles appear to depart significantly from exponentials were analyzed in a somewhat different manner. In almost all cases the peaks and dips in the profiles correspond to regions of exceptionally active star formation and spiral

structure. These dips and peaks will be discussed in detail later. In several galaxies there is evidence that the disk profile is exponential in regions away from this bright spiral structure. Consequently, we consider the non-exponential disks to have bright regions superposed on an underlying exponential disk. In some cases, we have fit an exponential to the faintest points in the disk-dominated part of the profile, and after subtracting this exponential from the observed profile, fit a de Vaucouleurs law to the inner regions. In other cases we have fit an exponential to the disk regions closest to the center and extrapolated this fit to the nucleus, then fit the remaining central light to a de Vaucouleurs law. In either case, the aim was to get a bulge magnitude only. This bulge magnitude was then subtracted from the total face-on magnitude listed in de Vaucouleurs et al. (1976) to give the disk magnitude. The disk correction was applied to these galaxies in an identical way as to those galaxies with exponential disks and the derived parameters are listed in Table 11. Also, the bulge profiles are shown in Figure 12, although the individual parameters may have little significance. The overall parameters, the disk-to-bulge ratio and the bulge luminosity, are almost as well determined as in those galaxies which could be accurately decomposed.

Following is a discussion of the decomposition of each galaxy individually.

NGC 488

This galaxy has a disk which is quite well fit by an exponential. There is no evidence that the profile departs from the sum of

the disk and bulge fits in the region between 23 and 70 arcseconds, which has not been used in the determination of either component.

NGC 628

This galaxy has an exponential disk, which is a little surprising considering the patchiness of the arms over which the profile has been integrated. The profile dips slightly below the sum of the components inside of about 60 arcseconds; this may be evidence for either a disk with a hole in the middle or a bulge which, in its outer regions, falls faster than a de Vaucouleurs law. The inclination is poorly determined because the bright spiral structure severely affects the individual profiles.

NGC 1058

This galaxy has a very patchy, disordered structure. Its disk departs from exponential in a way which illustrates the problem of understanding non-exponential disks. Three straight sections are evident, and it is unclear whether the disk gets fainter at small radii than the extrapolation of its exponential fit (Freeman's Type 2 profile), or if the profile between about 6 and 80 arcseconds represents a brightening due to active star formation on an underlying exponential disk, or, in fact, if the disk is best described as a series of steps, each roughly exponential with different scale lengths. The decomposition was made by iteratively fitting the inner part of the disk and the bulge to obtain the bulge magnitude.

NGC 2268

The disk of this galaxy departs from an exponential in that the inner parts (r = 25 to 65 arcseconds) are brighter than the exponential fit. This region is visible on the photograph as a dark area around the nucleus. Some structure is visible in this region so it is more likely to be an area of enhanced star formation than a smooth lens component.

NGC 2336

In this galaxy, the arms arise from a ring at a radius of about 35 arcseconds. A faint bar is seen within this ring at a position angle of about 120°. The profile dips below the exponential disk at small radii (< 70 arcseconds) and this feature seems unquestionably associated with the disk rather than the bulge.

NGC 2344

This profile is very interesting. The region between 25 and 80 arcseconds which is brighter than the fit corresponds to the entire optical disk visible in the picture. Clearly, the disk extends to fainter levels although there may be no spiral structure in this outer part.

NGC 2655

This is a very bulge-dominated system, and the disk parameters are not well determined.

NGC 2681

This is a peculiar galaxy although the profile shows little. It has a very bright nucleus, a faint bar with a position angle of about 80° terminating in two short arms. Outside of this there is a faint disk with a faint bar at a position angle of about 30° with a ring or low surface brightness arms around it. The profile looks quite normal except for the bump at about 17 arcseconds. This is caused by the short inner arms. The inner bar produces a large shift in the measured position angle of the bulge relative to the disk.

NGC 2775

This galaxy, in spite of prominent filamentary spiral structure, is bulge-dominated. A better picture of it can be found on page 10 of Sandage (1961). The profile shows two regions which depart from the model. The outer region (r = 30 to 65 arcseconds) is the area in which the spiral structure is most easily visible. Again, it is clear that the exponential disk does not produce a fit to the outer parts of the galaxy, even though spiral features are absent or much reduced in amplitude.

NGC 2841

This galaxy is the prototype of the filamentary armed Sb class (Sandage 1961). It fits the sum of the two components quite well except for a region in the inner part of the disk which is fainter than the model. There is known to be a hole in the HI disk (Bosma 1978) which begins at a slightly larger radius than this possible optical hole.

NGC 2855

This is a very early type spiral and is bulge-dominated.

NGC 2967

This galaxy has very short scale lengths, both for the bulge and disk. Because it is disk-dominated and the exponential fits well over many scale lengths, the disk parameters are quite well determined. The bulge parameters are very poorly determined because only a few points affect the bulge fit.

NGC 3147

This galaxy's profile is well fit by the model. The slight bump above the disk fit at about 45 arcseconds is due to the spiral arm visible on the north side of the galaxy. The position angles of the bulge and disk, both quite well determined, are almost 90° apart.

NGC 3277

This galaxy is extremely bulge dominated. The only evidence of spiral structure is a string of H II regions extending from south to west of the galaxy. The disk is poorly determined, so the profiles were not decomposed, but the bulge fit was used to calculate the bulge luminosity. This was subtracted from the total luminosity to get the disk luminosity.

NGC 3368

This galaxy is one of a group with a complicated morphological structure. There is an inner disk with bright spiral arms (to r = 85 arcseconds) and an outer pair of arms or a ring which arise from the

outer edge of the inner disk. The outer arms are faint and diffuse. The profiles of the disks of galaxies with these properties are never exponential. In this case, it appears that the outer disk is fit passably by an exponential. The inner disk does not dominate over a region large enough to use in a decomposition. The bulge luminosity has been determined by using for the disk the scale length measured from the outer region and increasing the central surface brightness until the disk profile passes through the inner disk points. Then the remaining central light was fit to the bulge.

NGC 3642

This galaxy appears at first glance to have a large bulge and a very faint disk. Closer examination, however, reveals that much of the bulge region shows spiral structure and is actually a section of the disk with a shorter scale length. On the profile, this is the region between 15 and 50 arcseconds. The faint outer disk is the region outside of 50 arcseconds. The bulge magnitude was determined by iterative decomposition limited to the inner disk and bulge regions.

NGC 3898

This galaxy fits the two component model well, and because of its high inclination, 67°, the bulge flattening, $b/a = 0.67$, is quite well determined.

NGC 4378

This galaxy has been extensively studied by Rubin et al. (1978). It has a prominent bulge and a disk whose profile is dominated by a

large bump at r = 90 arcseconds, due to a broad spiral arm. This profile could not be decomposed, so an exponential was approximated by the outer part of the profile, and the bulge was fit to the remaining luminosity.

NGC 4594

Clearly, any attempt to measure the photometric properties of the disk in this edge-on system is hopeless. Instead of a decomposition, the bulge luminosity was determined by fitting the outer regions of the minor axis (r = 70 to 205 arcseconds) to a de Vaucouleurs law. As expected, the de Vaucouleurs law becomes too faint at small radii where the disk contribution is non-negligible.

NGC 4725

This galaxy has a nonexponential disk whose slope is dominated by a ring of bright spiral structure. On the picture, this ring appears to be brightest at the points where it joins to a faint bar at position angles 30° and 210°. On the profile, this structure produces the extended bump from 90 to 185 arcseconds. The profile was decomposed by forcing an exponential through the points on either side of the bump, subtracting this from the observed profile, and fitting the bulge to the remaining central light.

NGC 4736

This galaxy, like NGC 3642, has an inner disk with a shorter scale length than the outer regions. The picture does not show all the structure in this galaxy well, as the inner portions are quite

saturated. This galaxy also has a large noncircular ring barely visible in this picture, but shown clearly in Sandage (1961).

NGC 4941

This galaxy was included in the sample because Sandage (1961) uses it as an example of an object with conflicting classification criteria. The arms are tightly wound as in an Sa, but the bulge is small as in an Sc (the galaxy is classified Sa). The profile shows that this is another object with an inner and outer component to the disk. The outer part is visible as a noncircular ring in the picture. The bulge luminosity was determined by fitting an exponential to the outer part of the inner disk.

NGC 5194

This galaxy also shows a nonexponential disk. In computing the averaged profile, the region around the companion, NGC 5195, was excluded. The profile is interpreted as follows: The outer disk, from r = 52 to 200 arcseconds is fairly flat (it has a large scale length) and ends abruptly at its outer boundary. Inside of this there is an inner disk with a short scale length, and a very small bulge. The inner disk and bulge were iteratively decomposed.

NGC 6340

This galaxy fits the two component model well. It is close to face-on and the bulge and disk position angles disagree.

NGC 7217

This galaxy has an obvious ring of intense spiral structure which is responsible for the lump in the profile at about 150 arcseconds. The arms also become bright inside of 70 arcseconds and produce the smaller bump visible in the profile. The bulge luminosity was determined with the same procedure as in NGC 3368

NGC 7331

This galaxy has an exponential disk and a surprisingly large bulge-to-disk ratio. The small b/a found for the bulge may be a result of strong dust absorption on the west side.

Discussion

The data described in the previous section contain a tremendous amount of information, both on the individual galaxies and on the properties of spiral galaxies in general. To attempt to analyze all aspects of this information is a project beyond the scope of this study, the prime motive for which was to quantify the large scale structure for a sample of spirals. In keeping with that aim, we will limit the discussion to two areas. First, we will attempt a qualitative explanation of the properties of the profiles. Second, we will examine the correlations among the parameters derived in this study and qualitative classification systems.

The profiles fall into two categories: those for which the de Vaucouleurs law plus exponential model fits the data points and those which show large departures from the model. Fifteen of the 26 galaxies have profiles which approximate the models closely enough to be

decomposed iteratively, as described in the previous section. Nine of the galaxies have large bumps or dips which we have interpreted as non-exponential disks. Two of the galaxies could not be decomposed for other reasons, NGC 3277 because it is so bulge-dominated that disk parameters could not be accurately determined, and NGC 4594 because of its inclination.

Those galaxies which fit the model reasonably well show smaller departures of two types. Three of the galaxies, NGC's 628, 2336, and 2841, have observed profiles which dip below the sum of the bulge plus disk models just outside the crossover point where bulge and disk contribute equally. In NGC 628 and NGC 2841, the observed profile never falls below the disk model alone, so it is impossible to determine whether the effect is due to a hole in the disk, as hypothesized by Kormendy (1977c) for compact SO's, or to an outer region in the bulges of these galaxies where the luminosity falls off faster than the de Vaucouleurs law. This latter explanation may be slightly difficult to understand on theoretical grounds as two effects are thought to be able to flatten bulges in the z-direction, the opposite to what is seen. First, while ellipticals are apparently not supported by rotation (Illingworth, 1977), preliminary evidence indicates that bulges do rotate (Kormendy and Illingworth 1980). Second, while ellipticals fight only against their own self-gravity to maintain their shape, bulges must fight the additional flat potential of the disk, which may dominate. These two effects should make bulges more extended in the plane of the disk than an elliptical of the same luminosity and central concentration.

The other departure from exponential disks is seen in those profiles which have extended regions brighter than the models. These, with the possible exception of NGC 2775, are invariably associated with spiral structure in the galaxy. NGC's 2268, 2344, and 2681 all show this effect clearly. This correlation suggests that all positive departures from exponential disks (observed profile brighter than model profile) are a result of a region of enhanced star formation. This idea is supported by the galaxies in which the departures are much larger also. NGC's 4378 and 4725 show bumps corresponding to obvious regions of vigorous star formation. In galaxies with innner and outer disk structure such as NGC's 4736, 4941, and 5194, the brighter inner parts always show more intense spiral structure.

This is not a startling idea as it is easy to imagine that if one starts with an exponential disk and then makes stars on top of it in spiral or other patterns, those regions will appear brighter. However, it is interesting to note that some galaxies show obvious star formation, and yet no departures from the exponential disk are visible. NGC 488 is a good example of this. Tightly wound spiral structure is easily visible in the picture from 45 to 90 arcseconds radius, but the profile shows no departure from a smooth exponential. The most obvious interpretation of this fact is that the increase in brightness obtained by averaging the arms into the underlying disk is a fraction which is constant or varies linearly with radius. Thus, one sees an exponential disk whether one looks at the underlying disk between the arms or the peaks of star formation at the centers of the arms.

The explanation for those galaxies which have apparently non-exponential disks follows simply from this idea. The spiral structure or star formation in these systems is constrained to or enhanced in certain ranges of radii in the disk. Thus, we see systems like NGC 7217 which have rings of star formation and therefore bumps in their profiles, or we see systems like NGC's 4941 and 5194 which have brighter inner disks with active star formation. It appears that scale lengths can either be the same or different (usually steeper) in the regions of enhanced star formation. For example, NGC 5194 and NGC 3642 have inner disks much steeper than their outer disks, while NGC 3368 and NGC 4941 have inner disks with scale lengths not very different from their outer disks.

A final comment is on the cause of these regions of enhanced star formation. Of the 9 galaxies which show strongly nonexponential disks, one (NGC 1058) is in a tight group, one (NGC 4725) has a bar, one (NGC 5194) has a companion, and three (NGC's 3368, 4736, and 4941) show oval outer rings. Of the galaxies which show exponential disks, the frequency of such perturbing morphological features is very much lower. The evidence certainly suggests that these features drive or are at least correlated with the regions of enhanced star formation.

The second point we will discuss is the interpretation of the variations of physical parameters in terms of qualitative morphological classification. This is important both because we would like to know which physical properties affect the appearance of spiral galaxies, and because we would then like to use the easily determined qualitative classification to learn about the variation of basic physical

parameters. The two classification systems we will examine are the Hubble system and the Yerkes system. The Yerkes system, or really, the one dimension of it in which we are interested, is a sequence in the degree of central concentration of luminosity (Morgan and Mayall 1957; Morgan 1958, 1959). The Yerkes types of the galaxies in this sample run from af, a disk-dominated system with very little central concentration, to k, a system dominated by a smooth, amorphous central component. We expect these types to be closely related to our quantitative bulge-to-disk ratios. The Hubble system is somewhat more complex, using three criteria to classify galaxies (Hubble 1938, Sandage 1961). These, in order of decreasing importance, are the tightness of the winding of the spiral arms, the texture of the arms (smooth vs. patchy and resolved), and the bulge-to-disk ratio. These are usually well correlated, but occasionally (NGC 4941), the criteria will conflict. The Revised Morphological Type system (T types) is based on the Hubble system, and types in this system and the Yerkes system have been obtained from de Vaucouleurs et al. (1976).

Figure 13 diplays plots of the log of the observed and corrected bulge-to-disk ratios against T types and Yerkes types. As expected, the tightest correlation with the observed bulge-to-disk ratios is the Yerkes types. The T types also show a good correlation with observed log B/D ratio. Because the primary parameter of the Hubble classification scheme is the pitch angle of the arms which is thought to depend on the central mass concentration of the galaxy (Roberts, Roberts, and Shu 1975), it is a little surprising that the corrected B/D ratios do not reduce the scatter.

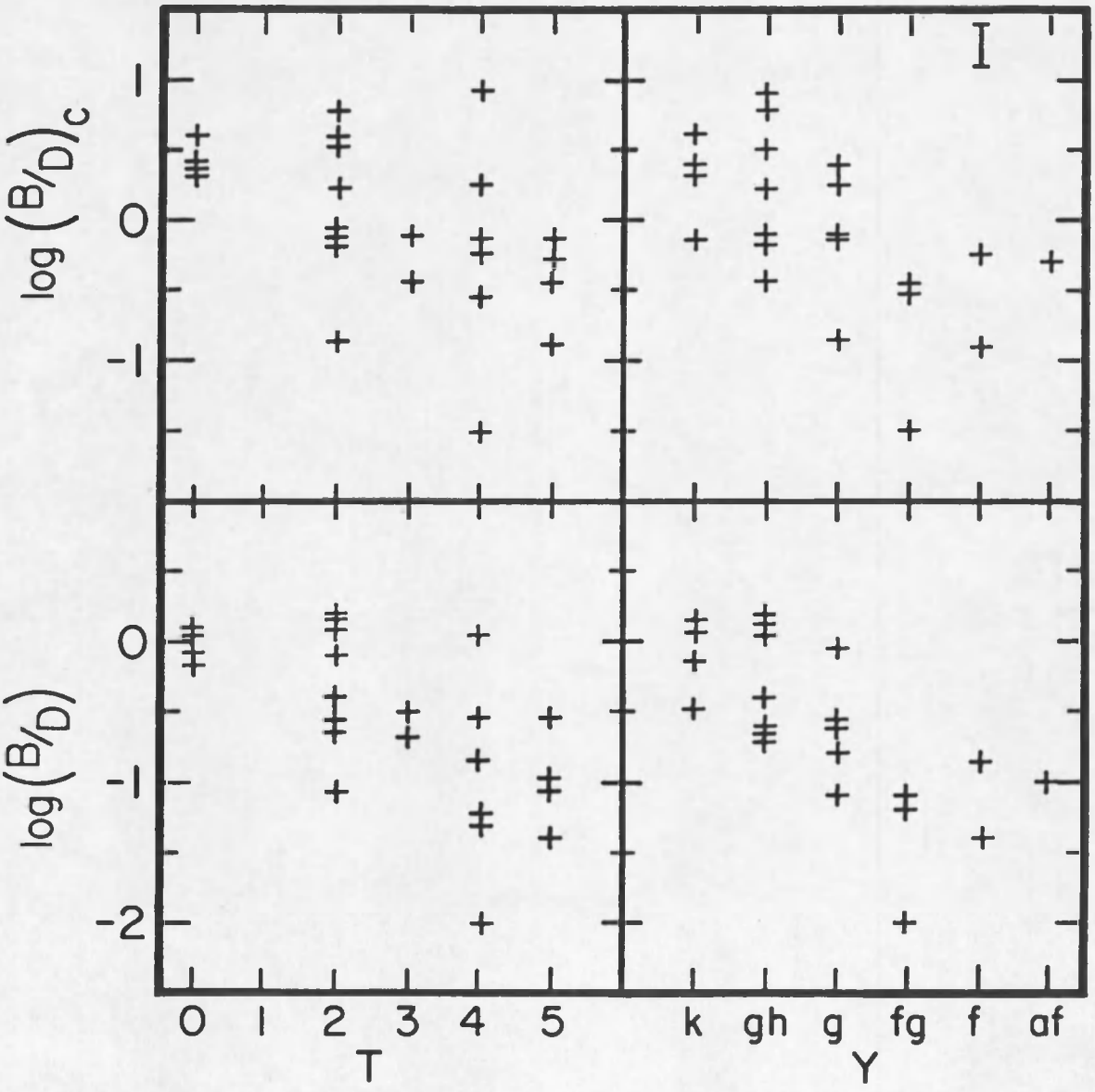

Figure 13. The relations between bulge-to-disk ratios and qualitative classifications -- The logarithms of the bulge-to-disk mass ratios (upper panels) and the logarithms of the bulge-to-disk luminosity ratios (lower panels) are plotted against T types (left panels) and Yerkes types (right panels). An estimated error bar for the bulge-to-disk ratios is shown in the upper right.

In order to determine whether the observed scatter in the plot of observed log B/D against T type is due to a combination of measurement and classification uncertainties, we estimate these errors. The B/D ratios are distance independent and thus, their accuracy depends only on the decomposition of the profiles. We judge that, in general, the maximum error possible in our determination of bulge luminosities is about 1/2 magnitude. This translates to an uncertainty in the log B/D of 0.15. The classification uncertainty quoted by de Vaucouleurs et al. (1976) is 1 for the T types. Thus classification errors dominate. We can fit a line to the log B/D - T type relation assuming all errors to be in the T types, and then use a chi-square determination to test the possibility that the observed scatter is due to classification errors alone. This test indicates a probability of only about 0.5% that the observed scatter is due to uncertainties in the classifications if we have estimated these uncertainties properly.

We next attempted to find another physical parameter which correlates with the residuals in the log (B/D) vs. T type diagram. In particular, we found no correlation between these residuals and (1) absolute magnitude corrected for disk color (2) absolute magnitude relative to other galaxies of the same T type, (3) disk scale length, and (4) $B_e - B(0)_c$. In the belief that the residuals might be associated with some measure of the disk's ability to maintain prominent spiral arms, we searched the literature for H I measurements of the galaxies in the sample. Table 12 lists H I flux integrals, masses, and the logarithm of the ratio of H I mass to disk luminosity in solar units. The disk luminosity in the last of these has been corrected

Table 12. H I Properties of Program Spirals

NGC	Flux integral	H I Mass (10^9 $M_\odot$)	log $(M_{H\ I}/L_D)_c$	Reference[a]
488	14.0	4.1	-1.02	F
628	533.0	18.7	0.60	G,C
1058	59.0	1.4	0.36	F
2268	25.1	8.5	-0.06	F,G
2336	42.5	13.6	-0.27	F
2344	12.7	0.7	-0.19	C
2655	<7.3	<1.1	<-0.98	B
2681	31.8	1.8	-0.37	B,C
2841	103.0	6.0	-0.44	A,C,F
2855	<8.7	<1.3	<-0.48	D
3368	62.0	1.5	-0.51	B,C,F
3898	37.0	2.2	0.07	F
4725	78.0	5.6	-0.51	F
4736	90.0	0.6	-0.89	E
4941	9.3	0.5	-0.97	B,C
5194	120.0	2.1	-0.69	F
6340	12.1	3.1	-0.44	A,B,C
7217	20.1	0.8	-1.17	B,C
7331	225.0	5.1	0.16	C,G

[a]References: A = Bottinelli et al. (1970); B = Balkowski et al. (1972); C = Balkowski (1973); D = Gallagher, Faber, and Balick (1974); E = Bosma, van der Hulst, and Sullivan (1977); F = Dickel and Rood (1978); G = Shostak (1978).

to reflect a mass estimate. References for the flux integrals are also listed.

Figure 14 shows the log $(M_{H\ I}/L_D)_c$ values ploted against the residuals. A correlation is clearly present (significant at the 99.5% level) and a line has been fit with the residuals as the dependent variable. One must be a little bit careful with this correlation because there is another possible reason for it. Since both axes depend on the disk luminosity, an error in this quantity will tend to extend the distribution of points in the direction of the line in Figure 14. We can only argue that if this is the case and we have made the correlation from what was originally a scatter diagram, then the average error required is about a factor 3 in the bulge-to-disk ratios. We do not believe an error this large could have been made.

We can now define a quantitative classification based on two parameters, the observed B/D ratio and the log $(M_{H\ I}/L_D)_c$:

$$T_{calc} = 2.26 - 1.91 \log(B/D) + 1.78 \log(M_{H\ I}/L_D)_c.$$

A chi-square test now indicates a probability of 24% that the distribution of differences between our T_{calc} and the tabulated T types could be explained by the classification uncertainties. We understand this quantification of the Hubble sequence in the following way. The three classification criteria, as stated above, are spiral arm pitch angle, spiral arm texture, and bulge-to-disk ratio. According to the density wave theory of spiral structure (Roberts et al. 1975), the pitch angle of the arms is essentially determined by the bulge-to-disk ratio or degree of central concentration of the galaxy. Thus, the bulge-to-disk

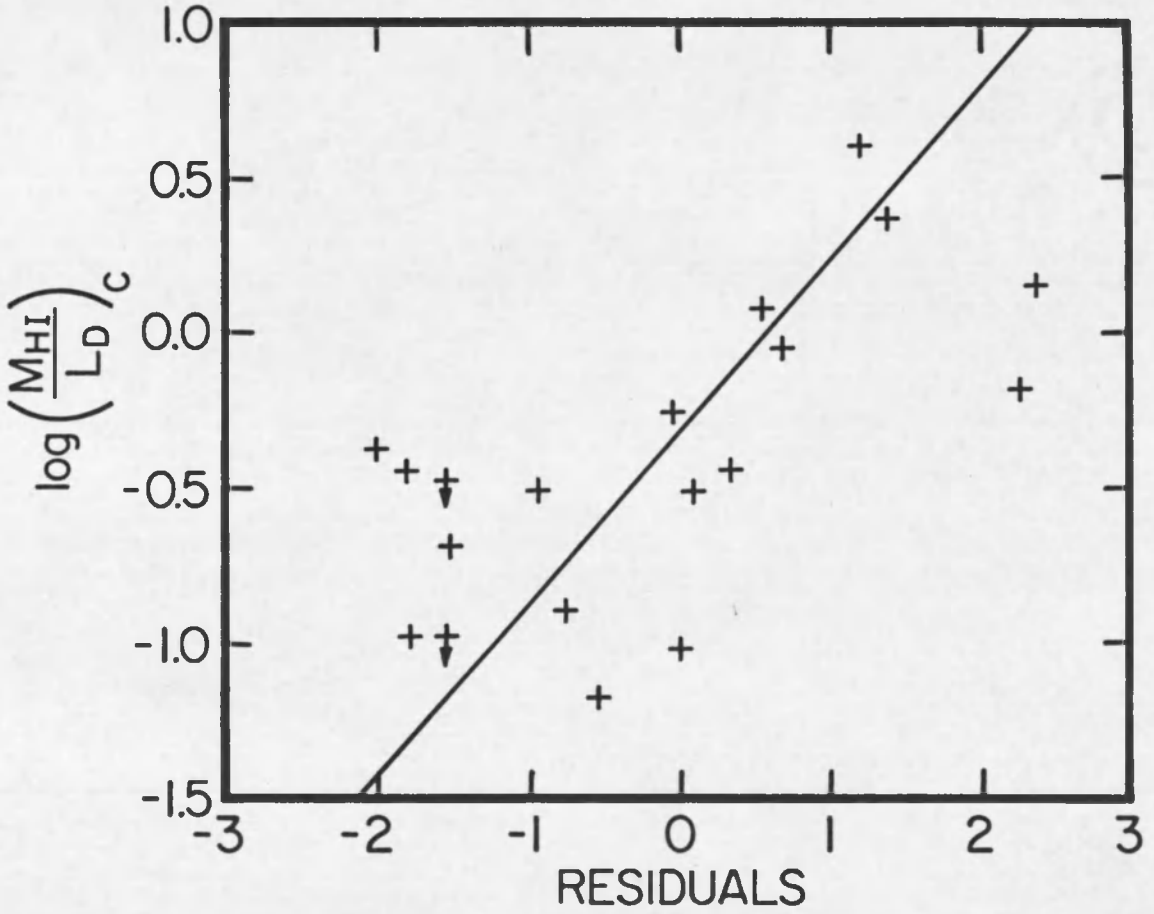

Figure 14. The residuals of the relation between T type and log (B/D) plotted against an indicator of the fraction of the disk in neutral atomic hydrogen.

ratio term accounts for the first and third criteria. The $\log(M_{H\,I}/L_D)_c$ term might reasonably be expected to determine the texture of the arms, in that a disk with a relatively small fraction of gas in it may not produce stars as vigorously as one in which there is a much larger gas content. For this reason, at a given bulge-to-disk ratio and pitch angle, a galaxy with lower contrast arms due to a relative deficiency of hydrogen gas will be classified earlier than one with arms which can easily be seen on top of the underlying disk. In support of this interpretation, we find that the $\log(M_{H\,I}/L_D)_c$ parameter is very well correlated with the (B-V) color of the disk, in the sense that high gas content disks are bluer in color.

Finally, we examine the distribution of two of the parameters we have obtained from our decomposition, disk central surface brightness and bulge flattening. Freeman (1970), in his pioneering work on disks of spiral galaxies, found that 28 of the 36 galaxies he examined had disks with a central surface brightness of 21.65 ± 0.30 Bμ. Kormendy (1977c) has pointed out that this result could be an artifact of the decomposition procedure that Freeman used. Thus, it is of interest to compare the distribution of $B(0)_c$, which has been defined in the same way as Freeman (1970), with the distribution found by Freeman. Figure 15 shows a comparison of these two distributions. It is obvious that although the present distribution is centered at roughly the same surface brightness, the contrast of the spike is much lower than in Freeman's distribution. The present distribution suggests that 21.65 is not a "preferred" value but is in the middle of the range of easily observable surface brightnesses.

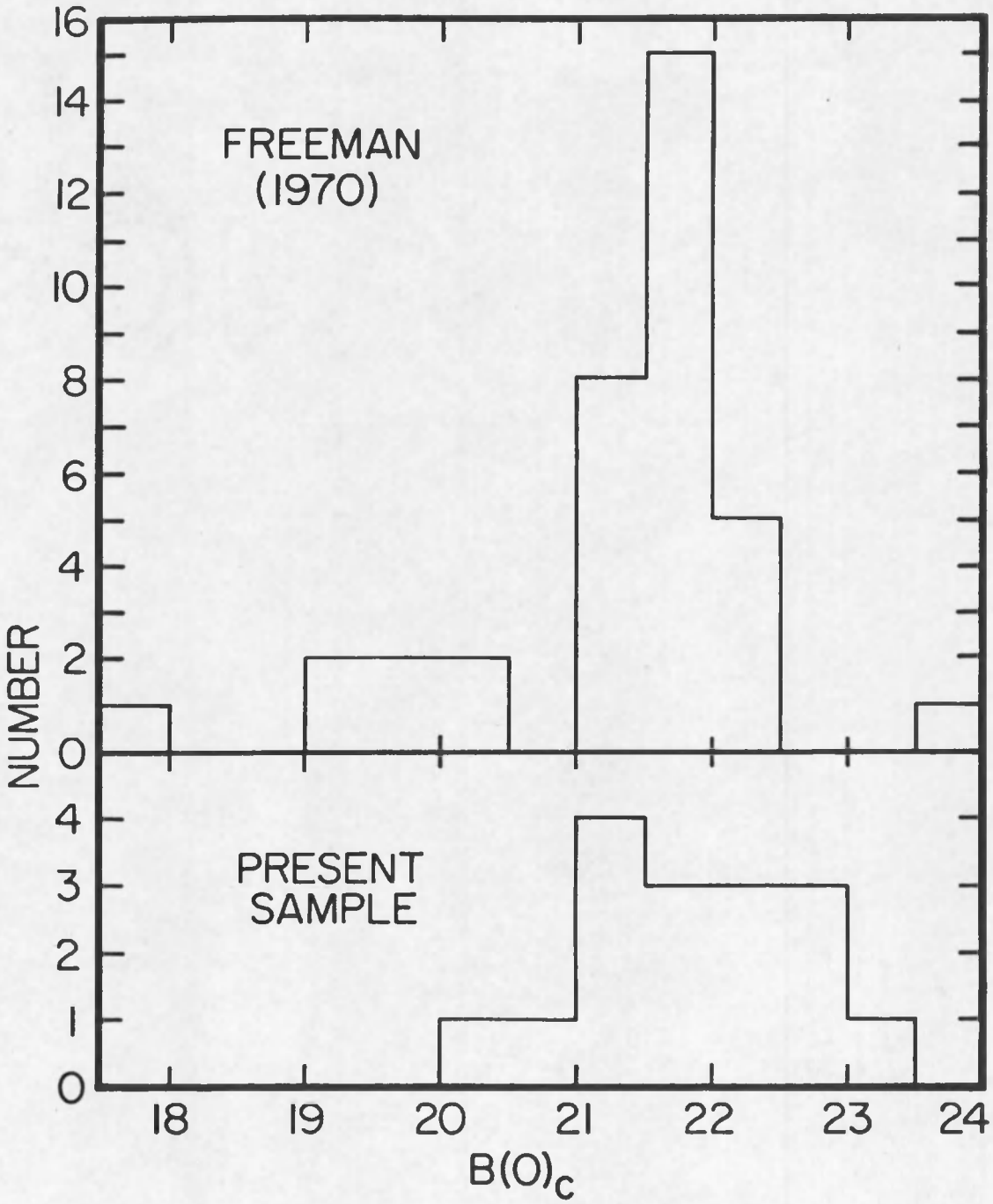

Figure 15. The distribution of disk central surface brightnesses in this study (lower panel) and in the study of Freeman (1970) (upper panel).

Figure 16 shows the distribution of $(b/a)_{true}$ values for the nine galaxies in the sample for which this quantity could be determined. The measurement for NGC 7331, shown as a dotted line, is considered unreliable because of strong dust absorption on one side of the bulge. Superposed on this histogram is the distribution of elliptical flattenings derived by Sandage, Freeman, and Stokes (1970). Although the number of objects in this sample is admittedly small, the bulges appear to be, if anything, more spherical than the elliptical galaxies. This is curious for the reasons discussed earlier in this chapter; rotation and the disk gravitational potential should make the bulge flatter than the elliptical galaxies. The flattening due to the presence of the disk has been quantified by Monet, Richstone, and Schechter (1980). These authors find that a spherical massless bulge is converted into an oblate ellipsoid with $b/a = 0.5$ in the potential of an infinite disk. This calculation ignores the effects of rotation, which is suspected of playing a role in the dynamics of spiral bulges, and anisotropic velocity dispersions, which are thought to be important in ellipticals. Both effects would increase the flattening. Thus, the data suggest that either bulges are, in general, isotropic and not rotating, or the gravitational potential is dominated by a more spherical mass distribution than that of the disk. A simple test of the effect of the disk potential is to examine the relation between the bulge flattening and the bulge-to-disk mass ratio. These two variables show no significant correlation, suggesting that the gravitational field of the disk is not the dominant factor in determining the bulge shape, but a larger sample is needed for a definitive test.

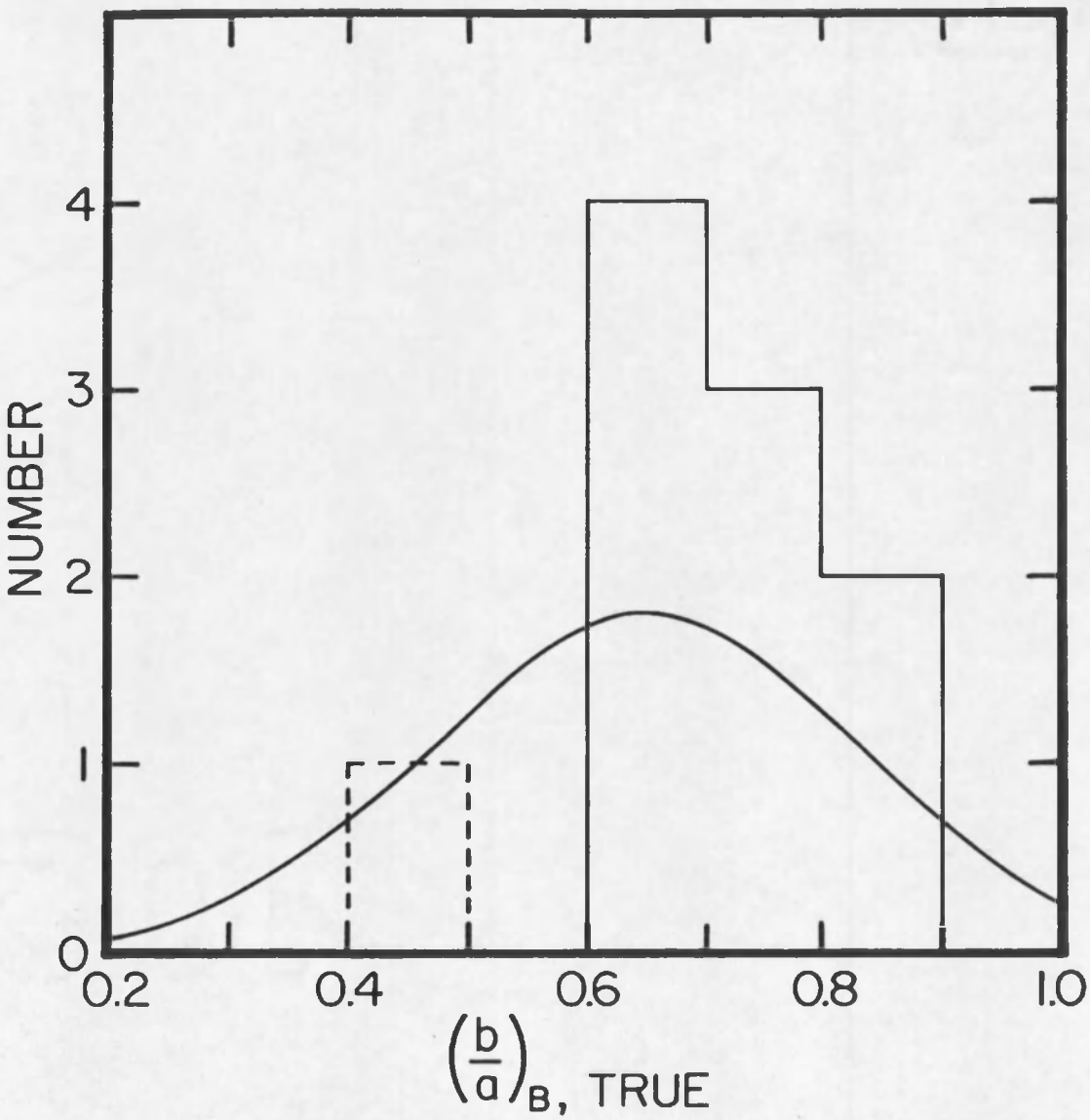

Figure 16. The distribution of true bulge flattenings in this study -- The column representing NGC 7331 is dashed because it is suspected that this measurement is anomalously low because of strong dust absorption on one side of the galaxy. The smooth curve is the distribution of flattenings for oblate elliptical galaxies determined by Sandage et al. (1970).

Conclusions

We have obtained and studied photographic surface brightness distributions for 26 spiral galaxies. Fifteen of these galaxies show exponential disks and have profiles which could be iteratively decomposed into bulge and disk components. The remaining objects were decomposed by estimating the bulge magnitude from the profiles. The following parameters were derived for all but two of the galaxies: bulge luminosity, bulge-to-disk ratio, total absolute magnitude corrected to a B-V color of 0.90, and bulge-to-disk ratio after this correction has been applied. Additionally, for the galaxies with well behaved profiles, the disk central surface brightness, $B(0)_c$; the disk scale length, r_o; the bulge effective surface brightness, B_e; the bulge effective radius, r_e; and the inclination of the galaxy were determined. For nine objects, the true bulge flattening is calculated.

Inspection of the profiles suggests that departures from exponential disks arise when the star formation is enhanced in certain regions. This enhancement seems to be often related to the presence of morphological features such as bars, rings, and companions which may be responsible.

It has been shown that the Hubble sequence is correlated with bulge-to-disk ratio, but with surprisingly large scatter, and that the residuals in this relation are correlated with the ratio of neutral hydrogen mass to disk luminosity. These two quantities define the revised morphological type to within the classification uncertainties. We also find that the disk central surface brightness distribution is not highly peaked at 21.65 magnitudes per square arcsecond as found by

Freeman (1970), but that this value is roughly at the center of the distribution. Finally, we note that the bulge flattenings are inconsistent with the idea of bulges being like elliptical galaxies but further flattened by the disk potential. Further observations are required to distinguish between the possibilities that the gravitational potential of a disk galaxy is dominated by a spherical mass distribution, or the bulges are not flattened by anisotropic velocity distributions as elliptical galaxies are.

CHAPTER IV

THE METALLICITY-LUMINOSITY RELATION FOR SPIRAL GALAXIES

As detailed in Chapter I, the metallicity-luminosity relations for galaxies of various types may provide information on physical conditions at the time of galaxy formation. Comparison of these relations for different types of galaxies may indicate in what aspects the formation of ellipticals, SO's, and spirals differed. The details of the metallicity-luminosity relations may discriminate between various scenarios of galaxy formation as well as the several proposed mechanisms for establishing such relations.

We begin by reviewing the theoretical expectations and previous observational results. The four theoretically justified possible relations are:

1. A correlation between metallicity and bulge luminosity identical to the metallicity-luminosity relation for ellipticals.
2. A correlation between metallicity and total luminosity identical to the metallicity-luminosity relation for ellipticals.
3. A correlation between metallicity and bulge luminosity offset to lower metallicity than the elliptical relation and a correlation between this offset and bulge-to-disk ratio (lower metallicity for smaller B/D).
4. A correlation between metallicity and total luminosity offset to lower metallicity than the elliptical relation and a

correlation between this offset and bulge-to-disk ratio (lower metallicity for smaller B/D).

The observational evidence is mostly relevant to S0 galaxies. A color-magnitude study by Visvanathan and Sandage (1977) and a line-strength study by Burstein (1979a) indicate that for S0 galaxies, the metallicity-total luminosity relation follows that for elliptical galaxies, with slightly increased scatter. Since almost all S0 galaxies tend to have bulge-to-disk ratios close to unity (Burstein 1979b), this result could be interpreted as a metallicity-bulge luminosity correlation in which the bulge of an S0 has a higher metallicity (by an amount corresponding to 0.75 magnitudes in the elliptical metallicity-luminosity relation) than an elliptical of equal luminosity. This seems unlikely as theoretical arguments maintain that if the metallicity-luminosity relation for disk systems is offset from that of elliptical galaxies, it should be toward lower metallicities, not higher.

Color-magnitude observations of early type spirals have been obtained by Visvanathan and Griersmith (1977). They find for these spirals the same result as for S0's: that the metallicity-total luminosity relation is indistinguishable from the elliptical relation. This study can be criticized, however, because the colors measured are sensitive to reddening effects and the unknown population mix.

We now have the data to construct the metallicity-luminosity relation for spiral galaxies using the results of Chapters II and III. We list in Table 13 the relevant quantities. For each galaxy we give

Table 13. Metallicity-Luminosity Data for Program Spirals

NGC	$(Mgb)_c$	M_O^T	$(M_O^T)_c$	M_{Bulge}	$\log(B/D)_c$
224	.295	-20.47	-19.90	-18.63	-.35
488	.240	-21.91	-21.44	-20.00	-.44
628	.195	-20.95	-19.05	-17.63	-.43
2268	.218	-21.34	-19.98	-18.87	-.25
2336	.200	-22.34	-20.78	-19.14	-.55
2344	.226	-18.52	-17.71	-16.77	-.14
2655	.209	-21.50	-21.30	-21.07	0.62
2681	.221	-20.19	-19.82	-19.40	0.33
2775	.264	-20.00	-19.61	-19.32	0.52
2841	.322	-21.40	-20.67	-19.74	-.13
2855	.249	-19.97	-19.87	-19.52	0.42
3031	.277	-20.54	-20.20	-19.16	-.21
3147	.194	-22.00	-21.36	-20.41	-.14
3277	.272	-19.36	-18.98	-18.81	0.78
3368	.170	-20.21	-19.81	-19.23	0.23
3642	.199	-20.83	-19.32	-18.84	0.25
3898	.302	-19.71	-19.45	-19.21	0.60
4378	.271	-21.10		-20.79	
4594	.339	-22.35		-22.63	
4725	.263	-21.56	-20.72	-19.74	-.17
4736	.228	-20.00	-19.26	-18.36	-.12
5194	.238	-21.08	-19.58	-15.88	-1.52
6340	.269	-21.14	-20.65	-20.26	0.37
7217	.332	-20.89	-20.39	-19.50	-.10

its $(Mgb)_c$ index, that is, a metallicity indicator corrected for the effects of a young component of the population. From the photometric parameters measured and calculated in Chapter III, we list a bulge magnitude, a total face-on magnitude corrected for the color of the disk, and a bulge-to-disk ratio, also corrected for the color of the disk. We also list total face-on uncorrected magnitudes, using the B_o^T values tabulated in de Vaoucouleurs et al. (1976). Distances used are listed in Chapter I. For NGC 224 and NGC 3031, we have derived parameters in a manner similar to the other galaxies, using bulge luminosities given by Whitmore, Kirshner, and Schechter (1979).

We will use several statistical procedures and tests in the analysis of these data. It is clear that the elliptical galaxy sample and the spiral galaxy sample explore somewhat different regions in the metallicity-luminosity diagram. For example, the mean Mgb index of the elliptical sample is 0.272, while for the spiral sample it is 0.248. Similarly, since we will consider both bulge luminosities and total luminosities in comparison with the elliptical sample, we can be sure that one, if not both of these parameters will have a mean value significantly different from the ellipticals (see Figure 18, p. 155). The implication of this is that we cannot directly compare the distribution of elliptical data points in the metallicity-luminosity diagram with the distribution of spiral data points. We must instead assume a functional form for one distribution, extrapolate it to the region occupied by the other distribution, and see if it is compatible.

This type of comparison will be performed using a standard least squares technique to fit a straight line to each data set.

Several properties of this type of fitting scheme should be kept in mind. Least squares minimizes the sum of the squares of the deviations from a line in a direction parallel to one axis. Thus, the implicit assumption is made that one variable is independent and has no uncertainties in its measurements, and that the other variable is dependent and scatter around the best fit line represents inaccuracies in the determination of this variable. This assumption is invalid in two respects for the analysis to be considered here. First, there are uncertainties associated with the determination of both the metallicities and the luminosities. The metallicities suffer both from observational errors ($\pm$ 10% as deduced in Chapter II) and random and systematic errors intrinsic to the correction for the dilution by the young component of the stellar population. These may be due to the uncertainty in the position of the metallicity line in the CN39-Mgb diagram used in Chapter II, or to variations in the age of the young component of the stellar populations in different spiral galaxies. They may also be proportional to the amount of correction required. The uncertainties in the luminosities arise from two effects. If the distance moduli used are incorrect due to departures from the Hubble flow not accounted for, then the luminosities will be in error. The other uncertainty, a factor for the spiral galaxies only, is the decomposition; zero-point errors, errors in the density-to-intensity conversion, or in the actual procedure of decomposition propagate to the bulge luminosities. A further uncertainty, which affects the total corrected luminosities, is related to the correction for the disk color, which is dependent on both the

accuracy of the decomposition and the correctness of the assumed expression for the magnitude of the correction.

The other intrinsic problem involving the use of the least squares fitting technique is that a straight line may not be the proper functional form with which to fit the distribution of points in the metallicity-luminosity diagram. It is known that the scatter around the best fit line in the metallicity-luminosity diagram for elliptical galaxies is larger than would be consistent with observational errors (Faber 1977). Thus, the best fit line is not expected to be extremely well defined, and a goodness-of-fit test may yield what would otherwise be only a marginally significant result.

Four simple statistical formulae will be used in the following analysis. For completeness and accuracy, we list and explain them here. A more detailed discussion of these tests and their uses may be found in Bevington (1969). In the following, x represents the independent variable, y the dependent variable, and N the number of data points in the sample. It is assumed that the uncertainties of all points in each sample are equal; i.e., the points are weighted equally. The intercept of the least squares fit line (the y-value at x = 0) is given by:

$$a = \frac{\Sigma x_i^2 \Sigma y_i - \Sigma x_i \Sigma x_i y_i}{N\Sigma x_i^2 - (\Sigma x_i)^2} \quad .$$

The slope is given by:

$$b = \frac{N\Sigma x_i y_i - \Sigma x_i \Sigma y_i}{N\Sigma x_i^2 - (\Sigma x_i)^2} \quad .$$

The correlation coefficient, r, measures the effect of exchanging the dependent and independent variables. It is defined:

$$r = \frac{N\Sigma x_i y_i - \Sigma x_i \Sigma y_i}{(N\Sigma x_i^2 - (\Sigma x_i)^2)^{1/2}(N\Sigma y_i^2 - (\Sigma y_i)^2)^{1/2}} .$$

This parameter is distributed in a well defined way between -1 and +1 for an uncorrelated sample. Thus, the value of r for a sample can be expressed in terms of the probability that an uncorrelated sample would produce a correlation coefficient as large as that determined.

Finally, the χ^2 parameter is defined:

$$\chi^2 = \Sigma\left(\frac{y_i - a - bx_i}{\sigma_i}\right)^2 .$$

χ^2 is a measure of the accuracy with which the line fits the data in comparison with the measurement uncertainties, σ_i. Its value is expected to be about N-2 if the fit is satisfactory. N-2 is the number of degrees of freedom in this case. Actually, what we will be concerned with in regard to the χ^2 parameter is a measure of the uncertainties in the slope and intercept of the line we have fit to the data. According to the decomposition theorem (see Margon et al. 1975 and references therein), the difference between χ^2_{min}, that is, the χ^2 for the least squares fit line, and the χ^2 at some other values of the parameters a and b is distributed as χ^2 with 2 degrees of freedom. Now, since the χ^2_{min} is quite a bit larger than N-2 because of the fact, discussed above, that the straight line is not a very good approximation to the true distribution, we normalize the χ^2 values:

$$\chi^2_{excess} = \left(\frac{\chi^2}{\chi^2_{min}} - 1\right)(N-2)$$

This χ^2_{excess}, evaluated at any values of a and b, should be distributed as χ^2 with two degrees of freedom, and thus, gives a probability that a point as far from the least squares solution as a and b could be the true solution. Be evaluating a grid of a and b values around the least squares solution, we can draw 1 sigma ellipses (corresponding to $\chi^2_{excess} = 2.30$) in the a-b plane.

There are two sorts of questions we wish to ask about the relation between central metallicity and luminosity in spiral galaxies. First, is there a statistically significant correlation? Second, is the distribution of points consistent with any of the four hypothetical relations we listed at the beginning of this chapter? The first question can be answered in a straightforward way. In Table 14 we list the correlation coefficients and significance levels for several pairs of variables: (1) the elliptical galaxy metallicity-luminosity relation, i.e., total absolute magnitude vs. Mgb index; (2) the spiral galaxy metallicity-bulge luminosity relation, i.e., bulge absolute magnitude vs. Mgb index corrected for dilution by the young component of the population; (3) the spiral galaxy metallicity-total luminosity relation, i.e., total absolute magnitude corrected to be a mass estimate comparable to elliptical galaxies vs. corrected Mgb index; and (4) the spiral galaxy metallicity-total luminosity relation, i.e., total uncorrected absolute magnitude vs. corrected Mgb index. The quantities used for the elliptical sample can be found in Chapters I and II; the

Table 14. Statistical Tests

Sample	Indep. (x)	Dep. (y)	Number (N)	r	Conf. level	Inter-cept	Slope
Ellip. (E)	M_o^T	Mgb	19	-.59	99.2%	-.156	-.021
Spiral (B)	M_{bulge}	$(Mgb)_c$	22	-.36	90. %	0.013	-.012
Spiral (C)	$(M_o^T)_c$	$(Mgb)_c$	20	-.05	<50. %	0.187	-.003
Spiral (U)	M_o^T	$(Mgb)_c$	22	-.04	<50. %	0.200	-.002
Spiral	resid(B)	$\log(B/D)_c$	20	0.00	<50. %		
Spiral	resid(C)	$\log(B/D)_c$	20	0.16	50. %		
Spiral (Sample includes M31, M81)	resid(B)	Dist.	22	0.55	99.1%		
Spiral (Sample does not include M31, M81)	resid(B)	Dist.	20	0.34	88. %		

spiral values are listed in Table 13. NGC 224 and NGC 3031 have been excluded from the calculations for the spiral galaxies because their small distances ensures that a much smaller region has been sampled than in the other objects. In addition, NGC 4378 and NGC 4594 have been removed from the spiral sample for the metallicity-total corrected luminosity relation because corrections could not be determined for these two objects.

It can be seen that none of the relations involving the spiral sample shows as tight a correlation as the elliptical sample. The spiral metallicities appear uncorrelated with total luminosity, corrected or uncorrected. The bulge magnitudes are marginally correlated with the metallicities. That the correlations are poorer for the spirals is not surprising; both metallicities and luminosities are more uncertain for the spiral sample than for the ellipticals. The metallicities have the added errors contributed by the removal of the young population contamination. The bulge luminosities have the uncertainties inherent in the profile decomposition, and the corrected total magnitudes have the additional errors associated with the color correction. Thus we do not consider the absence of a strong correlation evidence against the presence of any of these relations, although the 90% confidence level of the metallicity-bulge luminosity relation is suggestive that this relation should be favored over the other two.

The other question we wish to ask of these relations is somewhat more difficult to answer. Are any of these relations consistent with those expected on theoretical grounds? In order to test relations 1 and 2 (as listed at the start of this chapter), we need only fit a straight

line to each pair of variables in Table 14 and determine whether the parameters of each line are consistent with those for the elliptical sample. These fits have been made assuming that the metallicity variable is dependent and the luminosity variable is independent. The slope and intercept parameters are listed in Table 14.

As explained above, by mapping out variations of χ^2 with respect to its minimum value, we can estimate the likelihood of any point in the slope-intercept plane being the correct solution. Figure 17 shows 1 sigma ellipses for the elliptical relation (labelled E), the bulge luminosity relation (labelled B), the corrected total luminosity relation (labelled C), and the uncorrected total luminosity relation (U). It can be seen that the B relation is the only one which is quite compatible with the E relation, although the others cannot be ruled out with a high degree of certainty. It should be kept in mind that the ellipses represent the regions outside of which the true parameters will fall approximately 32% of the time. Thus, while there is a considerable joint probability that both C and E relations have parameters falling outside their 1 sigma ellipses, the probability that they both fall in the small region where the ellipses are close is somewhat smaller. We hesitate to make a more quantitative statement of the results, but we conclude that relation 1 is consistent with our data and relation 2 is marginally inconsistent.

We turn to relations 3 and 4 and investigate the possibility that there is a bulge-to-disk ratio dependence in the residuals of the B or C relations. Listed in Table 14 are correlation coefficients between the residuals of these two relations and $\log(B/D)_c$. No

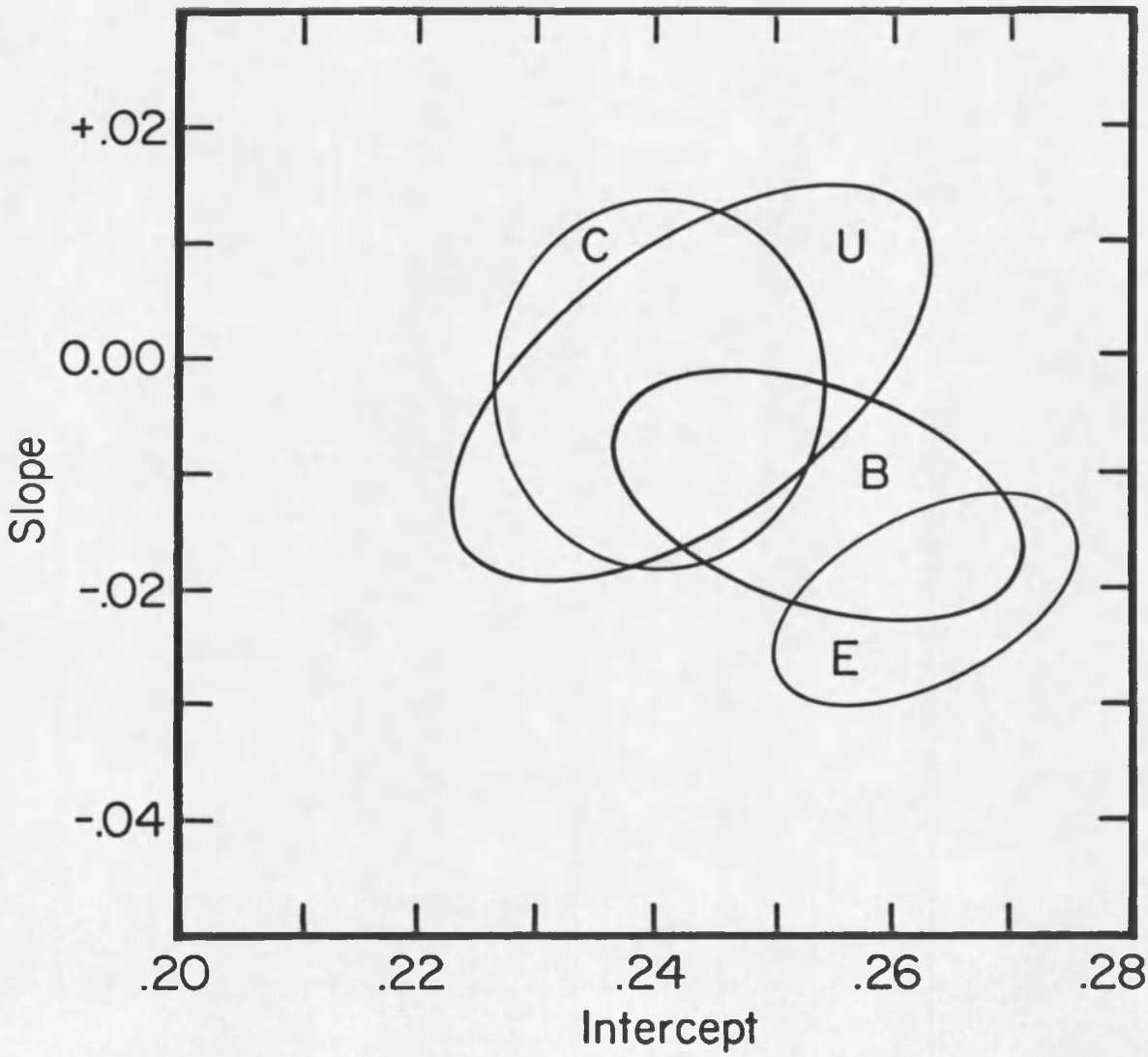

Figure 17. One sigma error ellipses showing possible values of slope and intercept for the first four pairs of variables listed in Table 14.

significant correlation is seen. Note that the expected offset in intercept in these relations should have no effect on the expected correlation, since it changes all of the residuals by a constant amount. Thus, we believe that relations 3 and 4 can be ruled out. Plotted in Figure 18 are the elliptical data points and the adopted metallicity-luminosity relation, and the spiral points in relation B.

Lastly, we investigate the evidence for radial metallicity gradients by examining the relation between the residuals in the spiral metallicity-bulge luminosity relation and the distances to the individual galaxies. Since a smaller area is sampled in a closer galaxy, it is expected that the metallicity in a nearby galaxy will appear greater than in a distant galaxy with identical properties. This effect is seen in Table 14 in the final 2 rows, where the residuals in the B relation have been compared with the distances in megaparsecs as listed in Chapter I. When M31 and M81 (NGC's 224 and 3031) are included, this effect is quite strong because the sample is strongly influenced by these nearby objects. When they are removed, the significance of the correlation is reduced. Thus, there is evidence for radial gradients, although this evidence is weak, apart from the two very close objects. This might be interpreted as an indication that the gradient is very steep at small galactocentric radii and gets flatter further out.

Discussion

The conclusions of the preceding sections are: (1) although the evidence is not extremely strong, it appears that central metallicity in the bulges of spiral galaxies is more closely related to the bulge

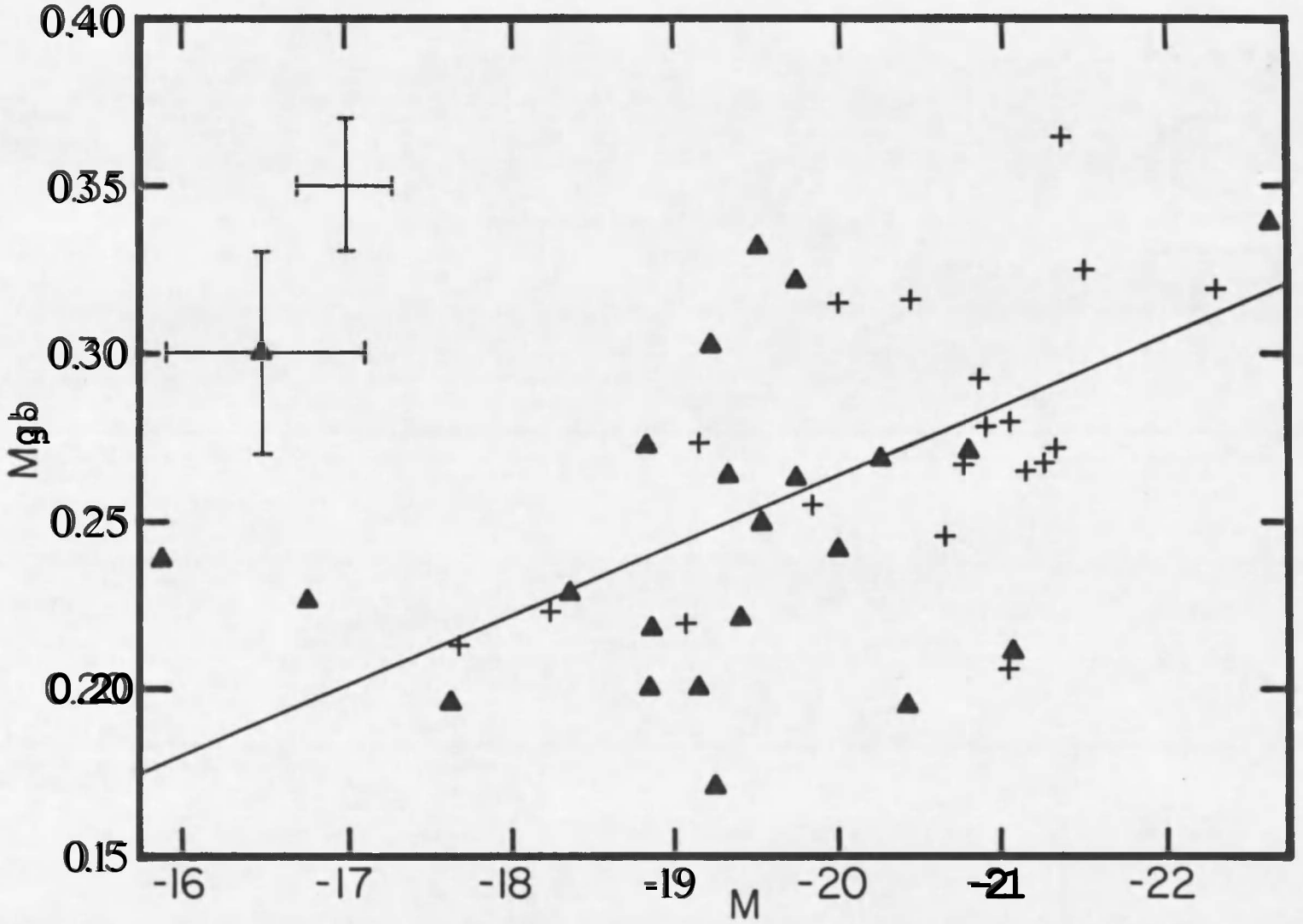

Figure 18. The metallicity (Mgb) vs. luminosity (M) diagram for elliptical galaxies (crosses) and spiral bulges (triangles) -- Estimated error bars are shown in the upper left. The line is the adopted relation for elliptical galaxies.

luminosity than to the total luminosity or total mass of the galaxy, and (2) there is no additional dependence on the bulge-to-disk ration of the galaxy. How can these results be interpreted in terms of the theoretical expectations presented in Chapter I?

Bot the lack of correlation with bulge-to-disk ratio and the preference for the bulge magnitudes over total magnitudes point toward the idea that the central metallicity in the bulge is set up without much influence from the disk or the material which will become the disk. This can be interpreted as evidence for one of two different types of scenarios. One possibility is that the presence of the disk is incapable of affecting the processes which are responsible for the metallicity-luminosity relation. A specific example of this idea might be a picture in which the central metallicity is determined by the epoch at which supernova-driven winds can blow the remaining gas out of the bulge region of the forming galaxy. The difference between this scenario and the application of supernova-driven winds to elliptical galaxies (Larson 1974b) is that in the proto-spiral, the star formation is not coeval. If the timescales are such that the disk has not yet begun intense star formation when the bulge blows out its gas, this gas could settle into the existing disk. The requirement that disks not undergo an early period of very active star formation is reasonable in light of the fact that the disks of spirals retain gas today. If early star formation in disks was as vigorous as in bulges or elliptical galaxies, we might expect that they would have removed their gas as well.

An equally valid situation which would produce the observed metallicity-bulge luminosity relation is one in which the disk material has not yet accreted on to the galaxy at the time that the central metallicity is determined. It is obvious that any scenario in which the disk forms after the metallicity-luminosity relation is established will produce the right answer. We illustrate this with a picture in which the bulge is formed by mergers of small subsystems of stars, in which residual gas forms stars after each merger. As detailed in Chapter I, it can be shown that the efficiency of star formation might reasonably be expected to depend on the amount of compression that the gas undergoes in the merger. This compression is related to the total mass of the system, and so a metallicity-luminosity relation arises. Now, if spiral bulges form in this manner, and disks are accreted afterward from low density outlying intergalactic gas clouds, the observed result would be expected.

Because many different specific pictures can be imagined to explain the result, it may be more instructive to ask what sorts of models are ruled out. The implication of the spiral metallicity-bulge luminosity relation is that pictures in which the disk material is undifferentiated from the bulge material at the time that the relation is set up are excluded. That is, the gas which is in the merging subsystems in those models cannot be the material which becomes the disk, for instance. Also, the parameter which determines the bulge-to-disk ratio of the galaxy, the density in the collapse models, cannot have an important effect on bulge star formation or central metallicity.

It is clear that the scenarios which have been proposed for galaxy formation are very complex and fairly ill defined. Furthermore, it is likely that in reality, the processes are even more complex than the models. Therefore, one of the most straightforward aspects of this study is a comparison of what might be two very similar types of systems, spirals and SO's. It has been found, in work described at the beginning of this chapter and in Chapter I, that when large aperture color or line strength measurements of SO galaxies are considered, their relation with the total luminosity of the galaxy is indistinguishable from what we have called the elliptical metallicity-luminosity relation. That finding is in contrast to this study of spiral galaxies, and the qualifications and implications of this distinction should be considered.

There are two limitations to a comparison of the results of this study with similar studies of SO galaxies. The first of these is related to bulge-to-disk ratios. It might be imagined that small bulge-to-disk spirals could have somewhat different bulge properties than large bulge-to-disk spirals. Clearly we would like to compare spirals and SO's with the same bulge-to-disk ratios. Figure 19 shows histograms of the bulge-to-disk mass ratios for spirals studied here and for SO's as measured by Burstein (1979b). Selection effects are expected to play an important role in the distribution of bulge-to-disk ratios for each sample, and in fact, it is thought that the selection effects bias the samples in opposite directions. Burstein states that he tried to include SO's with particularly small bulge-to-disk ratios; in this study the trend was toward spirals with large bulge-to-disk ratios. It is important to note also that large bulge-to-disk ratio SO galaxies are

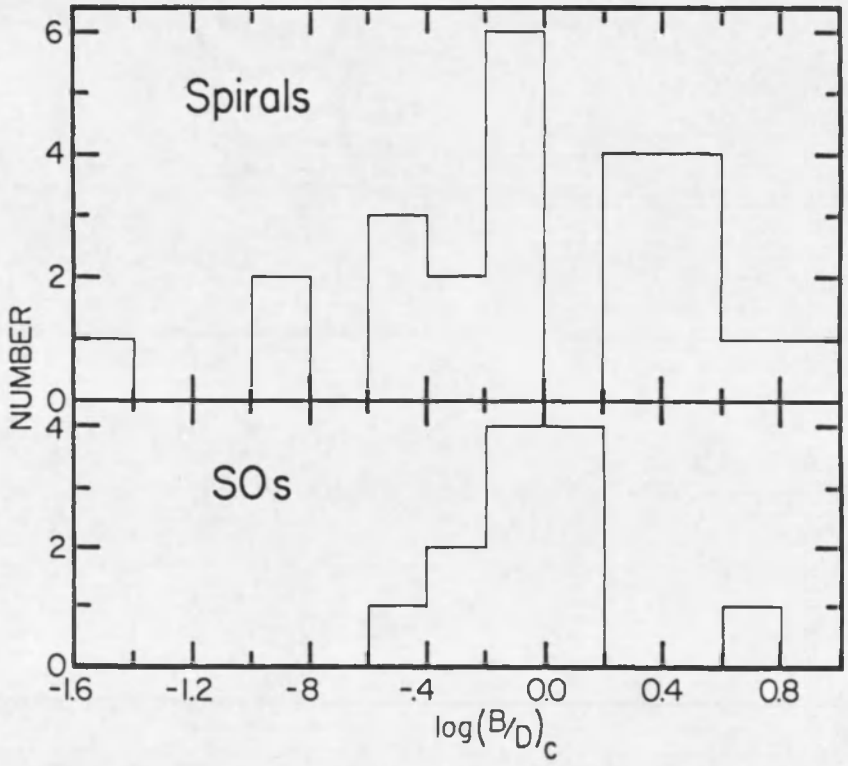

Figure 19. Histograms of the observed distributions of bulge-to-disk mass ratios for spirals (from this study) and for SO's (from Burstein 1979b).

especially difficult to distinguish from elliptical galaxies, particularly if the galaxy is pole-on. In the light of the obvious effects we interpret the bulge-to-disk ratio distributions as follows. In both spiral and S0 samples there is a broad peak in the distribution centered at a bulge-to-disk ratio of about unity. In the S0 sample, the deficiency of bulge-to-disk ratios to the right of the center of the peak is most likely due to the selection effects discussed above. The spiral sample clearly persists to much lower bulge-to-disk values than the S0 sample, and no doubt the extent and amplitude of this "tail" has been underestimated because of the bias toward bulge-dominated systems. It can be seen, however, that aside from the three very small bulge-to-disk spirals, the distribution of bulge-to-disk ratios for spirals and S0's in these samples is quite similar.

The second qualification we must consider in comparing the spiral and S0 results is the results of radial gradients. It was stated earlier that the S0 measurements were obtained through large apertures while the spiral measurements represent nuclear metallicities. Is it possible, considering this difference, to find a situation which allows the spirals and S0's to have the same properties and yet produce the observed distinction? Yes, such a picture is possible although it requires a rather special coincidental difference between gradients in the bulges of disk systems and elliptical galaxies. If the radial gradients in bulges are not as steep as in elliptical galaxies, then, when the nuclear metallicities are the same, a larger aperture will find a higher mean metallicity in the bulge than in the elliptical. If, moreover, the difference in the gradients is precisely right, the amount

by which the mean metallicity in bulges exceeds that in ellipticals for the same nuclear value could correspond to the factor of two difference between the bulge luminosity and the total luminosity in SO's. This scenario would explain the apparently different metallicity-luminosity relations for spiral and SO galaxies. Although, of course, this explanation is a possibility, the fact that it requires the two effects, difference in gradient and bulge-to-disk ratio, to conspire to agree, suggests to us that it is unlikely.

If in fact the metallicity-luminosity relations for spirals and SO's differ in the way that the evidence suggests, this discrepancy constitutes fairly solid proof that SO galaxies were not at one time spiral galaxies, as has been proposed. Specifically, it implies that in contrast to the spiral result, the metallicity at the centers of SO galaxies <u>is</u> influenced by the disk material. This requires a wholly different picture of the processes at the time of galaxy formation. In particular, this result might be interpreted as evidence that star formation in the disks of SO's takes place earlier than in spirals, or even that the material in SO disks takes part in the protogalactic collapse, whereas the material in spiral disks does not. However, the gradient question is still an uncertainty, and a detailed comparison of the metallicity-luminosity relation for spiral and SO galaxies will have to await the measurement of nuclear metallicities in a sample of SO galaxies.

In summary, we have shown that the nuclear metallcities in the bulges of spiral galaxies are related to the bulge luminosities in the same way that nuclear metallicity is related to total luminosity in

elliptical galaxies. This is interpreted as evidence that the disk material has little influence on the processes which affect star formation in the bulge. Specifically, formation scenarios which predict this result are those in which the bulge and disk are physically separate or in which the disk material has not yet accreted on to the galaxy at the time when the nuclear metallicity is determined. This result is contrasted with studies of SO galaxies, and, unless radial gradient effects conspire in an unlikely way, the difference between the metallicity-luminosity relations strongly suggest different origins for these two types of galaxies.

REFERENCES

Aaronson, M. 1977, unpublished thesis, Harvard University.

Aaronson, M. 1980, research associate, Steward Observatory, private communication.

Aaronson, M., J. G. Cohen, J. Mould, and M. Malkan 1978, Ap. J., 223, 824.

Aaronson, M., J. Huchra, and J. Mould 1979, Ap. J., 229, 1.

Balkowski, C. 1973, A. Ap., 29, 43.

Balkowski, C., L. Bottinelli, L. Gouguenheim, and J. Heidmann 1972, A. Ap., 21, 303.

Baum, W. A. 1959, P. A. S. P., 71, 106.

Bevington, P. R. 1969, Data Reduction and Error Analysis for the Physical Sciences (McGraw-Hill, New Yok).

Bosma, A., J. M. van der Hulst, and W. T. Sullivan, III 1977, A. Ap., 57, 373.

Bottinelli, L., P. Chamaraux, L. Gouguenheim, and R. Lauque 1970, A. Ap., 6, 453.

Burkhead, M. S., and J. K. Kalinowski 1974, A. J., 79, 835.

Burstein, D. 1979a, Ap. J., 232, 74.

Burstein, D. 1979b, Ap. J., 234, 435.

Burstein, D. 1979c, Ap. J., 234, 829.

Burstein, D. 1979d, Ap. J. Supp., 41, 435.

Cohen, J. G. 1978, Ap. J., 221, 788.

de Vaucouleurs, G. 1953, M. N. R. A. S., 113, 134.

de Vaucouleurs, G. 1959, Handbuch der Physik, 53, 311.

de Vaucouleurs, G. 1961, Ap. J. Supp., 5, 233.

de Vaucouleurs, G., and M. Cappaciolli 1979, Ap. J. Supp., 40, 699.

de Vaucouleurs, G., A. de Vaucouleurs, and H. G. Corwin, Jr. 1976, Second Reference Catalog of Bright Galaxies (University of Texas Press, Austin).

de Vaucouleurs, G., and J.-L. Nieto 1978, Ap. J., 220, 449.

de Vaucouleurs, G., and J.-L. Nieto 1979, Ap. J., 230, 697.

Dickel, J. R., and H. J. Rood 1978, Ap. J., 223, 391.

Faber, S. M. 1972, A. Ap., 20, 361.

Faber, S. M. 1973, Ap. J., 179, 792.

Faber, S. M. 1977, in The Evolution of Galaxies and Stellar Populations, ed. B. M. Tinsley and R. B. Larson (Yale University Observatory, New Haven), p. 157.

Faber, S. M. 1979, Professor of Astronomy, University of California, Santa Cruz, private communication.

Freeman, K. C. 1970, Ap. J., 160, 811.

Frogel, J. A., S. E. Persson, M. Aaronson, and K. Matthews 1978, Ap. J., 220, 75.

Gallagher, J. S., S. M. Faber, and B. Balick 1975, Ap. J., 202, 7.

Gott, J. R., and T. X. Thuan 1976, Ap. J., 204, 649.

Hege, E. K., R. H. Cromwell, and N. J. Woolf 1979, Adv. Electronics and Electron Physics, 52, 397.

Hubble, E. 1930, Ap. J., 71, 231.

Hubble, E. 1936, The Realm of the Nebulae (Yale University Press, New Haven).

Huchra, J. 1977, Ap. J., 217, 928.

Illingworth, G. 1977, Ap. J. (Lett.), 218, L43.

King, I. 1962, A. J., 67, 471.

Kormendy, J. 1977a, Ap. J., 214, 359.

Kormendy, J. 1977b, Ap. J., 218, 333.

Kormendy, J. 1977c, Ap. J., 217, 406.

Kormendy, J., and G. Illingworth 1980, in Photometry, Kinematics and Dynamics of Galaxies, ed. D. S. Evans (University of Texas, Austin).

Larson, R. B. 1974a, M. N. R. A. S., 166, 585.

Larson, R. B. 1974b, M. N. R. A. S., 169, 229.

Larson, R. B. 1975, M. N. R. A. S., 173, 671.

Larson, R. B. 1976, M. N. R. A. S., 176, 31.

Larson, R. B., and B. M. Tinsley 1978, Ap. J., 219, 46.

Lasker, B. M. 1970, A. J., 75, 21.

Margon, B., M. Lampton, S. Bowyer, and R. Cruddace 1975, Ap. J., 197, 25.

Monet, D., D. O. Richstone, and P. L. Schechter 1980, in prep.

Moore, E. 1968, unpublished thesis, University of Arizona.

Morgan, W. W. 1958, P. A. S. P., 70, 364.

Morgan, W. W. 1959, P. A. S. P., 71, 394.

Morgan, W. W., and N. U. Mayall 1957, P. A. S. P., 69, 291.

Morgan, W. W., and D. E. Osterbrock 1969, A. J., 74, 515.

Mould, J. 1978, Ap. J., 220, 434.

O'Connell, R. W. 1976, Ap. J., 206, 370.

O'Connell, R. W. 1980, preprint.

Pritchet, C. 1977, Ap. J. (Supp.), 35, 397.

Roberts, W. W., Jr., M. S. Roberts, and F. H. Shu 1975, Ap. J., 196, 381.

Rubin, V. C., W. K. Ford, Jr., K. M. Strom, S. E. Strom, and W. Romanishin 1978, Ap. J., 224, 782.

Sandage, A. R. 1961, The Hubble Atlas of Galaxies (Carnegie Institution of Washington, Washington).

Sandage, A. R., K. C. Freeman, and N. R. Stokes 1970, Ap. J., 160, 831.

Schmidt, M. 1959, Ap. J., 129, 243.

Searle, L., W. L. W. Sargent, and W. G. Bagnuolo 1973, Ap. J., 179, 427.

Shostak, G. S. 1978, A. Ap., 68, 321.

Spinrad, H. 1966, P. A. S. P., 78, 367.

Spinrad, H., and B. J. Taylor 1971, Ap. J. Supp., 22, 445.

Terlevich, R., R. L. Davies, S. M. Faber, and D. Burstein 1980, preprint.

Tifft, W. G. 1969, A. J., 74, 354.

Tinsley, B. M., and J. E. Gunn 1976, Ap. J., 203, 52.

Tinsley, B. M., and R. B. Larson 1979, M. N. R. A. S., 186, 503.

Turnrose, B. E. 1976, Ap. J., 210, 33.

Visvanathan, N., and D. Griersmith 1977, A. Ap., 59, 317.

Visvanathan, N., and A. R. Sandage 1977, Ap. J., 216, 214.

White, S. D. M., and M. J. Rees 1978, M. N. R. A. S., 183, 341.

Whitford, A. E. 1977, Ap. J., 211, 527.

Whitmore, B. C., R. P. Kirshner, and P. L. Schechter 1979, Ap. J., 234, 68.

Wilkinson, A., and L. Searle 1977, unpublished report, Hale Observatory.

Williams, T. B. 1976, Ap. J., 209, 716.

Wood, D. B. 1966, Ap. J., 145, 36.

Young, P. J., J. A. Westphal, J. Kristian, C. P. Wilson, and F. P. Landauer 1978, Ap. J., 221, 721.